

# Master Thesis

The applicability of the ASED-sensor for measuring bed level changes in intertidal areas



MASTER THESIS IN  
WATER ENGINEERING AND MANAGEMENT  
FACULTY OF ENGINEERING TECHNOLOGY  
UNIVERSITY OF TWENTE

April 18, 2019

**Author:** A. (Anja) Mus  
**Student number:** s1871587  
**Location:** Enschede and Yerseke  
**Organization:** University of Twente and Royal  
Netherlands Institute of Sea  
Research (NIOZ)

**Graduation committee:**

*University of Twente*  
Ir. P.W.J.M. Willemsen  
Dr. Ir. B.W. Borsje  
Prof. Dr. S.J.M.H. Hulscher

**Experimental support:**

NIOZ  
Prof. Dr. T.J. Bouma  
J. van Dalen



# Preface

This report is the final product of my master thesis in the Water Engineering and Management (WEM) department of the University of Twente and Royal Netherlands Institute of Sea Research (NIOZ). The research is executed under the supervision of Prof. Dr. T.J. Bouma, J. van Dalen from NIOZ, Prof. Dr. S.J.M.H. Hulscher, Dr. Ir. B.W. Borsje and Ir. P.W.J.M. Willemsen of the University of Twente. The major part of the study was conducted at the University of Twente, whereas lab and field experiments were executed during a period of one month at NIOZ in Yerseke.

Finishing this report marks the end of my time as a student, which I have very much enjoyed over the past years. I have had great experiences and met wonderful people and would like to thank everyone involved in this period of my life.

This report could not have been made without the help of some people. Firstly, I would like to thank my supervisors, with in particular P.W.J.M. Willemsen for the weekly support and revisions during the study. Furthermore, I would also like to thank F. van Maarseveen and B. Denissen for explaining the ASED-sensor in detail, R. Maaskant for helping me through the entire process, and H. Maaskant for reviewing my report during the final stages of the thesis.



# Abstract

The Acoustic Sediment Elevation Dynamics (ASED)-sensor is a stand-alone measuring device designed by NIOZ, to study bed level dynamics within intertidal areas. The ASED-sensor was used to study the morphological behaviour of intertidal flats. However, the sensor was not yet properly tested and lacked an algorithm and autonomous script for translating raw intensity data into bed level data. Therefore, the objective of this study is to assess the applicability of the ASED-sensor for measuring bed level changes in intertidal areas. It includes developing the raw data processing algorithms and their implementation in Python scripts.

The ASED-sensor uses a pulsed acoustic signal of approximately 300 kHz to measure bed levels during submerged conditions. The reflected signal by the bed is detected by a sudden increase in amplitude. The travel time of the signal from the sensor to the bed and vice versa needs to be converted to a distance, to obtain bed levels. The sensor will be tested both in the lab and in the field. Lab experiments need to be collected to verify whether the ASED-sensor can detect the echo and measure the travel time in a range of environmental conditions in the water tank and wave flume at NIOZ in Yerseke. The environmental conditions consisted of water depths, soil types, dilutions of soil types, and waves and current forcing. Thereafter the ASED-sensor was deployed to measure in the field. The field experiments were performed in the Eastern Scheldt, next to NIOZ, and in the Western Scheldt at the Kapellebank. The Eastern Scheldt experiment was performed during a weekend, while the Western Scheldt experiment collected data for 19 days. The lab experiments and the Eastern Scheldt experiment were validated with a manual measurement using a tape measure. The validation of the Western Scheldt experiment's data was accomplished by a tape measure and erosion pins.

At the start of the study, the ASED-sensor lacked an autonomous script for translating raw intensity data into bed level data. Therefore, three algorithms were tested, consisting of Fast Fourier Transform, envelope method and the Kalman filter. The Kalman filter method showed the most promising results, with the lowest standard deviation and lowest computation time. Parameter settings within the script were determined using the lab and field experiments. The parameter settings are filtering noise and searching the start of the sudden increase in amplitude of the first strong signal reflected by the bed. These parameters tune the bed detection of the ASED-sensor.

The practical measurement domain for the ASED-sensor is from 0.20 m to 0.45 m, according to the raw data analysis of all lab experiments. The coefficient of determination ( $R^2$ ) between the newly developed script and the manual measurements was 0.99 for the lab experiments. The bed could be detected during the field experiments. The actual accuracy is 2 mm to 4 mm, obtained from the lab experiments. The predecessor Sediment Elevation Dynamics (SED)-sensor scores 4 mm for the accuracy (De Mey, 2016). The light cells based SED-sensor cannot measure during nocturnal and submerged conditions. The hydrodynamics are only active during submerged conditions and thus morphological changes cannot be observed by the SED-sensor but can be observed by acoustic instruments. Most acoustic instruments have the same accuracy but have a high unit cost and labour-intensive deployments. The ASED-sensor, with its high vertical accuracy, low labour-intensive deployment cost and reasonable cost, is well suited for monitoring bed level dynamics in intertidal areas.

# List of abbreviations

ADCP	Acoustic Doppler Current Profiler
ADV	Acoustic Doppler Velocimeter
ASED-sensor	Acoustic Sediment Elevation Dynamics sensor
FFT	Fast Fourier Transform
GNSS	Global Navigate Satellite System
GPS	Global Positioning System
MBES	Multi Beam Echo Sounder
NIOZ	Royal Netherlands Institute of Sea Research
PEEP-sensor	Photo-Electronic Erosion Pin sensor
RPM	Rotation Per Minute
RTK	Real Time Kinematic
SBES	Single Beam Echo Sounder
SED-sensor	Sediment Elevation Dynamics sensor
SSC	Suspended Sediment Concentration
WEM	Water Engineering and Management

# Contents

<b>1</b>	<b>INTRODUCTION.....</b>	<b>1</b>
1.1	BACKGROUND .....	1
1.2	RESEARCH GAP AND RELEVANCE .....	3
1.3	RESEARCH OBJECTIVE .....	4
1.4	RESEARCH QUESTIONS.....	4
1.5	REPORT OUTLINE.....	4
<b>2</b>	<b>METHODS .....</b>	<b>5</b>
2.1	THE ASED SENSOR.....	5
2.2	STUDY SITES .....	8
2.3	LAB AND FIELD EXPERIMENTS .....	11
2.4	CONVERTING RAW DATA TO BED LEVELS.....	15
<b>3</b>	<b>RESULTS .....</b>	<b>22</b>
3.1	MEASURING WITH THE ASED-SENSOR .....	22
3.2	COLLECTING RAW DATA .....	23
3.3	CONVERTING RAW DATA TO BED LEVEL DATA .....	30
3.4	THE ACCURACY OF THE ASED-SENSOR .....	42
<b>4</b>	<b>DISCUSSION.....</b>	<b>43</b>
4.1	MEASURING WITH THE ASED-SENSOR .....	43
4.2	COLLECTING RAW DATA .....	45
4.3	CONVERTING RAW DATA TO BED LEVEL DATA .....	46
4.4	COMPARISON WITH THE SED-SENSOR.....	48
4.5	FURTHER POSSIBILITIES ASED-SENSOR .....	49
4.6	EXTRA MEASUREMENTS .....	50
<b>5</b>	<b>CONCLUSIONS .....</b>	<b>51</b>
<b>6</b>	<b>RECOMMENDATIONS .....</b>	<b>52</b>
<b>A</b>	<b>APPENDICES .....</b>	<b>57</b>
A.1	ASED-SENSOR.....	57
A.2	SEDIMENT DISTRIBUTION.....	65
A.3	FLUME CALIBRATION .....	66
A.4	SSC LAB EXPERIMENT .....	67
A.5	ANALYSED METHODS .....	69
A.6	FORMULAS OF THE SPEED OF SOUND .....	78
A.7	EXTRA RESULTS EXPERIMENTS .....	82
A.8	INUNDATIONS OF THE FIELD EXPERIMENTS.....	87
A.9	PERFORMED EXPERIMENTS.....	90



# 1 Introduction

## 1.1 Background

The ability of salt marshes and tidal mudflats to aggrade vertically to maintain their position in the intertidal region has been the focus of numerous studies over the last 50 years (Ranwell, 1964; Leonard *et al.*, 1995; Möller *et al.*, 2014). During the present era of sea-level rise and increasing storminess, sustainable coastal protection requires in-depth understanding of their long-term lateral dynamics and their ability to survive the changing conditions (Callaghan *et al.*, 2010; Yang *et al.*, 2012; Bouma *et al.*, 2014; Möller *et al.*, 2014). Coastal ecosystems, such as tidal flats and salt marshes (Figure 1.1), mangrove forests and reefs, can contribute to coastal protection and flood risk reduction by surge attenuation (Wamsley *et al.*, 2010), wave energy dissipation and erosion reduction (Gedan *et al.*, 2011).

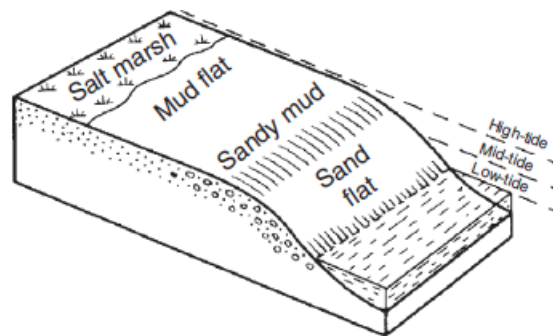


Figure 1.1: Exposed, sand-rich tidal flat and salt marsh (Friedrichs, 2012)

The morphological evolution (i.e., the balance between erosion and accretion) of tidal flats and salt marshes are influenced by tidal currents and waves (van der Wal *et al.*, 2008; Callaghan *et al.*, 2010). Morphodynamical changes in salt marshes are suppressed by vegetation, but dynamics at tidal flats occur much faster due to the absence of vegetation (Möller *et al.*, 1999; Hu *et al.*, 2015).

Three different types of measurements showed, that sediment deposition occurred on the marsh surface during rising tides at tidal elevations ranging from those barely flooding the creek bank to high spring tides, and that sediment was not remobilized by tidal flows after initial deposition (Christiansen *et al.*, 1999). Flooding is the main mechanism for sediment delivery to the marsh platform, salt marshes are therefore inevitably linked to sea level and tidal oscillations (Fagherazzi *et al.*, 2012). Sediment deposition occurred on the marsh surface largely because fine sediment in suspension formed flocs. The processes controlling sediment deposition did not vary among tides. However, Suspended Sediment Concentration (SSC) near the creek bank increased with increasing tidal amplitude, consequently promoting higher rates of deposition with higher tides (Christiansen *et al.*, 1999). If vertical sediment accretion is smaller than sea-level rise, marshes are at risk of drowning and suffer “coastal squeeze” when dykes prevent (high) marshes to recede inland (Doody, 2004). Besides all this, there is a seasonal influence of waves on the shore and mudflats. Winter has higher waves whereby the sediment is placed further outwards and the beach becomes steeper. The beach steepness is low in summer, due to the calmer waves and more deposition of sand on the beach.

High hydrodynamic energy either from waves or current velocity, and lack of sediment will generally cause mudflat–salt marsh ecosystems to reduce in size due to erosion. The

inverse, high sediment availability combined with low hydrodynamic energy, most likely results in vertical accretion and/or lateral extension (Bouma *et al.*, 2005, 2016). The waves and current forcing generate bottom shear stresses, which are relevant for sediment erosion and deposition. The bottom shear stress at the bed is a combined effect of non-linear interactions between the mean flow and the waves (Le Hir *et al.*, 2000). As mentioned before the tidal flat topography is continuously shaped by hydrodynamic force from tidal currents and wind waves (Hu *et al.*, 2015). As such forces have great temporal and spatial variability on short time scales, they may impose short-term surface elevation (Le Hir *et al.*, 2000; Green *et al.*, 2014). The short-term bed level change information is vital to identify the effect of current hydrodynamic forcing and to understand fundamental processes in sediment transport (Friedrichs, 2012; Green *et al.*, 2014). Wave forcing is known to vary strongly with wave direction, wave period, wave height and tidal phase or water depth (Nielsen, 2009). Current forcing varies hourly with the tidal phase, and the tidal range varies fortnightly with the spring/neap cycle (Bouma *et al.*, 2005). Waves and current field measurements on tidal flat and salt-marsh ecosystems indicated that the hydrodynamic forcing on the bottom sediment was strongly influenced by wind-generated waves, more so than by tidal- or wind-driven currents (Callaghan *et al.*, 2010). The measurements further showed that the hydrodynamic forcing decreased considerably landward of the marsh cliff, highlighting a transition from vigorous (tidal flat and pioneer zone) to sluggish (mature marsh) fluid forcing (Callaghan *et al.*, 2010).

Within the estuarine and coastal environment, tidal flats and salt marshes play an important role as essential habitats for plants and animals and as sinks and/or source for nutrients, pollutant and sediment (Figure 1.1; Allen, 2000; Doody, 2004). They also play a significant role in coastal defence, enhancing coastal sedimentation, as the intertidal vegetation decreases water movements and binds sediments (USACE, 1989). Sediment-rich environments with gentle bed slopes are a common representation of the tidal flats (Figure 1.1; Friedrichs, 2012). The vegetation in salt marshes ensures a stable sediment bed. Despite the absence of vegetation in the tidal flat, bed level changes are influenced by ecology, due to the seasonal presence of stabilizers and destabilizers bio-engineers on tidal flats, like algal tufts for the stabilizing effect and lugworms for destabilizing (Volkenborn *et al.*, 2008; Hu *et al.*, 2015). The wave attenuation by vegetation generally causes an exponential decline of wave energy with distance across salt marshes (Bouma *et al.*, 2005; Möller *et al.*, 1999; Yang *et al.*, 2012). Comparisons show that wave attenuation across salt marshes is determined by vegetation characteristics, hydrodynamics, and sediment bed and can show spatial and temporal variations (Yang *et al.*, 2012).

To identify the short-term bed level changes an instrument is needed which can monitor those changes. Several instruments such as: Photo-Electronic Erosion Pin (PEEP) sensor and the SED-sensor are used to measure bed level changes. A big limitation of these instruments is that they cannot measure during submerged and nocturnal conditions (Lawler, 2008; Hu *et al.*, 2015). Another instrument, the electro-resistivity sensor, which uses the difference in the electrical conductivity of seawater and sediment, has a low (10-30 mm) vertical resolution (Ridd, 1992; Hu *et al.*, 2015). As alternative different acoustic instruments have been used, such as: ALTUS (Ganthy *et al.*, 2013), Acoustic Doppler Velocimeter (ADV) (McLelland *et al.*, 2000), Acoustic Doppler Current Profiler (ADCP) (Horstman *et al.*, 2011), Single Beam Echo Sounder (SBES) (Kongsberg Maritime AS, 2017) and Multi Beam Echo Sounder (MBES) (Kongsberg, 2017). The acoustic instruments generally have the highest vertical resolution (within 2 mm). However, most of these

methods require external power and an on-site data-logging system, which leads to high unit cost and labour-intensive deployment (Hu *et al.*, 2015). The acoustic instruments cost more than €8000. Conventional discontinuous surface-elevation monitoring typically has a coarse temporal resolution (weeks to months), determined by resurvey frequency (Lawler, 2008; Nolte *et al.*, 2013).

The NIOZ developed a new sensor called the ASED-sensor. The ASED-sensor is a standalone device, like the predecessor SED-sensor. The ASED-sensor measures the propagation time of the signal reflected by the bed using an acoustic signal with a measurement frequency of approximately 300 kHz (Appendix A.1.1). This allows the sediment dynamics to be measured continuously during submerged conditions (Thorne *et al.*, 2002). This study is the first time that the ASED-sensor is tested thoroughly. First, the ASED-sensor will be validated during lab experiments before the data of the ASED-sensor can be trusted in the field.

## 1.2 Research gap and relevance

Estuarine tidal flats and salt marshes are important ecosystems, providing coastal protection (Allen, 2000; Callaghan *et al.*, 2010). Hydrodynamic energy either from waves or current velocity and sediment will cause the salt marsh and tidal flat to laterally grow and retreat (Bouma *et al.*, 2005). The size of the system influences the contribution to wave energy reduction and thereby on coastal protection (Vuik *et al.*, 2016); therefore, it is important to monitor bed level changes. The morphological development of the bed is driven by the hydrodynamic characterisation of a mudflat-salt marsh ecosystem. Yet, there is not much known about the relationship between the hydrodynamics and the morphological changes of the seabed. Therefore, an instrument is needed to measure in high resolution these morphological changes to understand the underlying processes. Accordingly, NIOZ designed a novel stand-alone instrument called the ASED-sensor. The ASED-sensor detects sediment surface position by an acoustic signal and is developed to measure with a high vertical resolution. The ASED-sensor has a high battery and storage capacity. Therefore, the surface elevation dynamics can be measured with a high temporal resolution. The problem with the predecessor SED-sensor not continuously measuring during submerged conditions has been solved. It is important to measure during submerged conditions because the hydrodynamics are only active during submerged conditions and thus morphological changes can be observed. This sensor is relatively cheap compared to the other acoustic instruments and should have similar accuracy. Since the sensor is cheap, a network of ASED-sensors could be placed in intertidal areas to register not only temporal variations but also spatial variations.

### 1.3 Research objective

The objective of this study is:

*Assessing the applicability of the ASED-sensor for measuring bed level changes in intertidal areas.*

Waves, currents and vegetation are the influencing factors for morphological changes (Möller, 2006). The bed level changes occur mostly during submerged conditions. For the registration of bed level changes, the ASED-sensor has been used. A script is built to convert the raw data into bed levels. This might improve the understanding of the underlying processes for the bed level changes during submerged conditions. Climate change, land subsidence and population growth in coastal areas lead to an increase in flood hazards and in its consequent economic damage and loss of life (Mendelsohn *et al.*, 2011). The ASED-sensor, with its high vertical accuracy, low labour-intensive deployment cost and reasonable cost, is well suited for monitoring bed level dynamics in intertidal areas. Therefore, this study will give a better understanding of the short and long term morphodynamics using the ASED-sensor.

### 1.4 Research questions

Three research questions have been formulated to achieve the research objective.

- 1) What is the ASED-sensor?
- 2) For what range of environmental conditions can the ASED-sensor detect a bed?
  - a) Under controlled lab experiments?
    - i) The range of water depths?
    - ii) The range of soil types?
    - iii) The range of dilutions of the different soil types?
    - iv) During waves and current forcing?
  - b) During field experiments?
    - i) In the Eastern Scheldt?
    - ii) In the Western Scheldt?
- 3) What converting method is suitable for detecting the bed using the raw data of the ASED-sensor?

### 1.5 Report outline

Following this introductory chapter, the next chapter starts by explaining the ASED-sensor, describes the study sites for collecting the lab and field data and illustrates the methods for converting the raw data into bed levels. Consecutively, chapter 3 describes the results of the raw data of the ASED-sensor under several conditions and converting the raw data into bed levels. Thereafter discussions, conclusions and recommendations are provided in chapter 4, 5 and 6.

## 2 Methods

### 2.1 The ASED sensor

The ASED-sensor is a stand-alone device that measures the propagation time of the signal reflected by the bed using an acoustic signal with a measurement frequency of approximately 300 kHz (Appendix A.1.1). The ASED-sensor has a storage capacity of 8 GB. The ASED-sensor has an energy supply from a battery pack of 8 alkaline AA battery cells (F. van Maarseveen, personal communication, October 15, 2018). The sensor is made waterproof by the transparent polyester case (Figure 2.1). The ASED-sensor has one transmitting transducer and one receiving transducer. The transducers are made waterproof by a 4 mm layer of lime/sealer 604 of Ruplo (F. van Maarseveen, personal communication, October 15, 2018). Between the transducers and the lime/sealer no air is present (Figure 2.2). The acoustic signal propagates from the transmitter through the water to the seabed (green arrow; Figure 2.3) and reflects at the seabed returning to the receiver (red arrow; Figure 2.3). Therefore, to define the water depth the signal travel time needs to be divided by two and multiplied by the speed of sound (blue arrow; Figure 2.3). The speed of sound varies by the water temperature, water pressure and the salinity. The ASED-sensor measures the water pressure, in 0.1 mbar accurate, and the water temperature, 2 decimals accurate in degrees Celsius. Salinity is determined independently, by conductivity sensor or from Rijkswaterstaat (Dutch department of waterways and public works) in parts per thousand. The time of measurement is recorded in milliseconds from 1-Jan-2001. The voltage of the battery, the start and the end voltage of the transmission are stored in millivolt (F. van Maarseveen, personal communication, October 15, 2018).



Figure 2.1: The waterproof transparent polyester case of the ASED-sensor

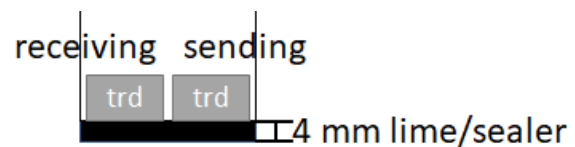


Figure 2.2: The head of the ASED-sensor with two transducers and the 4 mm thick lime/sealer.

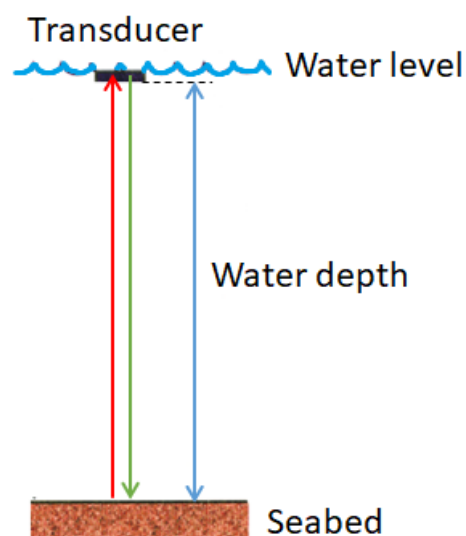


Figure 2.3: Signal transmission through the water

Before the signal can be sent into the water, the electric signal from the transducer needs to be transformed into an acoustic signal into the water and vice versa. The piezoelectric material in the transducer ensures these translations.

First, the transducer's analogue signal output is amplified and then passed through a bandpass-filter to lower the noise. It is then sampled at a 4 MHz sample rate with an 8-bit accuracy (F. van Maarseveen, personal communication, October 15, 2018).

During the transmission of the pulse, the data is not sampled. Therefore, the first 80 samples in time are not registered (F. van Maarseveen, personal communication, October 15, 2018). The ASED-sensor sends a burst of 5 pulses at approximately 300 kHz into the water. The transducer cannot produce a square wave and its best approach is a sine. The capacity of the electronics of the ASED-sensor and the mass of the water ensure a flattening of the square wave into the sine wave (F. van Maarseveen, personal communication, October 15, 2018).

The hardware consists of an 8-bit AD (analogue to digital) converter ( $2^8 = 256$ ), which results in an intensity range from -128 to 127 (F. van Maarseveen, personal communication, October 15, 2018). The AD converter has a reference voltage of 1 V for the translation of analogue voltage to the digital domain (F. van Maarseveen, personal communication, October 15, 2018). The digital domain has a sample rate of the 4MHz, with 4000-time steps of 250 ns each being recorded. The AD converter which is used is the AD9203 (Appendix A.1.2). The digital value of the AD converter represents the ratio of the measured voltage with respect to the reference voltage. The voltage can be calculated back when both voltages and the ratio are known. An amplifier is needed to get the voltage of the transducer for the AD converter to a sufficient level for passing the bandpass filter. A bandpass filter is a device that reduces the band noise and is a frequency selective filter (Corbishley *et al.*, 2007). The bandpass filter and amplifier only pass the 300 kHz signal and reject other frequencies or interferences. The ASED-sensor has a 3400x bandpass filter, the 3400 is the amplifier factor (F. van Maarseveen, personal communication, October 15, 2018). One reference voltage of the ASED-sensor and a 3400x bandpass filter give a  $\frac{1.0}{3400 \cdot 256} = 1.15 \mu V$ . The intensity range is from  $-0.147 mV$  ( $-128 * 1.15 \mu V$ ) to  $0.146 mV$  ( $127 * 1.15 \mu V$ ). One unit of intensity of the signal is  $1.15 \mu V$ .

The acoustic measurement interval of the ASED-sensor can be set with a Wi-Fi connection to the computer (Figure 2.4). Every single measurement can have an inter-measurement delay of a few milliseconds in a batch. The only requirement is that the signal should be back before the new signal is sent into the water. The output values which will be used for further analysis can be found in Appendix A.1.3.

# sediment002

## Diagnostics

```
(S) - System time : 2018-11-01 11:01:36
(W) - Postpone first wake-up until : 2018-11-01 10:53:20
(N) - ID : 2
(B) - Min. battery voltage : 8000 mV
(; ) - Remark :
(Y) - Sync marker threshold : 4096 bytes
(P) - Pressure sampling interval (0=off) : 0.2
(A) - Acoustic measurement interval (0=off) : 00:01:00
(M) - # Acoustic measurements : 8
(I) - inter measurement delay : 10 ms
(X) - Burst pattern : ++++++-----+++++
(D) - Recording delay : 533 (x 250ns)
(F) - First sample : 533
(G) - Flush after measurement : y
(T) - IR trigger off time : 2.0
(T) - IR trigger settling time : 0.035
(T) - IR trigger on time : 0.1
(T) - IR trigger verify time : 1.0
(T) - trigger debounce : 5000 ms
(N) - SSID prefix : sediment
(N) - SSID key : nioznioz
(B) - Minimum WiFi voltage : 7000 mV
(B) - # battery cells : 8
```

**Keyboard off**

Figure 2.4: ASED-sensor interface screen by Wi-Fi connection

After each burst electrostatic noise can occur or the internal mechanism could be vibrating (Riegl *et al.*, 2004; Lurton, 2010), which will result in noise at the beginning of the signal. Therefore, the first 533-time steps of the measurement are ignored which is approximately 0.10 m. This means that the first 613 (533 + 80) samples in time are not measured, which is  $153 \mu\text{s}$  ( $613 * 250 \text{ ns}$ ) in time. The speed of sound in seawater is assumed to be 1500 m/s. This results in  $\frac{613 * 250 \text{ ns} * 1500 \text{ m/s}}{2} = 11.5 \text{ cm}$  in water depth. The ASED-sensor measures with a 4 MHz sample rate during 1 ms (4000 samples), which can measure a water depth of  $\frac{4000 * 250 \text{ ns} * 1500 \text{ m/s}}{2} = 0.75 \text{ m}$ . Therefore, the theoretical measurement domain of the ASED-sensor is from 0.115 to 0.865 m. Based on the collected lab experiments, we assume a practical measurement domain from 0.20 to 0.45 m.

The transducer starts sending the signal by the provided square waves and the accumulated energy will be delivered in a few periods of decreasing intensity strength (F. van Maarseveen, personal communication, October 15, 2018). Since the transducer of the ASED-sensor sends 5 pulses, the bed detection will start at a sudden increase in return signal amplitude. The reflection of the bed is dependent on the roughness/ smoothness and the type of bed. The rougher the bed, the more diffuse scatter will occur, and the more energy will return to the receiver, like a rock bed. The smoother the bed, the more specular the scatter, with that energy not returning to the receiver and being lost, like a very fine silt bed (Riegl *et al.*, 2004; Lurton, 2010).

The files from the ASED-sensor can be downloaded using a Wi-Fi connection. The file name of a certain ASED-sensor is 002-003A.SE2. Where 002 denotes the sensor-id, 003A is the measurement sequence number (in hex coding) and SE2 is the output format (Appendix A.1.4).

## 2.2 Study sites

### 2.2.1 Lab experiments

The travel time of the signal from the ASED-sensor to the bed and vice versa needs to be converted to a distance, to obtain a water depth. Therefore, analytic software needs to be developed. Before this can be done, lab experiments need to be collected to verify whether the ASED-sensor can measure the travel time in a range of environmental conditions. The lab experiments are measured under controlled environmental conditions. Thereafter the ASED-sensor will be used in the field. All lab experiments were obtained in a 300-litre water tank and in the wave flume at NIOZ. The water tank is placed outside, next to the greenhouse, at the NIOZ terrain in Yerseke (51°29'17" N; 004°03'26" E; Figure 2.5). Water from the Eastern Scheldt is used, which has an average salinity of 31.7 parts per thousand.

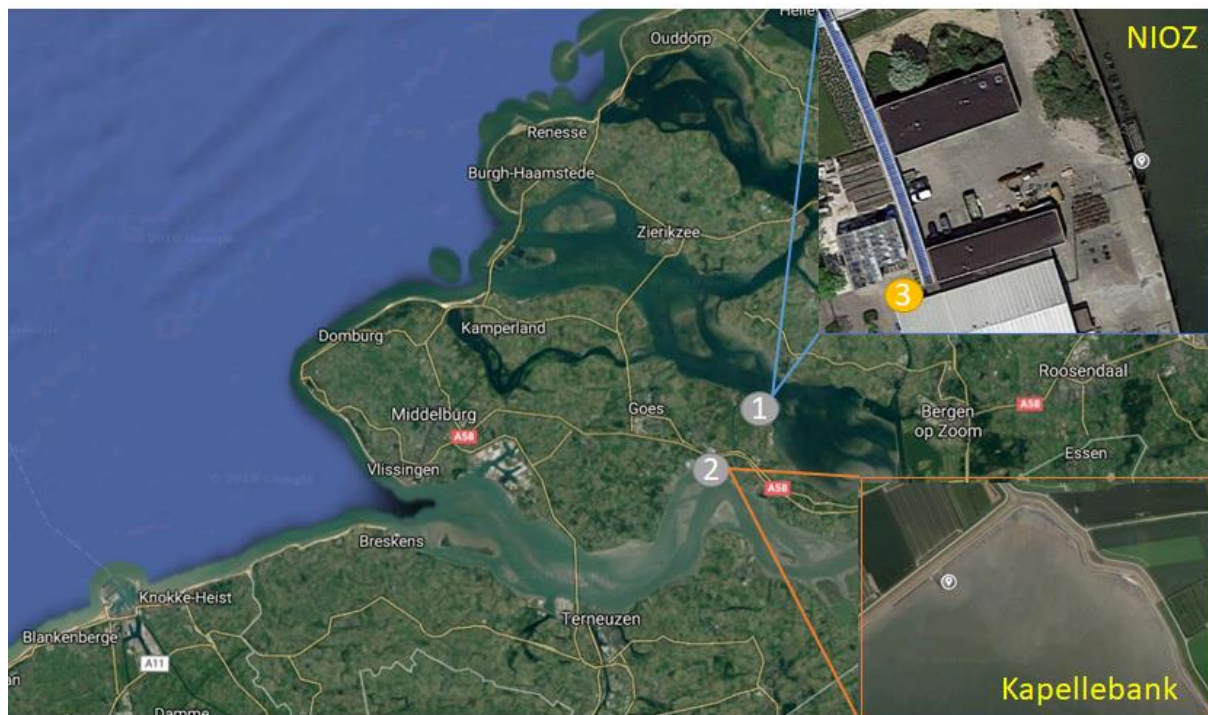


Figure 2.5: Location of the study sites. Location 1 is next to NIOZ which is in the Eastern Scheldt. Location 2 is the Kapellebank which is in the Western Scheldt. Location 3 is the greenhouse at the NIOZ terrain.

The wave flume of NIOZ (Figure 2.6) is used for testing the ASED-sensor during controlled waves and current forcing. The dimensions of the wave flume are 17 m long (2 m test section) x 0.6 m wide x 0.4 m deep (Figure 2.6). The current velocity can be changed from 0 to 80 cm/s and small regular waves can be made. The maximum wave height which can be created by the wave flume was 9.5 cm. The wave flume is filled with 30 cm of water from the Eastern Scheldt. First, the water from the Eastern Scheldt is saved in a big water tank and thereafter put in the wave flume. The same occurs when the water needs to be emptied from the wave flume. The big water tank is used to split the added chemicals from the water before the water is deposited in the Eastern Scheldt. The salinity in the wave flume is 31.2 parts per thousand.



Figure 2.6: The wave flume of NIOZ (NIOZ website)

Waves will propagate through the entire wave flume. At the end of the test section, the wave break material is placed under a gradient to damp the wave and reduce reflection (Figure 2.7). The experiment with current forcing does not have wave break material. Therefore, the current forcing could circulate through the entire wave flume. The set-up of the ASED-sensor for both waves and current forcing experiments is shown in Figure 2.8.



Figure 2.7: Wave break material for damping the waves



Figure 2.8: Set-up of the ASED-sensor for the waves and current measurements

### 2.2.2 Field experiments

The field experiments are performed in the Eastern Scheldt and in the Western Scheldt (Figure 2.5 location 1 and 2 resp.). Because the Eastern Scheldt was closed off from freshwater input from the Rhine, Meuse and Western Scheldt since 1969, the Eastern Scheldt formed a tidal bay (De Leeuw *et al.*, 1992). Since then, the salinity remained nearly constant (De Leeuw *et al.*, 1992). The tides are semidiurnal, with a tidal range of 4 m (data derived from Rijkswaterstaat (Ministry of Transport and Public Works)). The soil type of the Eastern Scheldt is sandy. The ASED-sensor is placed next to NIOZ (Yerseke) in a sand

soil type in the Eastern Scheldt (51°29'18" N; 004°03'29" E; Figure 2.5 location 1 resp.; Figure 2.9). The salinity is assumed to be 31.7 parts per thousand at the experiment location in the Eastern Scheldt.

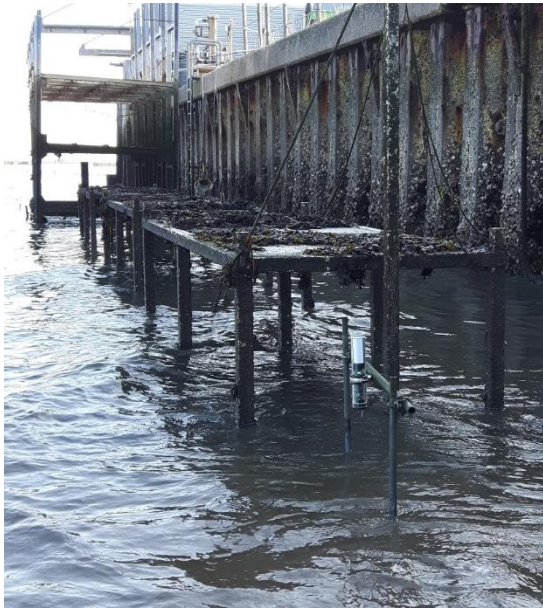


Figure 2.9: Set-up of the field measurement in the Eastern Scheldt next to NIOZ



Figure 2.10: Western Scheldt experiment set-up ASED-sensor

The Western Scheldt is a well-mixed estuary and is exposed to semidiurnal tides (Van den Berg *et al.*, 1996; Horstman *et al.*, 2011). Salinity at the mouth of the Western Scheldt (near Vlissingen ) is around 25 parts per thousand and around 10 parts per thousand at the Dutch-Belgian border, increasing during summer and decreasing during winter (Van Damme *et al.*, 2005). The salinity is assumed to be 25 parts per thousand at the experiment location in the Western Scheldt (Figure 2.5 location 2 resp.; Figure 2.10). The tidal range in the Western Scheldt increases from approximately 4.2 m at the mouth (near Vlissingen) to 5.2 m at Hansweert (data derived from Rijkswaterstaat). The bed sediment of the Western Scheldt predominantly consists of well-sorted medium to fine grained sand (Van den Berg *et al.*, 1996). The ASED-sensor is placed at the Kapellebank (51°27'35" N; 003°58'15" E; Figure 2.5 location 2 resp., Figure 2.10 and Figure 2.11). The soil type of the Kapellebank is for 88% silt and the median grain size (D50) is 16  $\mu\text{m}$ . The silty sediment of the Kapellebank can easily get in suspension. The SSC in the Western Scheldt has a high seasonal and tidal dependency (Fettweis *et al.*, 1998). In the winter the SSC is 2 times larger than in the summer. This is explained by the freshwater discharge of the river. The tide average mud concentration is 1.3 to 1.7 times higher during a spring tide than during a neap tide (Fettweis *et al.*, 1998). This encourages sediment deposition during the spring tide. If the ASED-sensor can measure the bed during these circumstances, the ASED-sensor should be applicable at all coasts, with a silty bed, as the Kapellebank.



Figure 2.11: The field experiment in the Westerschelde at the Kapellebank

## 2.3 Lab and field experiments

### 2.3.1 Lab experiments

The lab experiments are conducted from 16<sup>th</sup> of October till 30<sup>th</sup> of October 2018. As mentioned above the ASED-sensor is evaluated during lab experiments in a water tank. The dimensions of the water tank (Figure 2.12.1) are  $a = 57.4$  cm,  $b = 72$  cm,  $c = 84$  cm,  $d = 42$  cm and  $e = 56$  cm. The corners of the water tank give a strong reflection. Therefore, the ASED-sensor is not placed symmetrically in the water tank. The ASED-sensor is mounted using a steel ring whose inside is covered with rubber (Figure 2.12.3). With a bolt the ASED-sensor can be mounted on a wooden frame (Figure 2.12.3 and Figure 2.12.4).

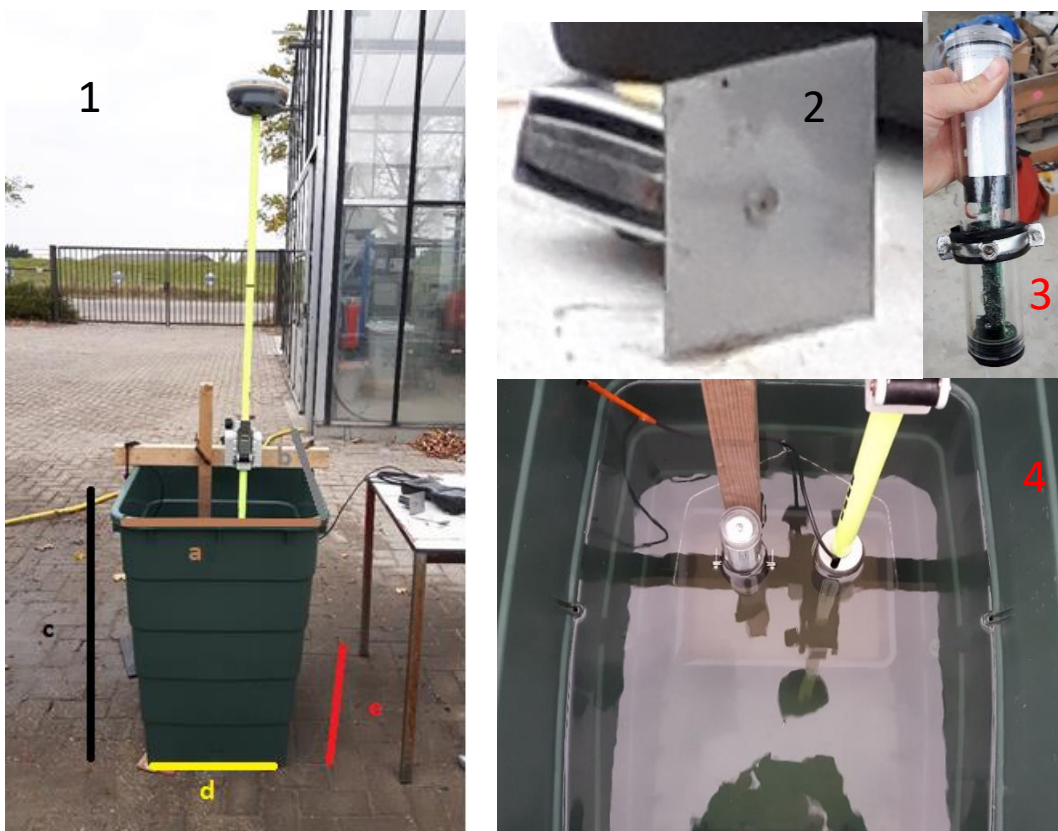


Figure 2.12: ASED-sensor in lab set-up next to the greenhouse at the NIOZ terrain. Picture 1 is the front view of the lab set-up. Picture 2 is the tape measure with a metal plate. The clip surrounding the ASED-sensor can be seen in picture 3. Picture 4 is the top view of the lab experiment. The ASED-sensor is mounted on a wooden pole. The echologger is mounted on the yellow pole with on top the Global Positioning System (GPS) receiver.

All the experiments are validated with manual measurements, by a tape measure. The tape measure has a metal plate at the end of the tape (Figure 2.12.2) and the benefit is that the metal plate did not disappear in the soft soil type. This improves the accuracy of the manual measurement up to 3 mm.

For all the experiments the ASED-sensor will use a measurement frequency of approximately 300 kHz and, 8 individual measurements form a batch. Every individual measurement elapses 1 ms ( $=250\text{ns} * 4000$ ) and the inter-measurement delay is 200 ms. The ASED-sensor has a short-term memory, which can be extended with SD-card. As the ASED-sensor measures, the measurements are first stored in the short-term memory and thereafter flushed to the SD-card. The short-term memory can only store 60 measurements, which are 7 full batches. As the measurements are sent in batches the flush from the short-term memory to the SD-card will be during the batches (60 measurements / 8 = 7.5). The ASED-sensor cannot store data during the data transfer from internal memory to external memory (SD-card). Therefore, immediately after a batch, the data is transferred from the short memory to the SD-card. This takes 1.3 seconds in time. Therefore, a measurement interval of 3 seconds between each batch is required.

#### 2.3.1.1 Water depths

First, the ASED-sensor is tested at different water depths. From this, the measurement domain can be obtained. A metal plate, which gives a strong reflection, covered half of the bottom of the water tank. The height of the ASED-sensor above the metal plate varies between 10 and 55 cm, with a distance interval of every 5 to 10 cm. The manual measurement was obtained by measuring from the metal plate to the waterline and from the waterline to the bottom of the ASED-sensor. The salinity is 31.7 parts per thousand during the experiments.

#### 2.3.1.2 Soil types

In tidal-flats different soil types occur, ranging from silt to mud to sand (Adam *et al.*, 2006). Each soil type gives a different reflection of the acoustic signal. This depends on the absorption rate and the saturation rate of the soil type (Lurton, 2010). The different soil types will be put in a bucket below the ASED-sensor in the water tank (Figure 2.12.4). The bucket can carry 13 litres and the dimensions are width 21 cm x length 31 cm x height 19.4 cm. First, the soil was mixed well before putting the soil in the bucket. The bucket was filled with 10 cm soil and is covered with bubble plastic. Some seawater is put above the bubble plastic; therefore, the soil will not get in suspension in the water tank. The bubble plastic floated as the water in the water tank increased and the bubble plastic was removed. The measurements are done at depths of 20 and 40 cm.

Six different soil types are used in this experiment. The first soil type is pure sand from the construction market. The second is silt obtained from Kapellebank (Western Scheldt) (Figure 2.5 location 2). Then, four different mixtures were made of these two soils. The idea is to add 20% silt to the sand and some salt water when needed to mix the new soil type. A 1.0 fraction of sand, 0.8 fraction of sand, 0.6 fraction of sand, 0.4 fraction of sand, 0.2 fraction of sand, and silt were expected. Because the obtained silt from the Westerschelde already had 0.12 fraction of sand in the soil, it was not possible to create these exact mixtures. Of each soil type, 3 samples were taken. The samples were freeze-dried in the laboratory, and the sediment distribution (Appendix A.2) of the soil was determined using a Malvern laser particle sizer. The eventually mixed results are 1.0,

0.80, 0.65, 0.48, 0.40 and 0.12 fraction of sand. A 0.80 fraction of sand means that the soil type contains 0.20 fraction of silt, which is defined as a grain size smaller than  $63 \mu\text{m}$ .

### 2.3.1.3 Dilutions of soil types

When rough weather occurs, heavy wind and waves will get the upper layer of the bed in suspension. The sediment is mixed in the water. Therefore, it is necessary to know whether the ASED-sensor can measure the bed under these conditions. All soil types are used except 1.0 fraction of sand because it settles fast. Therefrom, the remained dilutions of the soil types were used. The dilutions are created by adding each time 20% water, so 80% soil and 20% water, 60% soil and 40% water and 40% soil and 60% water. The results of the different dilutions are tested at water depths of 0.20, 0.30 and 0.40 m (Table 2.1). The bucket with the dilutions of soil types was put in the water tank in the same way as described in 2.3.1.2. This experiment checks whether the ASED-sensor measures the upper layer of the dilution of the soil or it measures through the soil suspension and detects the bottom of the bucket. The manual measurement is obtained by first measuring the upper layer of the soil to the upper edge of the bucket (Figure 2.13 (1)). The tape measure continued from the bucket edge was measured to the waterline (Figure 2.13 (2)) and, from the waterline to the bottom of the ASED-sensor (Figure 2.13 (3)).

Table 2.1: Dilutions (percentage water in the soil) of the soil types at measured depths of 0.20, 0.30 and 0.40 m. The values between the x and y-axis are the dilutions of the conducted experiments.

Fraction sand in soil	0.80	0.65	0.48	0.40	0.12
0.20 m	16.37, 26.11	17.07, 18.12	19.95, 20.00	20.26, 21.75	
0.30 m	16.37, 26.11	17.07, 18.12	19.95, 20.00	20.26, 21.75	
0.40 m	26.93, 45.47	30.94, 43.86, 68.98, 90.37	41.27, 52.45	44.47, 52.42, 65.19	57.50, 63.13, 72.45

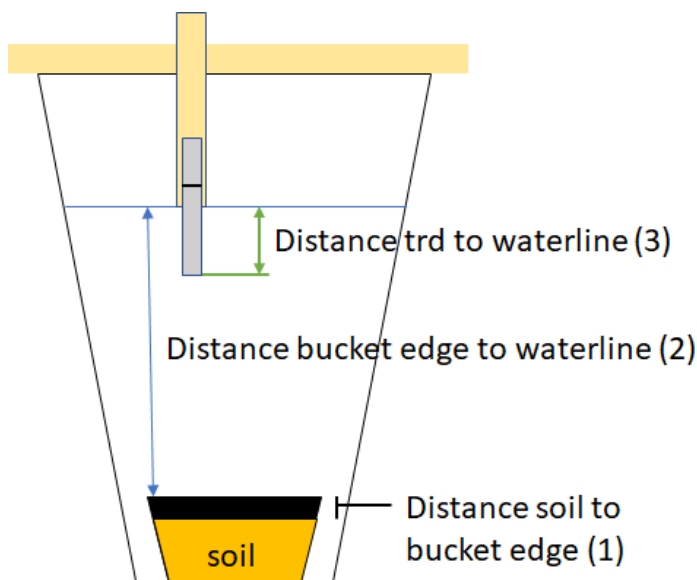


Figure 2.13: Manual measurement from the soil to the transducer



Figure 2.14: Mixer powered by an electrical drilling machine

### 2.3.1.4 Waves and current forcing

The purpose of this experiment is to determine whether the ASED-sensor can measure the bed in the presence of waves. Therefore, the ASED-sensor is positioned 0.183 m above the bed of the wave flume, and increasingly larger waves were generated in the flume. The measurement started with no waves to check whether the ASED-sensor could measure

the bed of the wave flume (Figure 2.8). Thereafter the waves started to increase every ten minutes by 1000 Rotations Per Minute (RPM). The RPM corresponds to a wave height (Table 2.2). The obtained experiments during waves are described in Table 2.2.

Table 2.2: RPM versus wave height in the wave flume

RPM	wave height in cm	extra information
1000	2	
1100	3	
1200	5	
1300	7	
1400	6.5	constant wave
1500	9	
1600	9.5	strong wave

Table 2.3: Flume settings for the current of the wave flume

flume setting in cm/s	velocity in cm/s
200	17
250	23
300	29
400	38
500	44
600	55
700	66

During the current forcing experiment, the height of the ASED-sensor above the bottom of the wave flume was 0.227 m. The current started at flume setting 250 cm/s which corresponds to a velocity of 23 cm/s. The ASED-sensor measured the reflection of the signal by the bed in time (depth) the entire night. In the morning the current is set back to flume setting 200 cm/s. Every minute the flume setting increased by 100 cm/s until flume setting 700 cm/s. It takes 5 seconds to increase the current velocity. The flume settings can be translated into velocities in cm/s (Table 2.3). The flume was calibrated (Appendix A.3) before the experiment started.

### 2.3.2 Field experiments

The ASED-sensor is also tested in the field. Therefore, the ASED-sensor was first placed next to NIOZ (Yerseke) in the Eastern Scheldt during the weekend of 20 October 2018. The Eastern Scheldt has a sandy bed and therefore a strong reflection of the signal by the bed is expected. The Western Scheldt has very fine silt. The Western Scheldt data is collected in three weeks from the 1<sup>st</sup> of November till 23<sup>rd</sup> of November 2018. The idea was to measure for two weeks, to measure during a full tidal cycle (spring and neap tides). The ASED-sensor is mounted on a frame (Figure 2.9 and Figure 2.10). The long vertical pipes give the frame stability during wavy conditions. Another benefit of this frame is that scouring does not occur as it did with the predecessor the SED-sensor (Hu *et al.*, 2015). Only point measurements at one location have been done, so only temporal variation can be observed. Each batch contains 8 measurements. The pressure sensor is enabled and set to a measurement interval of 5 Hz. Hereby, the waves are registered during the measurements in a submerged condition. For the determination of the inundation time, data from Rijkswaterstaat is used.

#### 2.3.2.1 Eastern Scheldt

The Eastern Scheldt is a tidal bay and sediment deposition occurs during rising tides. As flooding is the main mechanism for sediment delivery, the tidal flat is inevitably linked to sea level and tidal oscillations (Fagherazzi *et al.*, 2012). Therefore, a lot of bed level dynamics occur, and it is interesting to observe this with the ASED-sensor. The length of the vertical pipes of the frame which enter the ground are 1.5 m long. This length is enough for a sandy bed. The ASED-sensor measured with a measurement interval of every 5 minutes and was set at a height of 39.0 cm above the bed (Figure 2.9).

### 2.3.2.2 Western Scheldt

The Western Scheldt is a tidal bay as well, but here the bed is very silty. Therefore, the length of the vertical pipes of the frame which enter the ground are now 2 m long. This length is necessary for stability in the silty bed. The ASED-sensor had a measurement interval of every minute. The measurement interval was chosen to check whether waves affect the deformation of the bed. The manual measurement was at the start of the experiment at a depth of 0.258 m and after three weeks 0.270 m. The bed eroded in the three weeks. Three erosion pins (Stokes *et al.*, 2010; Gedan *et al.*, 2011) are located 2 metres from the frame (Figure 2.15). Erosion pins are used to record the local surface level. The erosion pin is a very thin metal rod (i.e., to prevent scouring) with a height marker on top and a ring around the pin. The pin was pushed into the sediment, with the marker at a fixed height above the sediment. A metal ring was placed around the pin on top of the soil surface. The distance from the marker to the soil surface and the ring buried into the sediment were measured (Willemsen *et al.*, 2018). The erosion pin showed an erosion of 0.009 m.



Figure 2.15: Three erosion pins (two erosion pins in the left red box) in the Western Scheldt experiment

## 2.4 Converting raw data to bed levels

Yet no analysing method existed at the start of this study. In the raw data of the ASED-sensor, a bed needs to be determined. As mentioned in paragraph 2.1, it is assumed when the amplitude suddenly increases, this denotes the reflection of the signal by the bed (Figure 2.16). Therefore, a method is required to find this sudden increase in amplitude. In general, the beginning of the signal has a lot of noise (Figure 2.16). As the ASED-sensor will be used in shallow water, multiple reflections of the bed level can occur. These reflections are reflected by the transition from water to air and by the bed. Figure 2.16 shows three reflections of the bed. In general, the first reflection has a higher intensity peak compared to the remained reflections and therefore the bed will be detected at the first strong reflection. The first strong reflection occurs around time step 600 ( $0.25 \mu\text{s}$ ), so the distance between the ASED-sensor and the bed is approximately

$\frac{1500m/s * ((613+600) * 0.25 \mu s)}{2} = 0.227 m$ . The other strong reflections occur around time step 1800 ( $\approx 600+613+600$ ) ( $0.25 \mu s$ ) and 3000 ( $\approx 1800+613+600$ ) ( $0.25 \mu s$ ).

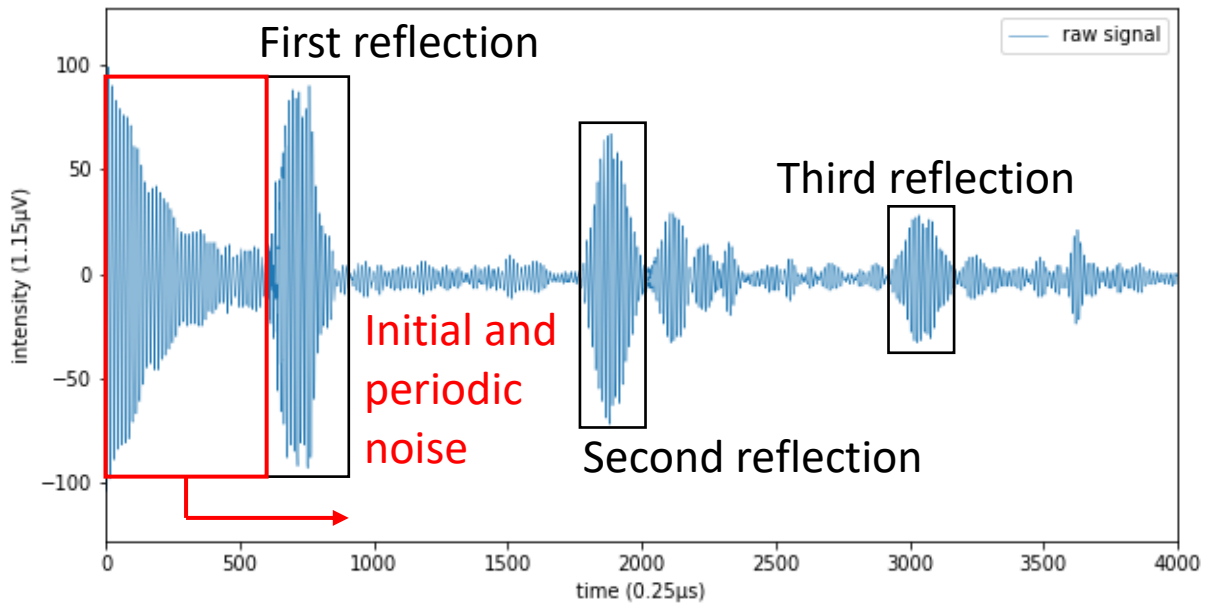


Figure 2.16: Raw data of the ASED-sensor above a metal plate

Multiple methods are tested to detect the first peak in the raw data so that it can be converted into bed levels. The chosen method must be applicable under various environmental conditions.

#### 2.4.1 Fast Fourier Transform

As the ASED-sensor sends one signal into the water, multiple frequencies return. This can be due to multiple reflections, noise, etc. The Fast Fourier Transform (FFT) analysis is done to convert a signal into its corresponding frequency components, therefore the signal can be better analysed (Appendix A.5.1; Figure A.6.4). The frequency with the highest amplitude is the frequency which occurs the most in the data (Figure A.6.4). As the data is not infinite and no periodicity occurs, spectral leakage will appear. Spectral leakage can be minimized using windowing. The Hanning window will be used for the FFT analysis (Appendix A.5.1.1). This analysis is done with the real numbers of the FFT analysis. Before the FFT analysis can be done all negative values need to be removed; therefore, the absolute is taken of the raw data. The wavelength can be calculated using the frequency with the highest amplitude. The FFT analysis also provides an imaginary number and the phase of the returned signal can be determined. A depth value can be calculated by the combination of the wavelength and the phase of the returned signal (Figure 2.17; Table 2.4).

#### 2.4.2 Envelope method

The sudden increase in amplitude can be found using the lower and upper envelope. The lower envelope are the minimum values of a line and the upper envelope are the maximum values of a line. The lower envelope is subtracted from the upper envelope, called delta envelope (Appendix A.5.2 Figure A.6.6).

1. Determine the sample with the maximum peak value;
2. Step back 300 (parameter) time steps;
3. From there determine the minimal value, going forward (i.e. towards the peak).

This will be the point used as the beginning of the reflection. To find this point, a few parameters can be set. The parameters which can be set are filtering initial and periodic noise (Figure 2.16, Figure 3.2 and Figure 3.3), strong reflections after the first reflection of the signal by the bed or a strong second part of the reflection (Figure 3.8), the point from which to start looking for the minimum. The bed detection range is  $400 \leq \text{time step} \leq 2000$ . This corresponds to the assumed practical measurement domain of 0.20 m to 0.45 m. Mostly, the sudden increase in amplitude and the maximum intensity peak take a time of less than 300-time steps. Therefore, the sudden increase in amplitude will be found starting from 300-time steps backwards in time to the maximum intensity peak. As the start of the sudden increase in amplitude is mostly the minimum value before the maximum intensity peak. To find this start of the sudden increase in amplitude a n-value will be introduced. The n-value is a horizontal line to find the minimum value before the maximum intensity peak of the delta envelope line. The n-value starts from value 1.0 and increases 0.1 as the minimum value is not found. The intersection between the delta envelope line and the n-value line is until n-value 20. Mostly, a lot of noise occurs at a n-value higher than 20, observed from the lab experiments. As the n-value intersects the delta envelope line that time step will be the bed detected depth in time. The bed detected depth in time needs to be converted into depth by  $\frac{(\text{time step}+613)*250 \text{ ns}*\text{speed of sound m/s}}{2} = \text{bed detected depth in metres}$ . A median filter is applied for the bed detected depths of each batch, because it effectively removes impulsive outliers from the signal. As the bed is undetectable with the parameter settings, the values are not saved. These parameters are set as default settings (Figure 2.17). All parameters can be manually adjusted.

### 2.4.3 Kalman filter

The final analysed method evaluated was the Kalman filter. The Kalman filter is one of the most widely used methods for tracking and estimation due to its simplicity, optimality, tractability and robustness (Julier *et al.*, 1997). The Kalman filter, rooted in the state-space formulation of linear dynamical systems, provides a recursive solution to the linear optimal filtering problem (Haykin, 2002). It applies to stationary as well as nonstationary environments. The solution is recursive in that each updated estimate of the state is computed from the previous estimate and the new input data, so only the previous estimate requires storage (Haykin, 2002).

The raw data (Figure 2.16) is made positive by taking the absolute of the raw data (Appendix A.5.3.1). Most of the noise is removed by applying the Kalman filter. All parameters described in paragraph 2.4.2 are used in the Kalman filter method as well. Mostly, the maximum intensity peak of the Kalman filter line is above an intensity value of 10 ( $1.15 \mu V$ ), observed from the lab experiments. This is an extra parameter addition to the envelope method. The Kalman filter, the window of the bed detection and parameters; the amount of time steps to find the minimum value from the maximum value and the n-value, are set as default settings (Figure 2.17). All parameters can be manually adjusted.

## 2.4.4 All methods

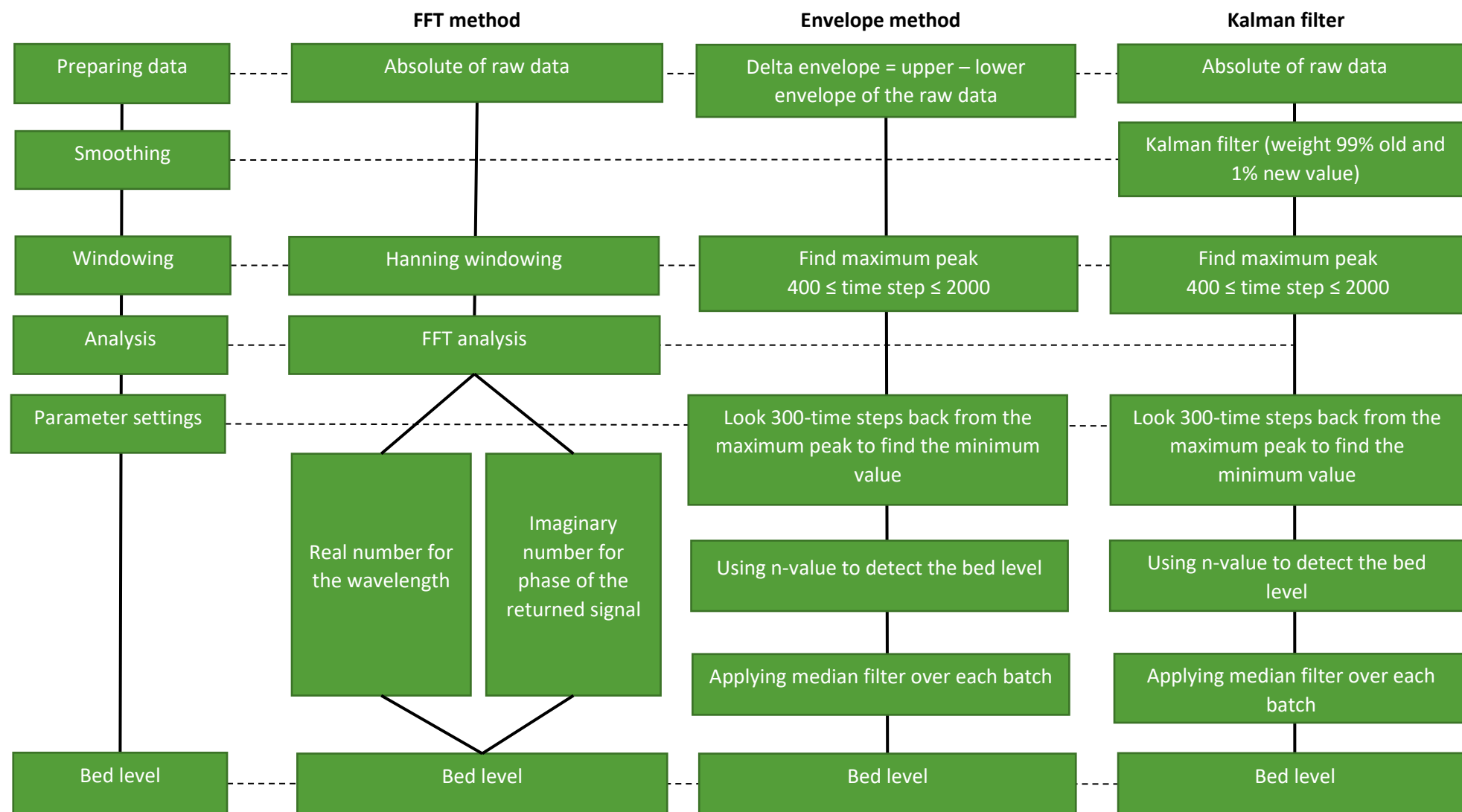


Figure 2.17: Flow chart of the converting methods

To test the three methods, the experiment was done above a metal plate at a fixed depth. The manually measured depth is 0.284 m. The experiment has 2583 measurements. A burst of 8 measurements is analysed.

First, the FFT method will be analysed. The difference between the first and the second measurement is 0.018 m (Table 2.4). This is due to the frequency fluctuations. The standard deviation of the FFT method is 0.008 m, for the envelope method 0.010 m and for the Kalman filter method 0.002 m (Table 2.4). The idea is that once a month the data is collected from the ASED-sensor. Therefore, another downside is the 5 minutes computation time of the envelopes of only 2583 measurements. The bed detection of the FFT yields 0.028 m deeper than the manual depth.

The converting methods are applied by using scripts written in Python version 3.6.

The envelope method and the Kalman filter method start increasing at the sudden increase in amplitude (Figure 2.18).

As the ASED-sensor is placed above soil type 0.48 fraction of sand at a manually measured depth of 0.210 m. The delta envelope bed detection starts before the sudden increase in amplitude and therefore this method detects the bed at too shallow depths (Figure 2.19). The Kalman filter bed detection starts when a sudden increase in amplitude appears (Figure 2.19).

The Kalman filter method will be used for analysing the bed detected depths and thus measuring sedimentation and erosion (Table 2.5).

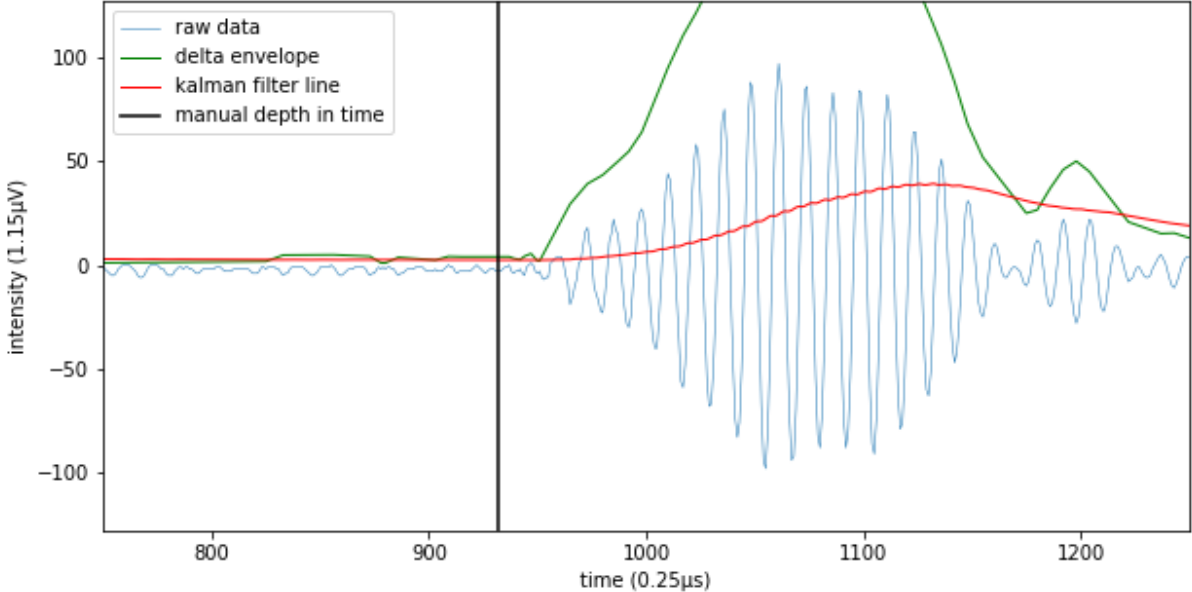


Figure 2.18: Comparison of the delta envelope and Kalman filter method. The ASED-sensor measures above a metal plate at a manually measured depth of 0.284 m = 932 (0.25 µs).

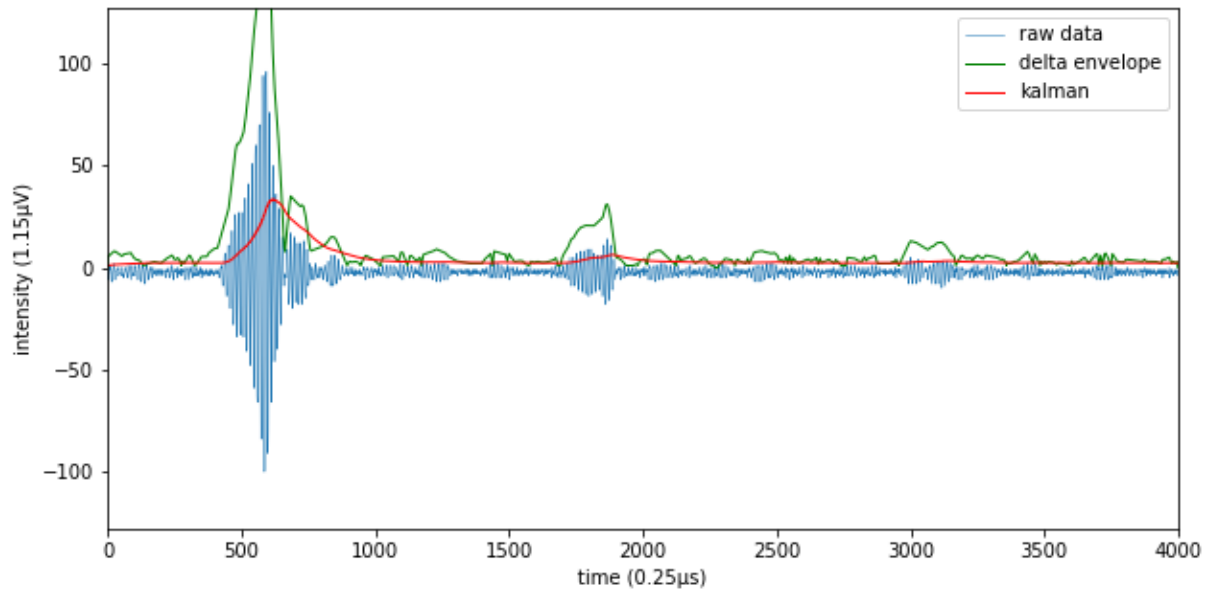


Figure 2.19: Comparison of the delta envelope and Kalman filter method. The soil type of the bed is 0.48 fraction of sand.

Table 2.4: All methods used to convert the raw data into bed levels. The first 8 single measurements (one batch) are observed. This measurement was applied above a metal plate at a depth of 0.284 m.

Single signal		1	2	3	4	5	6	7	8	Average [m]	Median [m]	Stdev [m]
<b>FFT</b>	freq [Hz]	325163	314157	325163	314157	314157	325163	325163	325163	321036	325162.581	5328.016
<b>FFT</b>	depth [m]	0.313	0.295	0.313	0.296	0.295	0.312	0.312	0.312	0.306	0.312	0.008
<b>Envelope</b>	depth [m]	0.288	0.255	0.284	0.287	0.286	0.286	0.278	0.286	0.281	0.286	0.010
<b>Kalman</b>	depth [m]	0.288	0.281	0.288	0.288	0.286	0.284	0.286	0.288	0.286	0.287	0.002

Table 2.5: The advantages and disadvantages of the converting methods for the raw data into bed levels.

	<b>Fast Fourier Transform</b>	<b>Envelope method</b>	<b>Kalman filter</b>
<b>Computation time</b>	2 minutes	5 minutes	40 seconds
<b>Bed detected depth fluctuates</b>	Frequency fluctuates and therefore bed detected depth fluctuates	High bed detected depth fluctuations	Bed detected depth fluctuates
<b>Bed detected depth standard deviation</b>	0.008 m	0.010 m	0.002 m
<b>Manual depth versus bed detected depth</b>	The bed detected depth is 0.028 m deeper the manual measurement	The bed detected depth is 0.002 m deeper the manual measurement	The bed detected depth is 0.003 m deeper the manual measurement
<b>Raw data reflection of the signal by the bed versus the bed detected depth</b>	The bed is detected too deep compared to the reflection of the signal by the bed	The bed is detected too shallow compared to the reflection of the signal by the bed	The bed is detected exactly where the sudden increase in amplitude occurs in the reflection of the signal by the bed

### 3 Results

Firstly, the raw signal of the ASED-sensor will be explained during the submerged and non-submerged conditions. Secondly, the raw signal of the ASED-sensor during the lab and field experiment will be clarified. Thirdly, the converted raw data to bed level data will be analysed. Finally, the obtained theoretical and actual accuracy of the ASED-sensor is described.

#### 3.1 Measuring with the ASED-sensor

##### 3.1.1 Being submerged or not

Due to tides, the ASED-sensor is half of the time submerged during the field experiments. The difference between the non-submerged and submerged conditions can be clearly recognized in the raw data of the ASED-sensor (Figure 3.1). During non-submerged conditions, the initial part of the signal (approximately from  $t = 0$  until  $t = 700$ ) has a lot of noise and no bed is detected (blue line; Figure 3.1). A little initial noise occurs during submerged conditions (orange line; Figure 3.1). The submerged signal has a bed reflection with an intensity of around 100 ( $1.15 \mu V$ ) time step 1600 ( $0.25 \mu s$ ; orange line; Figure 3.1).

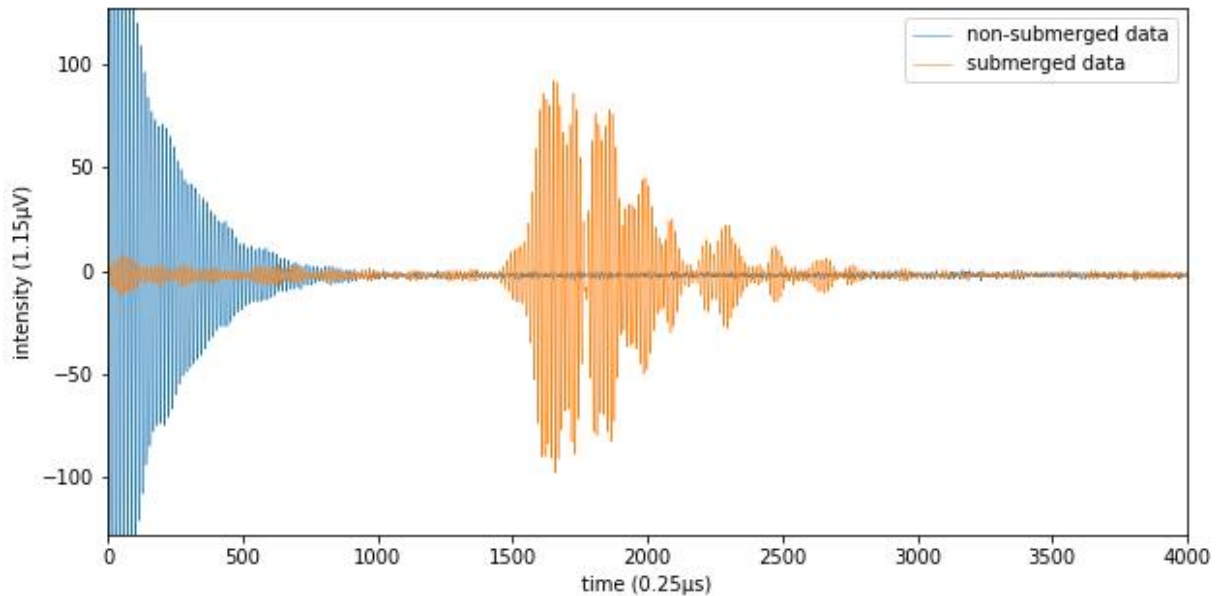


Figure 3.1: Non-submerged and submerged reflection of the raw signal of the ASED-sensor during the field experiment, Eastern Scheldt.

##### 3.1.2 The speed of sound in water

The obtained time needs to be converted to depth values by multiplying by the speed of sound ( $c$ ) to calculate the depth ( $d$ ), see Equation 1.

$$\frac{c \left[ \frac{m}{s} \right] * t[s]}{2} = d [m] \quad (1)$$

Four speed of sound formulas, namely Del Grosso (Appendix A.6.1), Coppens (Appendix A.6.2), Mackenzie (Appendix A.6.3), and UNESCO – Chen and Millero (Appendix A.6.4) are compared with each other. By the calculation of the speed of sounds different salinities, depths or pressures and temperatures were used (Appendix A.6.5). The speed of sound in water will be calculated using the formula of UNESCO – Chen and Millero.

## 3.2 Collecting raw data

### 3.2.1 Lab experiments

The ASED-sensor can detect the reflection of the signal by the metal plate as bed at a manually measured depth of 0.284 m (Figure 3.2). The ASED-sensor measured 295 bursts for 14.8 minutes during this experiment. The signal of the ASED-sensor does change over time, although the bed is fixed during the lab experiments. The first signal is the raw data collected by the first measurement of the experiment and the last signal is the raw data collected by the last measurement of the experiment. The first signal has less initial noise (approximately  $t = 0$  until  $t = 700$ ) than the last signal (Figure 3.2).

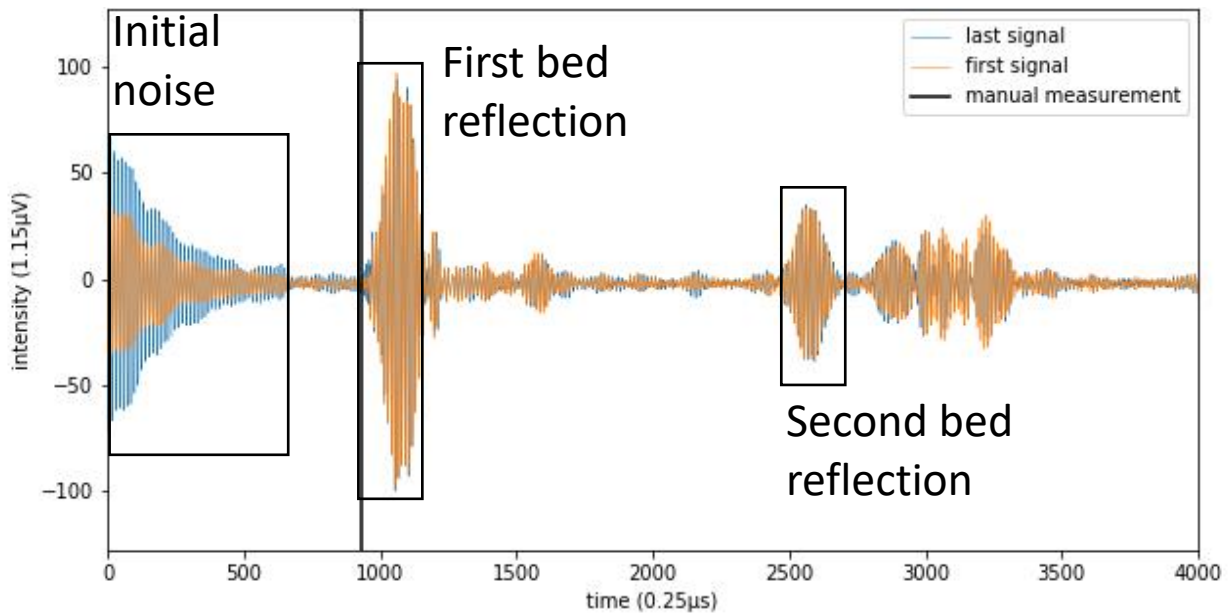


Figure 3.2: The first and last signal of the raw data of the ASED-sensor. The ASED-sensor is placed above a metal plate at a manually measured water depth of 0.284 m = 931 (0.25  $\mu$ s).

This time the experiment lasts for 20 minutes and the manually measured depth is 0.340 m. Both signals have a lot of initial and periodic noise (Figure 3.3). The reflection of the signal by the bed has a higher intensity for the first signal and a lower intensity for the last signal (Figure 3.3).

A combination of increasing initial noise and decreasing bed reflection intensity occurred over time. These circumstances can occur during all the experiments and therefore can possibly influence the conversion of the raw data into bed levels. The reflection of the signal by the bed occurs mostly deeper than or around the manual measurement. At depths before the manual measurement and the reflection of the signal by the bed mostly noise occurs (Figure 3.1, Figure 3.2 and Figure 3.3).

The 4 mm lime/sealer is added to the manually measured depths.

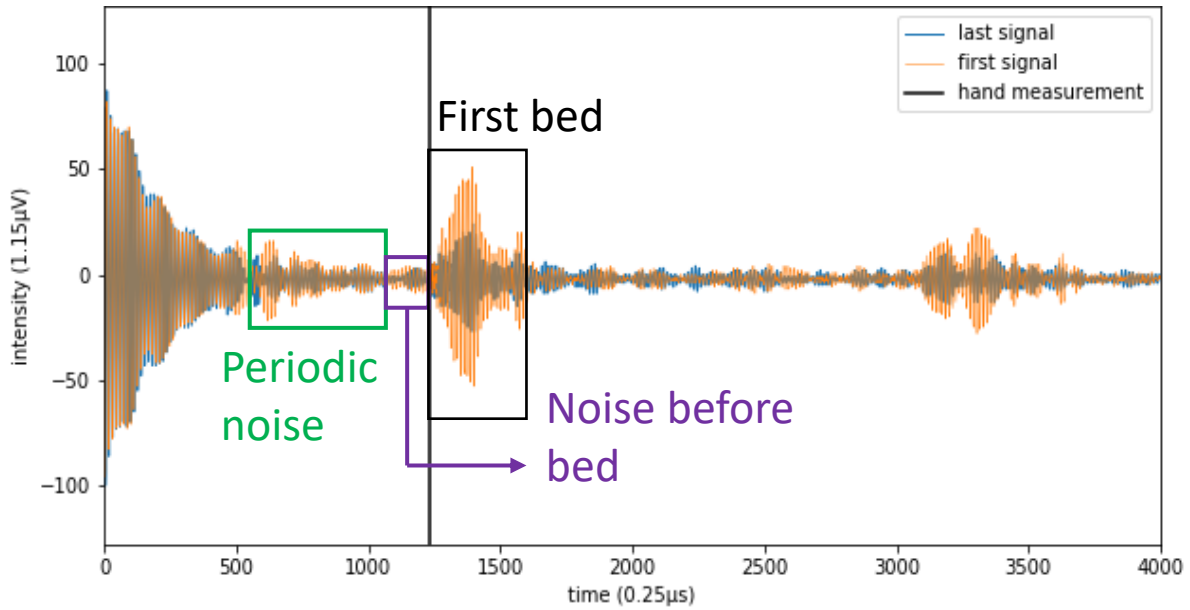


Figure 3.3: The first and last signal of the raw data of the ASED-sensor. The ASED-sensor is placed above a metal plate at a manually measured water depth of 0.340 m = 1230 (0.25  $\mu$ s).

### 3.2.1.1 Water depths

The ASED-sensor is tested at different depths measured above a metal plate at a manual depth of 0.115 m, 0.210 m, 0.284 m, 0.340 m, 0.395 m, 0.440 m, 0.497 m and 0.572 m (Table A.6.8).

The speed of sound is 1475.3 m/s during the manual depth of 0.115 m (Figure 3.4). The bed should be visible at time step  $\frac{0.115 \text{ m}}{1475.3 \frac{\text{m}}{\text{s}} * 250 \text{ ns}} * 2 - 613 = 11$ . Initial noise occurs at that time (Figure 3.4) and therefore the ASED-sensor is unable to detect the reflection of the signal by the bed. The second and the third reflection are easily detected at time step 700 and time step 1250 (Figure 3.4).

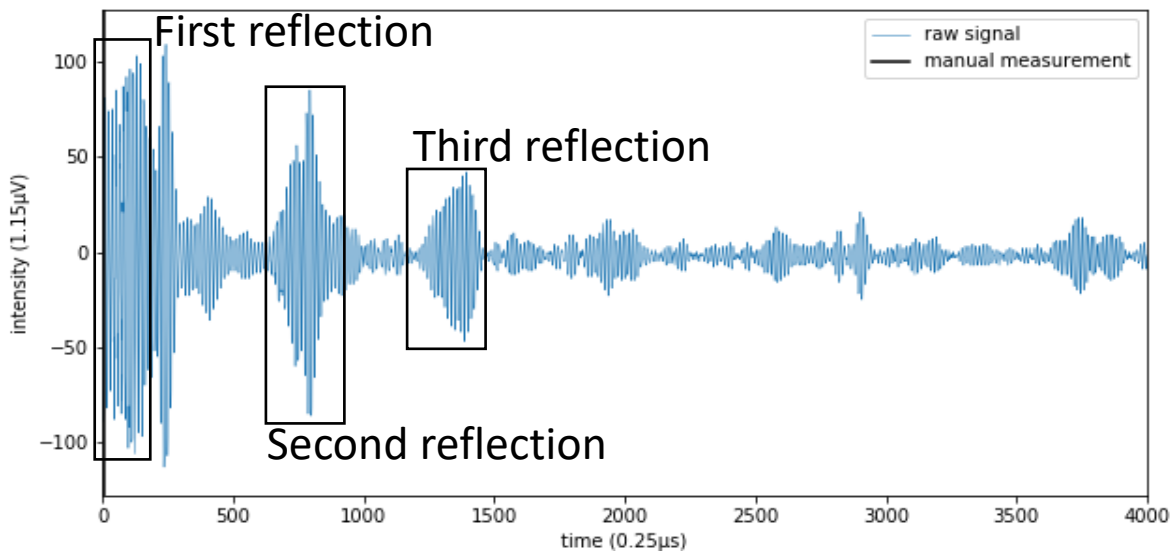


Figure 3.4: The ASED-sensor is placed above a metal plate at a manually measured water depth of 0.115 m = 11 (0.25  $\mu$ s).

The raw signal of the ASED-sensor at a water depth of 0.210 m and 0.284 m (depths  $\leq 0.30$  m) changes over time like in Figure 3.2. The raw signal of the ASED-sensor at a

water depth of 0.340 m, 0.395 m, 0.440 m, 0.497 m and 0.572 m (depths > 0.30 m) changes over time like in Figure 3.3. The shallow depths  $\leq 0.30$  m (Figure 3.2) have a narrower reflection of the signal by the bed and the intensity of the signal reflected by the bed is 100 ( $1.15 \mu\text{V}$ ). The deeper depths > 0.30 m (Figure 3.3) have a wider reflection of the signal by the bed, have an intensity of the signal reflection by the bed of around 50 ( $1.15 \mu\text{V}$ ) and the last signal has a lower intensity peak compared to the first signal (Figure 3.3). The second reflection cannot be observed for water depths from 0.440 m, because the second reflection occurs after the registration time frame (after time 4000 ( $0.25 \mu\text{s}$ ); Table A.6.8). The intensity of the reflection of the signal by the bed is low at a manually measured depth of 0.497 m and 0.572 m (Table A.6.8). Therefore, the bed cannot be detected.

### 3.2.1.2 Soil types

The bed reflection of 1.0 fraction of sand has a lot of initial noise at a manually measured depth of 0.186 m. The reflection of the signal by the bed cannot be detected (Table A.6.9). Soil type 0.8 fraction of sand has no initial and periodic noise and the reflection of the signal by the bed is easily detected (Figure 3.5; Table A.6.9). The second reflection by the bed is visible around time step 1800 ( $0.25 \mu\text{s}$ ) (Figure 3.5). The reflection of the last signal by the bed is shifted to the right (deeper) compared to the first signal for 0.40 fraction of sand (0.179 m). At a depth around 0.20 m 0.65, 0.48 and 0.12 fraction of sand have a clear bed detection and no to a little initial noise (Table A.6.9).

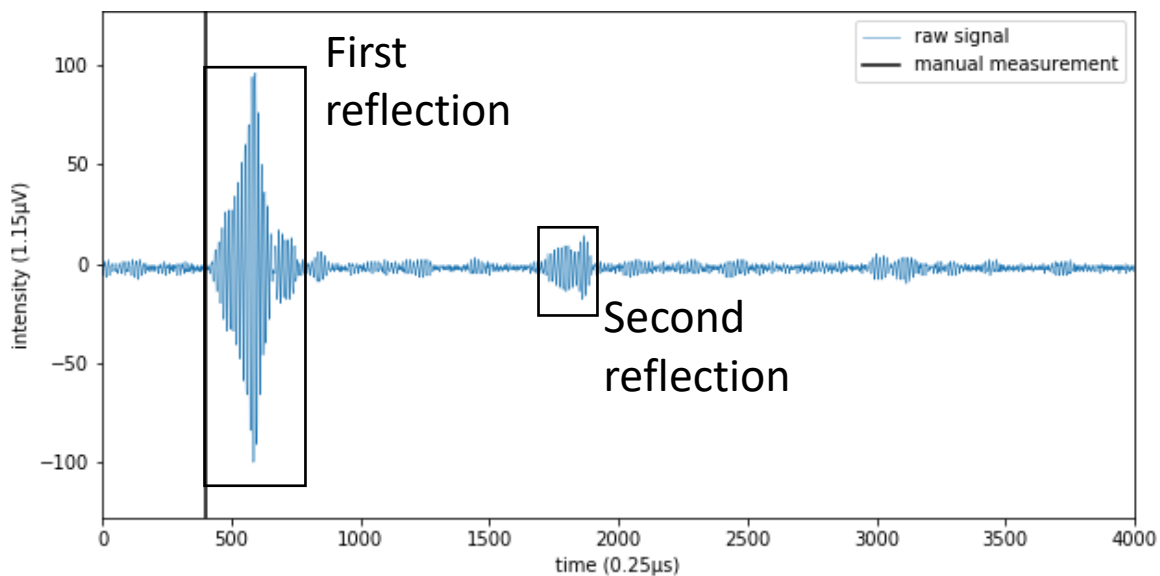


Figure 3.5: Soil type 0.8 fraction of sand at a manually measured depth of 0.188 m = 404 ( $0.25 \mu\text{s}$ ).

All soil types can detect the signal reflected by the bed at a manual measurement of around 0.40 m (Table A.6.9). Soil types 1.0, 0.65 and 0.48 fraction of sand of noise before the reflection of the signal by the bed and therefore are detected shallower than the manual depth.

The shape of the signal reflected by the bed changes for varying depths and having the same soil type. The shape of the signal reflected by the bed changes as well for the varying soil types at a constant depth. There is no consistency in the shape of the signal reflected by the bed for the soil types and the water depths. The deeper depths of around 0.40 m have a wider signal reflection by the bed compared to the shallower depths of around 0.20 m.

### 3.2.1.3 Dilutions

The ASED-sensor is tested for five different dilutions of soil types at a manually measured depth around 0.20, 0.30 and 0.40 m (Table 3.1). Unfortunately, some soil types were no longer in stock and these measurements could not take place.

Table 3.1: Manually measured water depths in metres of the soil type dilutions during the ASED-sensor measurement

Fraction sand in the soil	0.80	0.65	0.48	0.40	0.12
% of water in the soil	<b>16.37</b>	<b>17.07</b>	<b>19.95</b>	<b>21.75</b>	
	0.219	0.244	0.192	0.197	
	0.303	0.331	0.309	0.299	
% of water in the soil	<b>26.11</b>	<b>18.12</b>	<b>20.00</b>	<b>20.26</b>	
	0.212	0.197	0.179	0.205	
	0.307	0.305	0.295	0.287	
% of water in the soil	<b>26.93</b>	<b>30.94</b>	<b>41.27</b>	<b>44.47</b>	<b>57.50</b>
	0.393	0.365	0.368	0.385	0.366
% of water in the soil	<b>45.47</b>	<b>43.86</b>	<b>52.45</b>	<b>52.42</b>	<b>63.13</b>
	0.384	0.36	0.361	0.374	0.358
% of water in the soil		<b>68.98</b>		<b>65.19</b>	<b>72.45</b>
		0.389		0.380	0.357
% of water in the soil		<b>90.37</b>			
		0.427			

All dilutions of soil type 0.8 fraction of sand can detect a reflection of the signal by the bed, except dilution 26.11% (0.307 m; Table A.6.10). The reflection of the last signal has a lot of initial noise and is shifted to the right (deeper) for dilution 26.11% (0.307 m). The second reflection of the bed is well visible for dilutions 16.37% (0.219 m and 0.303 m) and 45.47% (0.384 m). The intensity of the second reflection for dilution 16.37% (0.303 m) is higher than the first reflection of the signal by the bed. But the intensity of the second reflection is for the last signal weaker than for the first signal.

Dilutions 17.07% (0.244 m and 0.331 m), 18.12% (0.197 m and 0.305 m) and 30.94% (0.365 m) of soil type 0.65 fraction of sand can be detected by the reflection of the signal by the bed (Table A.6.11). Dilution 43.86% has a lot of noise before the reflection of the signal by the bed and therefore the reflection of the signal by the bed cannot be detected. The first signal has a stronger intensity reflection of the signal by the bed for dilutions 43.86%, 68.98% and 90.37% (Figure 3.6). The reflection of the signal by the bed of the last signal is shifted to the right compared to the first signal for dilution 68.98%. The reflection of the signal by the bed is detected later than the manual depth for dilution 90.37% (Figure 3.6).

Dilutions 19.95% (0.192 m), 20.00% (0.179 m and 0.295 m) and 41.27% (0.368 m) of soil type 0.48 fraction of sand can detect a reflection of the signal by the bed (Table A.6.12). The periodic noise is weaker than the reflection of the signal by the bed for the first signal. But the periodic noise has a stronger intensity than the reflection of the signal by the bed for dilution 19.95% (0.309 m (Figure 3.7)). Therefore, the highest intensity peak will be detected earlier. The dilution of 52.45% has high intensities of periodic noise and therefore the reflection of the signal by the bed of is not easily detected.

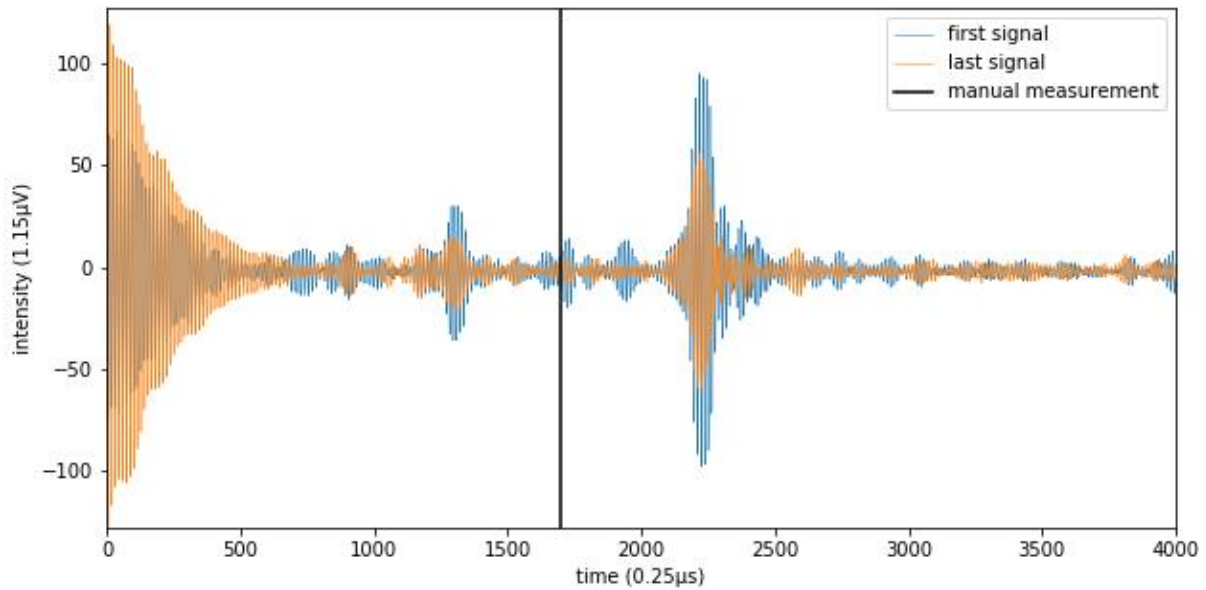


Figure 3.6: Soil type 0.65 fraction of sand with 90.37% water in the soil at a manually measured depth of 0.427 m = 1696 (0.25  $\mu$ s).

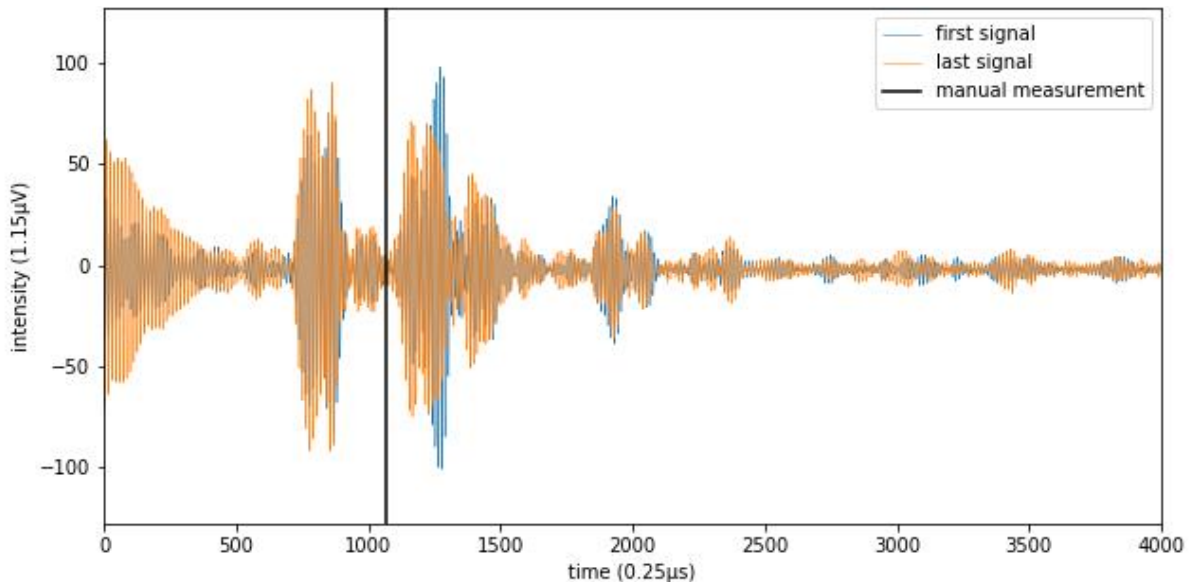


Figure 3.7: Soil type 0.48 fraction of sand with 19.95% water in the soil at a manually measured depth of 0.309 m = 1068 (0.25  $\mu$ s).

Dilutions 20.26% (0.205 m), 21.75% (0.197 m and 0.299 m) of soil type 0.4 fraction of sand can detect a reflection of the signal by the bed (Table A.6.13). The reflection of the signal by the bed is weak for dilution 20.26% (0.287 m) and 44.47% (0.385 m), therefore the reflection of the signal by the bed is not easily detected (Table A.6.13). Dilution 44.47%, 52.45% and 65.19% have high intensities of periodic noise and therefore it is not clearly visual which reflection of the signal is the bed reflection.

Dilutions 57.5% (0.370 m), 63.13% (0.358 m) and 72.45% (0.357 m) of soil type 0.12 fraction of sand have initial and periodic noise and the reflection of the signal by the bed cannot be detected (Table A.6.14).

There is no consistency in the shape of the signal reflected by the bed for the dilutions and the water depths.

#### 3.2.1.4 Waves and current forcing

First, the ASED-sensor measured in waves forcing conditions. No initial and periodic noise occur before the reflection of the signal by the bed. The reflection of the signal by the bed is easily detected during waves. The length of the wave forcing experiment lasted for 62 minutes.

Thereafter, the ASED-sensor measured in current forcing conditions. The length of the current forcing experiment lasted for 880 minutes = 14.7 hours. The raw data of the ASED-sensor has initial noise and low intensities of periodic noise. The reflection of the signal by the bed is easily detected. The intensity of the reflection of the signal by the bed is higher for the last signal than for the first signal. The shape of the signal reflected by the bed did not change significantly over time for the experiments during waves and current forcing.

The practical measurement domain is from 0.20 m to 0.45 m, according to the raw data analysis of all lab experiments.

### 3.2.2 Field experiments

From 19<sup>th</sup> of October until 22<sup>nd</sup> of October 2018 the ASED-sensor was placed in the Eastern Scheldt (Figure 2.5). During that period, the ASED-sensor is five times inundated by the tide.

Next, the ASED-sensor measured for 19 out of 23 days in the Western Scheldt (Figure 2.5). Because the battery dropped below 8 V. The ASED-sensor was inundated 37 times during this period.

#### 3.2.2.1 Eastern Scheldt

The raw data of all 5 inundations have been analysed. Starting with the first inundation, a little initial noise occurs (Figure 3.8). At the start of the first inundation, the shape of the reflection of the signal by the bed is different than for the middle and end of that first inundation. The reflection of the signal by the bed is split into 2 parts (Figure 3.8). The maximum intensity peak is higher in the second part of the first bed reflection for the start of the first inundation, this might influence the conversion of the raw data into bed levels. The middle and end of the first inundation have a higher maximum intensity peak in the first part of the first bed reflection (Figure 3.8). Therefore, the reflection of the signal by the bed can be detected at a deeper depth for the start of the first inundation than for the middle or end of the first inundation. At the end of the first inundation periodic noise occurs (Figure 3.8). The end of the first inundation has a higher intensity peak of the reflection of the signal by the bed than the start of the first inundation (Figure 3.8). The start of the reflection of the signal by the bed is clearly visual for the first inundation (Figure 3.8).

The beginning of the reflection of the signal by the bed starts later for the second inundation compared to the first inundation, this could imply erosion. The shape of the reflection of the signal by the bed is like the middle and end of the first inundation. The intensity of the reflection of the signal by the bed is constant during the second inundation. The reflection of the signal by the bed is the same for the second, third and start of fourth inundation. But the shape of the signal changes from the third to the fourth inundation. The fourth inundation has several peak intensities like the start of the first inundation (Figure 3.8). The middle and end of the fourth inundation have noise before the reflection of the signal by the bed. Therefore, the bed will probably be detected shallower than the bed at the start of the fourth inundation. The shape of the reflection of the signal by the

bed is the same for the fourth and fifth inundation. The fifth inundation does not have noise before the reflection of the signal by the bed. The maximum intensity peak of the raw signal moves to the right (deeper) during the last two inundations.

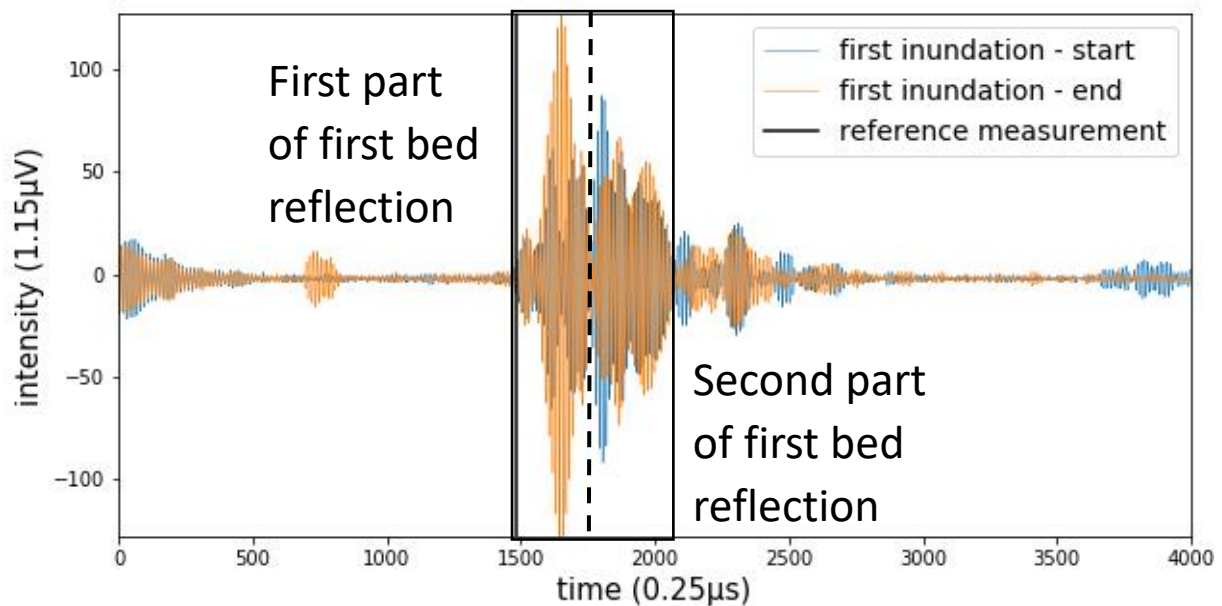


Figure 3.8: The start and end signal of the first inundation raw signal of the ASED-sensor in the Eastern Scheldt at a manually measured depth of  $0.394 \text{ m} = 1521 \text{ (} 0.25 \mu\text{s)}$ .

### 3.2.2.2 Western Scheldt

Initial noise occurs for the first inundation (Figure 3.9). The start of the reflection of the signal by the bed is easily detected. The reflection of the signal by the bed changes in a three-week time scale. At the end, the reflection of the bed is still easily detected, but a second part of the signal reflected by the bed has a higher intensity for the start-middle of the first inundation (orange line; Figure 3.9), which happened as well during the Eastern Scheldt experiment (blue line; Figure 3.8). When the ASED-sensor is recently submerged, mostly the reflection of the bed has a high intensity (Figure 3.10) compared to the signal when it has been submerged for a while (Figure 3.9). As the ASED-sensor gets from a submerged to a non-submerged condition the last signal of the reflection of the bed is the same as when recently being submerged (Figure 3.10). A lot of noise occurs and the intensities of the entire signal increase during that moment. Therefore, it is better to leave the first and last signals out for the conversion of the raw data into bed levels. During the experiment, the reflection of the signal by the bed moves to the right (deeper). Therefore, erosion will be expected.

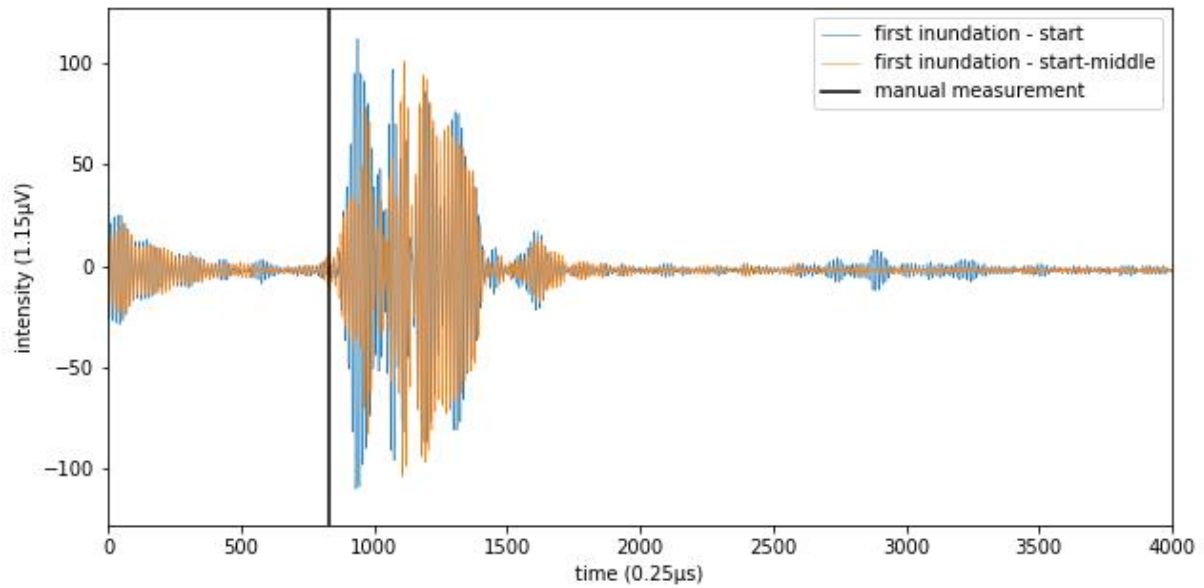


Figure 3.9: The raw signal of start and middle start of the first inundation of the ASED-sensor in the Western Scheldt at a manually measured depth of 0.262 m = 823 (0.25  $\mu$ s). (1632 vs 2168)

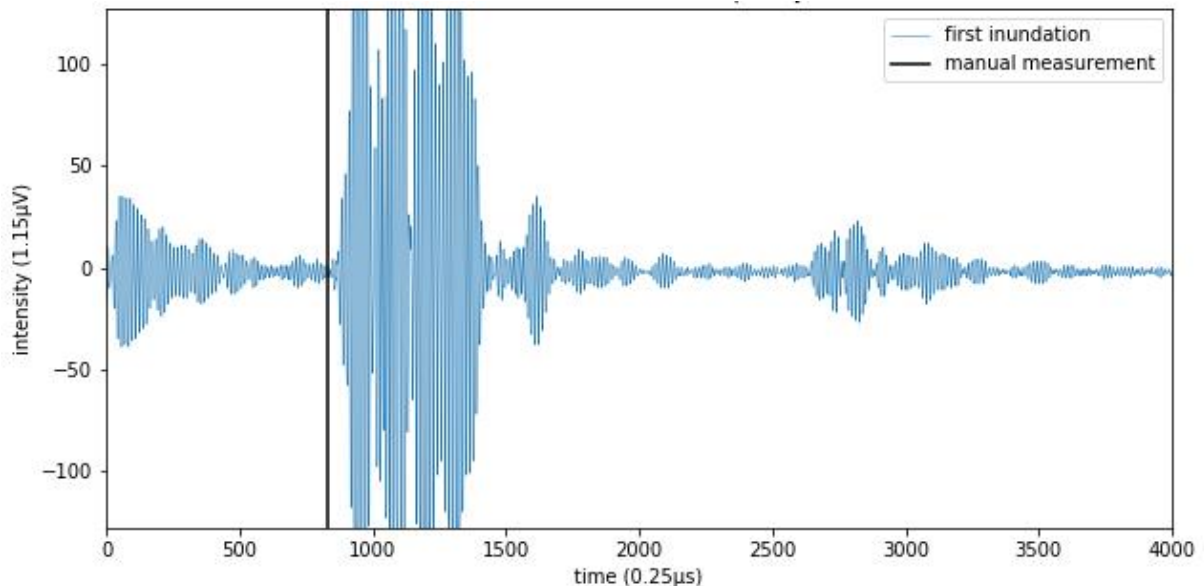


Figure 3.10: A just submerged raw signal of the first inundation of the ASED-sensor in the Western Scheldt at a manually measured depth of 0.262 m = 823 (0.25  $\mu$ s).

### 3.3 Converting raw data to bed level data

#### 3.3.1 Lab bed level

All lab experiments with a clear visible reflection of the signal by the bed are converted to bed level data. The reflections of the signals by the bed that could not be detected are not converted to bed level data.

##### 3.3.1.1 Water depths

Each bed level is continuously measured for a period of about 15 minutes. The n-value increases over time for water depths 0.210 (Figure 3.11), 0.284 m and 0.440 m (Table 3.2). The n-value decreases over time for water depths 0.340 m and 0.395 m (Table 3.2).

**Manual depth 0.210 m** - the bed detected depth is at 0.225 and 0.226 m for the first 10.4 minutes. Between 10.4 and 12.1 minutes, the bed detected depth is fluctuating between 0.225 m and 0.229 m. From 12.1 to 14.05 minute the bed detected depth is constant at 0.229 m and in the end, the bed detected depth fluctuates and ends at 0.225 m. Outliers occur between 0.225 and 0.229 m (Figure 3.11). The bed detected depth fluctuates during this measurement, while the bed is fixed.

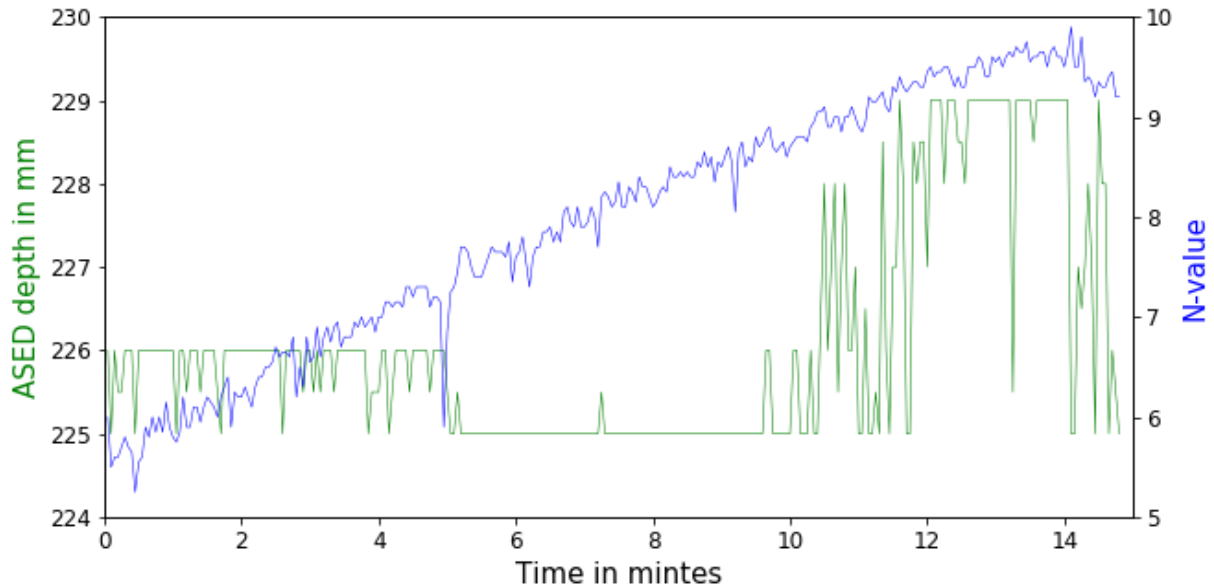


Figure 3.11: ASED-sensor measured above a metal plate at a manually measured water depth of 0.210 m. The n-value and the ASED-sensor measured depth in mm over the length of time of the experiment.

**Manual depth 0.284** - at the beginning the bed jumps between 0.285 m and 0.288 m and after 2.8 minutes the bed detected depth is constant at 0.286 m (Table 3.2).

**Manual depth 0.340** - at the beginning of the experiment, the reflected signal by the bed has a stronger intensity than the noise. After 45 seconds the noise has a stronger intensity than the reflected signal by the bed. Therefore, the bed cannot be detected with the default parameter settings and the parameter settings, need to be adjusted for searching the maximum intensity value from  $t=700$  ( $0.25 \mu s$ ). Three depths are detected by the ASED-sensor around 0.327 m, 0.330 m and 0.343 m (Table 3.2).

**Manual depth 0.395 m** - again, three depths are detected by the ASED sensor at 0.385 m, 0.386 m and 0.387 m (Table 3.2).

**Manual depth 0.440 m** - the bed detected depth increased from 0.424 to 0.445 m for the first 9.4 minutes (Table 3.2). Thereafter the maximum intensity of the reflected bed was lower than the intensity of the noise at the beginning of the signal and therefore the parameter settings need to be adjusted for searching the maximum intensity value from  $t=500$  ( $0.25 \mu s$ ).

Table 3.2: Bed detected depth above a metal plate at varying water depths.

Manual depth in m	0.115	0.210	0.284	0.340	0.395	0.440	0.497	0.572
Averaged ASED depth in m	-	0.226	0.286	0.339	0.386	0.436	-	-
Difference manual - ASED depth in m	-	-0.016	-0.002	0.001	0.009	0.004	-	-
Minimum ASED depth in m	-	0.225	0.285	0.323	0.382	0.423	-	-
Maximum ASED depth in m	-	0.229	0.288	0.346	0.394	0.445	-	-
Standard deviation ASED depth in m	-	0.0014	0.0005	0.0065	0.0011	0.0093	-	-
Averaged n-value	-	7.9	2.6	3.0	2.4	4.0	-	-
Minimum n-value	-	5.2	2.4	2.6	2.3	3.6	-	-
Maximum n-value	-	9.9	3.0	4.2	3.0	4.6	-	-
Standard deviation n-value	-	1.25	0.15	0.14	0.11	0.12	-	-

As the depth increases the n-value does not increase or decrease (Table 3.2). The n-value is independent of the ASED-sensor measured depth (Table 3.2).

The obtained ASED-sensor versus manual depths are close to the 1:1 reference line, which shows a good agreement between ASED-sensor and the manual depths (Figure 3.12). Using the data from the two methods, a fitted regression line can be obtained ( $R^2=0.997$ ). The slope of the fitted line is 1.10, that is a 10% deviation. Using the data from the two methods and a 1:1 reference line gives coefficients of determination  $R^2=0.987$ .

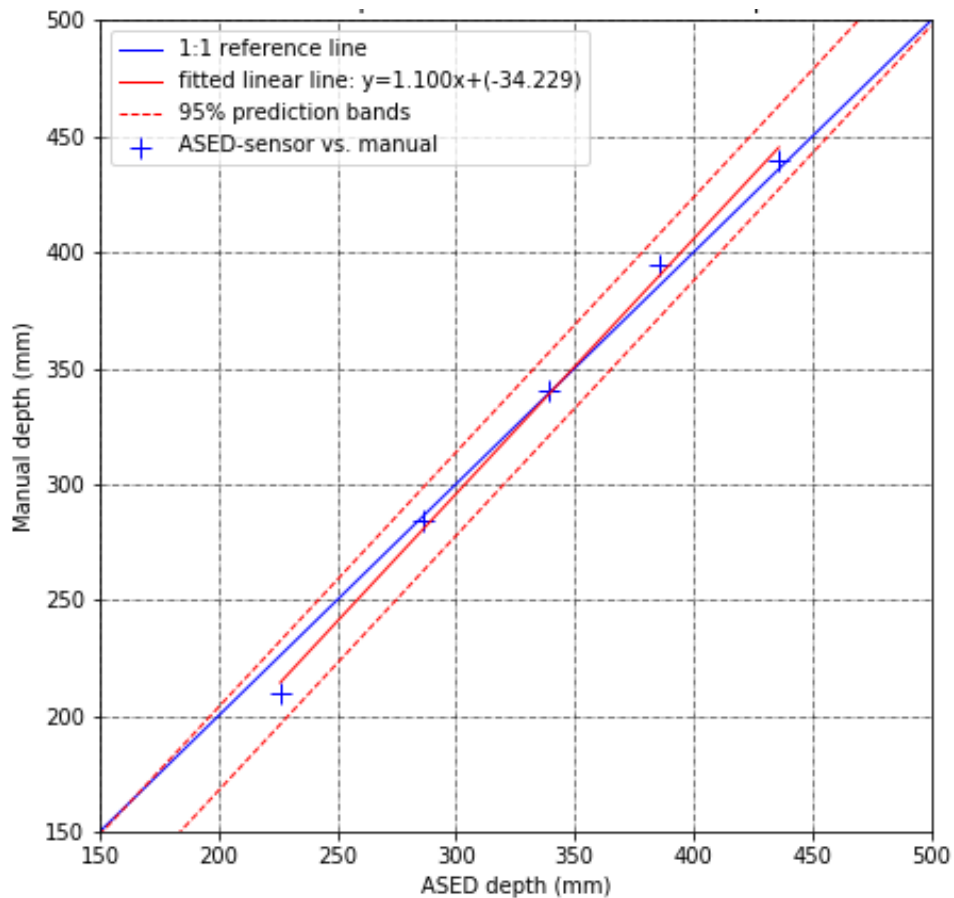


Figure 3.12: The water depths measured above a metal plate with the ASED-sensor and the manual measurement.

### 3.3.1.2 Soil types

All soil types are analysed at a depth of 0.20 m, except for the 1.0 fraction of sand (Table 3.3). The n-value is constant for 0.8 and 0.65 fraction of sand. The n-value increases for 0.48, 0.4 and 0.12 fraction of sand (Table 3.3). The bed detected depths are constant for 0.8 (at 0.193 m), 0.65 (at 0.189 m), 0.48 (at 0.188 m) and 0.4 (at 0.193 m) fraction of sand (Table 3.3). But for 0.65 fraction of sand, the bed detected depth suddenly decreases 3 mm for the last two minutes. The n-value decreases too at that moment. The same occurs for 0.4 fraction of sand, except the bed detected depth suddenly increases 12 mm, the n-value became inconsistent at that moment. The bed detected depth is increasing during the measurement for 0.12 fraction of sand, but the bed fluctuates a lot. The first 3 minutes the bed detected depth fluctuates from 0.177 m to 0.191 m. Thereafter, the bed detected depth fluctuates from 0.193 m to 0.198 m until the end of the experiment. A few outliers occur around the bed detected depth.

Table 3.3: The bed detected depth of all soil types at a depth around 0.20 m.

Fraction of sand	1.0	0.8	0.65	0.48	0.4	0.12
Manually measured depth in m	0.186	0.184	0.177	0.174	0.175	0.185
Averaged ASED depth in m	-	0.193	0.189	0.188	0.195	0.189
Difference manual - ASED depth in m	-	-0.009	-0.012	-0.014	-0.020	-0.004
Minimum ASED depth in m	-	0.190	0.186	0.188	0.192	0.177
Maximum ASED depth in m	-	0.193	0.189	0.188	0.207	0.199
Standard deviation ASED depth in m	-	0.0004	0.0008	0.0000	0.0043	0.0074
Averaged n-value	-	2.3	3.8	3.2	10.0	3.3
Minimum n-value	-	2.2	3.4	2.7	6.7	2.8
Maximum n-value	-	2.4	4.2	3.7	11.8	4.1
Standard deviation n-value	-	0.03	0.16	0.23	0.97	0.33

All soil types are analysed at a depth of 0.40 m. For all soil types, a minimal variation of the n-value occurs during the course of the experiment. The n-value is constant for 1.0 and 0.8 fraction of sand. The n-value decreases for 0.65, 0.48 and 0.12 fraction of sand and the n-value increases for 0.4 fraction of sand (Table 3.4). The bed detected depths are constant for 1.0, 0.8, 0.65 and 0.4 fraction of sand (Table 3.4). As bed detected depth suddenly increases from 0.393 m to 0.401 m, the n-value increases too for 0.48 fraction of sand (Table 3.4). For the first 40 seconds, the bed detected depth is 0.411 m thereafter the bed detected depth is constant at 0.414 m for 0.4 fraction of sand (Table 3.4). In the beginning, the bed detected depth is 0.408 m and after 2 minutes the bed detected depth increased to 0.410 m for 0.12 fraction of sand (Table 3.4). A few outliers occur around the bed detected depth.

Table 3.4: The bed detected depth of all soil types at a depth around 0.40 m.

Fraction of sand	1.0	0.8	0.65	0.48	0.4	0.12
Manually measured depth in m	0.400	0.396	0.393	0.396	0.400	0.393
Averaged ASED depth in m	0.404	0.407	0.392	0.396	0.414	0.409
Difference manual - ASED depth in m	-0.004	-0.011	0.001	0.000	-0.014	-0.016
Minimum ASED depth in m	0.404	0.407	0.392	0.391	0.411	0.393
Maximum ASED depth in m	0.405	0.408	0.394	0.403	0.414	0.411
Standard deviation ASED depth in m	0.0004	0.0003	0.0004	0.0040	0.0008	0.0028
Averaged n-value	5.1	4.1	3.5	5.4	5.9	5.9
Minimum n-value	4.8	4.0	3.3	4.7	5.4	5.1
Maximum n-value	5.3	4.3	4.0	6.3	6.3	6.6
Standard deviation n-value	0.09	0.07	0.17	0.45	0.23	0.29

All soil types yield an n-value between 2.2 and 11.8 at a water depth of 0.20 m. And for a water depth of 0.40 m, the n-value varied between 3.3 and 6.6. The n-value did not correlate between soil type and there is no correlation between depth and n-value (Figure 3.13).

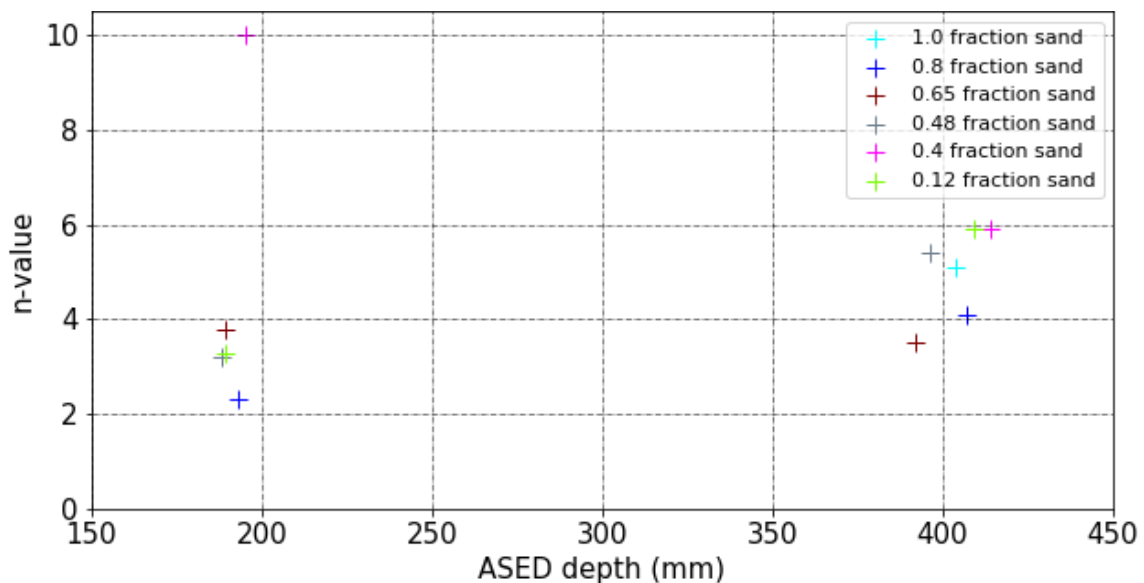


Figure 3.13: N-value versus the measured ASED-sensor depth in metres of all soil types at a depth of 0.20 and 0.40 m.

### 3.3.1.3 Dilutions

Before the reflection of the signal by the bed periodic noise occurs for dilution 16.37% (0.219 m; Figure 3.14) of 0.8 fraction of sand. The periodic noise influences the Kalman filter line (red line; Figure 3.14). Therefore, the bed is detected at the manual depth  $t=577$  ( $(0.25 \mu s) = 0.219$  m) instead of at  $t=515$  ( $=0.208$  m), where the sudden increase in the amplitude of the reflection of the signal by the bed occurs. The second strong reflection is 600-time steps after the first strong reflection, which is approximately 10 cm. The bucket was filled with 10 cm of the soil dilution. Therefore, this second reflection could be the reflection of the signal by the bottom of the bucket instead of by the bed of the soil dilution.

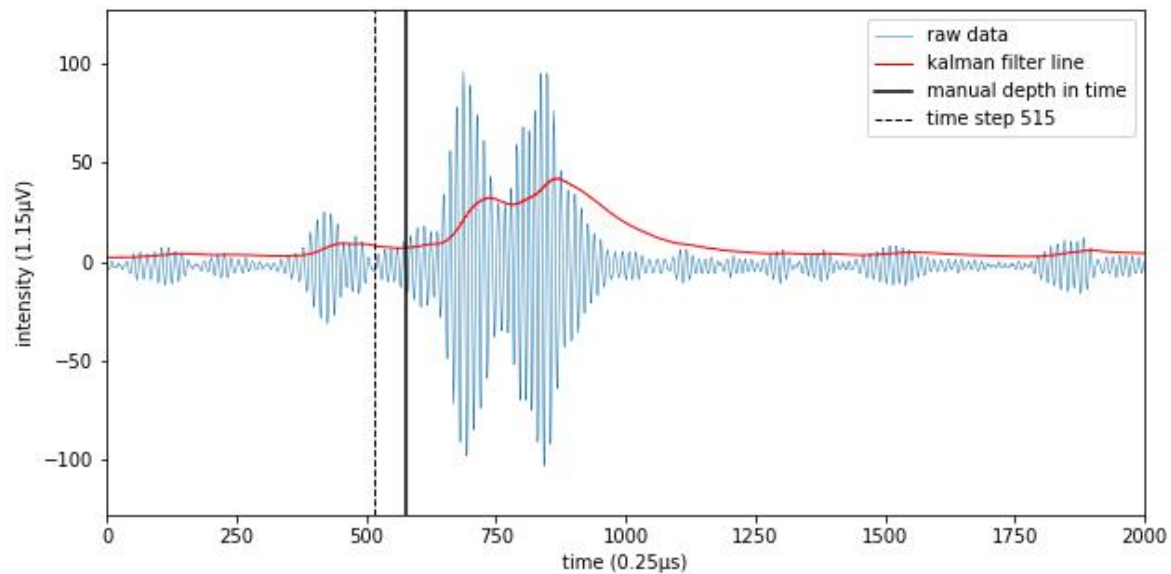


Figure 3.14: The raw signal and the Kalman filter signal of 0.8 fraction of sand with a dilution of 16.37% at a manually measured depth of 0.219 m = 577 (0.25  $\mu$ s).

For 0.8 fraction sand with a dilution of 16.37%, the reflection of the signal by the bed is detected shallower for the first signal compared to the last signal, due to noise before the first signal reflected by the bed. The bed detected depth increased from 0.219 m to 0.232 m for 15.3 minutes (Table 3.5). During this measurement the parameter settings have been adjusted, instead of looking from the maximum intensity value 300-time steps back in time, it is 400-time steps back in time. Due to the maximum intensity reflection is shifted to the right (deeper).

The same dilution of 16.37% (0.303 m), the bed detected depth is constant at 0.299 m (Table 3.5). The second reflection has a stronger intensity than the first reflection of the signal by the bed. During this measurement, the parameter settings have been adjusted, instead of searching for the maximum intensity peak from time step 400. The maximum intensity peak is searched from time step zero until time step 2000.

A dilution of 26.11% (0.212 m) has a varying bed detected depth between 0.183 and 0.212 m. Mostly, the bed detected depth is between 0.204 m and 0.208 m. The bed detected depth is around at 0.382 m for dilution 45.47% (Table 3.5).

Table 3.5: The bed detected depth of soil type 0.8 fraction of sand with different dilutions at different depths.

Dilution in %	16.37	16.37	26.11	26.93	45.47
Manually measured depth in m	0.219	0.303	0.212	0.393	0.384
Averaged ASED depth in m	0.227	0.300	0.201	0.398	0.382
Difference manual - ASED depth in m	-0.008	0.003	0.011	-0.005	0.002
Minimum ASED depth in m	0.219	0.299	0.183	0.398	0.379
Maximum ASED depth in m	0.232	0.300	0.212	0.398	0.384
Standard deviation ASED depth in m	0.0051	0.0004	0.0084	0.0000	0.0011
Averaged n-value	6.3	3.5	2.7	5.9	5.2
Minimum n-value	4.7	3.0	2.5	5.4	3.9
Maximum n-value	7.6	4.7	2.9	6.7	6.1
Standard deviation n-value	0.93	0.20	0.06	0.29	0.46

The bed detected depth decreases for dilutions 17.07% (0.244 m), increases for dilutions 17.07% (0.330 m) and 18.12% (0.305 m) and is constant for dilutions 18.12% at 0.202 m (0.197 m) and 30.94% at 0.388 m of soil type 0.65 fraction of sand (Table 3.6).

Dilution 17.07% (0.244 m) has a constant bed detected depth at 0.249 m for the first 6 minutes, surrounded by a few outliers. Until the end, the bed detected depth fluctuates between 0.239 m and 0.248 m (Table 3.6). During this measurement, the parameter settings have been adjusted, instead of looking from the maximum intensity value 300-time steps back in time, it is 400-time steps back in time. This because the second part of the reflection of the signal by the bed has a higher maximum intensity peak (as in Figure 3.8).

*Table 3.6: The bed detected depth of soil type 0.65 fraction of sand with different dilutions at different depths.*

<b>Dilution in %</b>	<b>17.07</b>	<b>17.07</b>	<b>18.12</b>	<b>18.12</b>	<b>30.94</b>
Manually measured depth in m	0.244	0.330	0.197	0.305	0.365
Averaged ASED depth in m	0.246	0.332	0.202	0.309	0.388
Difference manual - ASED depth in m	-0.002	-0.002	-0.005	-0.004	-0.023
Minimum ASED depth in m	0.239	0.331	0.200	0.309	0.387
Maximum ASED depth in m	0.250	0.336	0.202	0.310	0.388
Standard deviation ASED depth in m	0.0033	0.0011	0.0006	0.0004	0.0002
Averaged n-value	3.3	5.1	2.5	2.4	5.1
Minimum n-value	3.1	3.7	2.3	2.3	4.4
Maximum n-value	8.8	5.8	2.6	2.6	5.7
Standard deviation n-value	0.39	0.43	0.05	0.05	0.28

The bed detected depth decreases for 19.95% and 20.00% (0.179 m) and is constant for 20.00% (0.295 m) and 41.27% of soil type 0.48 fraction of sand (Table 3.7).

During the first 11 minutes, the bed detected depth is at 0.200 m and thereafter at 0.198 m, with a lot of outliers ranging from 0.190 m to 0.202 m for dilution 19.95% (Table 3.7). Dilution 20.00% (0.179 m) has a bed detected depth at 0.184 m for the first 2 minutes. Thereafter the bed decreases until a bed detected depth of 0.163 m (Table 3.7). When little initial and periodic noise occurs for the first and last signal. The first signal has a higher starting intensity for the Kalman filter line and the last signal a lower starting intensity for the Kalman filter line. Therefore, the last signal has an increasing Kalman filter line before the signal reflected by the bed. And the bed detected depth will be detected 300-time steps backwards from the maximum intensity peak. After two minutes, the bed cannot be detected for this dilution and depth by this method.

Table 3.7: The bed detected depth of soil type 0.48 fraction of sand with different dilutions at different depths.

Dilution in %	19.95	20.00	20.00	41.27
Manually measured depth in m	0.192	0.179	0.295	0.368
Averaged ASED depth in m	0.199	0.171	0.297	0.399
Difference manual - ASED depth in m	-0.007	0.008	-0.002	-0.031
Minimum ASED depth in m	0.190	0.163	0.297	0.399
Maximum ASED depth in m	0.202	0.187	0.298	0.400
Standard deviation ASED depth in m	0.0020	0.0073	0.0003	0.0000
Averaged n-value	3.1	2.7	5.7	6.0
Minimum n-value	2.6	2.3	5.1	5.4
Maximum n-value	4.3	4.1	6.6	6.4
Standard deviation n-value	0.25	0.34	0.25	0.19

The bed detected depth is constant for all dilutions of soil type 0.4 fraction of sand (Table 3.8). For dilution 20.26%, the maximum intensity value will be found from time step 500, instead of the default value time step 400. A lot of initial noise occurred, and the intensity of the signal reflected by the bed decreased over the measurement. Dilution 21.75% has a bed detected depth at 0.190 m, 0.191 m and 0.192 m, a few outliers occur around the bed detected depths. During dilution 21.75% (0.299 m) the parameter settings have been adjusted, instead of looking from the maximum value 300-time steps back in time it is 500-time steps back in time. This because the second part of the reflection of the signal by the bed has a higher maximum intensity peak (as in Figure 3.8).

Table 3.8: The bed detected depth of soil type 0.4 fraction of sand with different dilutions at different depths.

Dilution in %	20.26	21.75	21.75
Manually measured depth in m	0.205	0.197	0.299
Averaged ASED depth in m	0.217	0.191	0.304
Difference manual - ASED depth in m	-0.012	0.006	-0.005
Minimum ASED depth in m	0.216	0.187	0.304
Maximum ASED depth in m	0.217	0.192	0.305
Standard deviation ASED depth in m	0.0005	0.0012	0.0003
Averaged n-value	9.9	2.5	9.7
Minimum n-value	9.4	2.4	7.0
Maximum n-value	10.5	2.8	10.4
Standard deviation n-value	0.18	0.07	0.42

### 3.3.1.4 Waves and current forcing

At the beginning of the wave forcing experiment the bed detected depth starts at 0.195 m, the bed detected depth decreases to 0.191 m (Figure 3.15). Close to the end of the experiment, the ASED-sensor is manually vibrated to simulate waves breaking at the ASED-sensor (Figure 3.15). At that moment the bed detected depth decreases from 0.191 m to 0.188 m (Table 3.9). The n-value increases from 2.4 to 6.98 at that moment.

For the current forcing experiment, the last 5 minutes of the experiment the n-value suddenly increases, and the bed detected depth has more outliers during that moment. This is during the increasement of the current forcing; therefore, the ASED-sensor could vibrate a bit. The bed detected depth fluctuates between 0.229 m and 0.234 m (Table 3.9), with outliers at shallower depths.

Table 3.9: Bed detected depth during current and wave forcing.

	Wave forcing	Current forcing
Manually measured depth in m	0.187	0.228
Averaged ASED depth in m	0.193	0.232
Difference manual - ASED depth in m	-0.006	-0.004
Minimum ASED depth in m	0.188	0.215
Maximum ASED depth in m	0.195	0.235
Standard deviation ASED depth in m	0.0015	0.0017
Averaged n-value	2.4	2.4
Minimum n-value	2.3	2.3
Maximum n-value	6.7	7.0
Standard deviation n-value	0.32	0.15

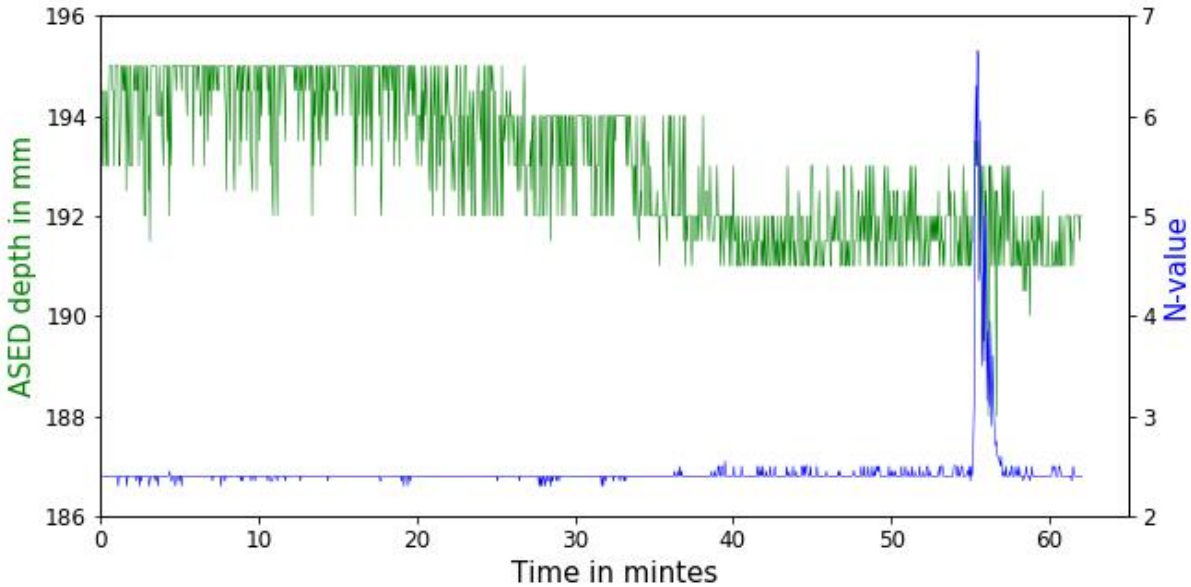


Figure 3.15: ASED-sensor measured during wave forcing at a manually measured water depth of 0.187 m. The n-value and the ASED-sensor measured depth in mm over the length of time of the experiment.

### 3.3.2 Field bed level

As the field experiments encounter inundations, the parameters will need to be reset. The maximum intensity will be found  $1000 \leq \text{time step} \leq 3000$ , instead of the default setting  $400 \leq \text{time step} \leq 2000$ . The sudden increase in amplitude will be searched for starting 400-time steps backwards from the maximum intensity, instead of 300-time steps backwards. The maximum intensity will be found  $900 \leq \text{time step} \leq 1500$  for the Western Scheldt experiment. The sudden increase in amplitude will be searched for starting 400-time steps backwards from the maximum intensity. The remaining parameters are the

same as the default setting. The bed level will not change hourly and therefore a median filter is used hourly. The outliers will be removed by the hourly median filter (Figure 3.16 and Figure 3.18).

### 3.3.2.1 Eastern Scheldt

The bed levels are stable during the first 3 inundations. The last 2 inundations have a lot of outliers and detect the depth deeper compared to the first 3 inundations (Figure 3.16 and Figure 3.17). This was as well observed during the raw data analysis. The first-hour median bed level is the null bed level and erosion and sedimentation can be observed (Figure 3.17). The detected erosion of the tape measure was 3 mm and by the ASED-sensor 5 mm (Figure 3.17). The tape measure has an accuracy of 3 mm.

The results of all inundations of the bed detected depths can be found in Appendix A.8.1.

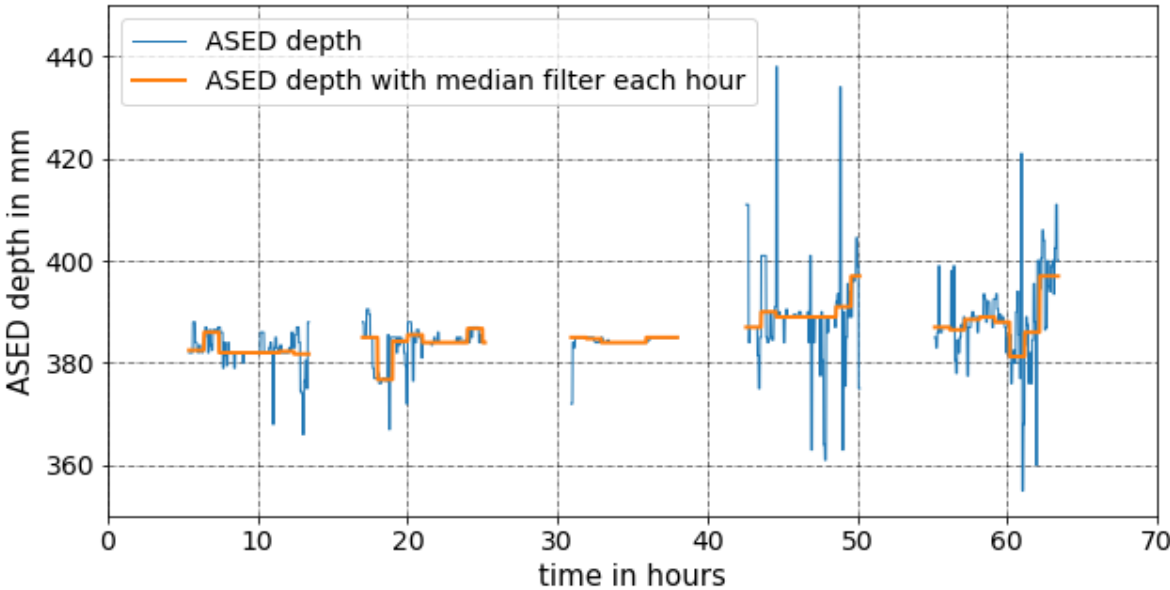


Figure 3.16: The ASED-sensor converted depth during the Eastern Scheldt experiment.

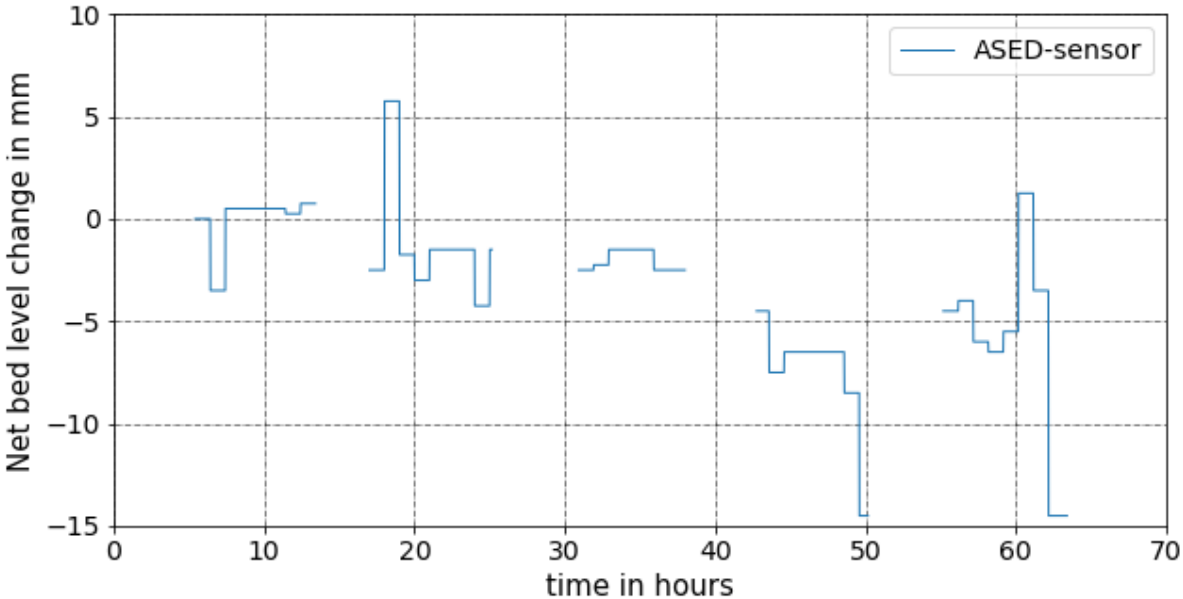


Figure 3.17: The negative values clarify erosion and the positive values indicate sedimentation during the Eastern Scheldt experiment.

### 3.3.2.2 Western Scheldt

The bed detected depth is not as stable as during the lab experiments (Figure 3.18). The bed level gets deeper during the experiment (Figure 3.18 and Figure 3.20). The raw data of the Western Scheldt experiment already showed that the shape of the signal reflected by the bed changes over times. The sudden increase in amplitude is shifted to the right (deeper) during the experiment.

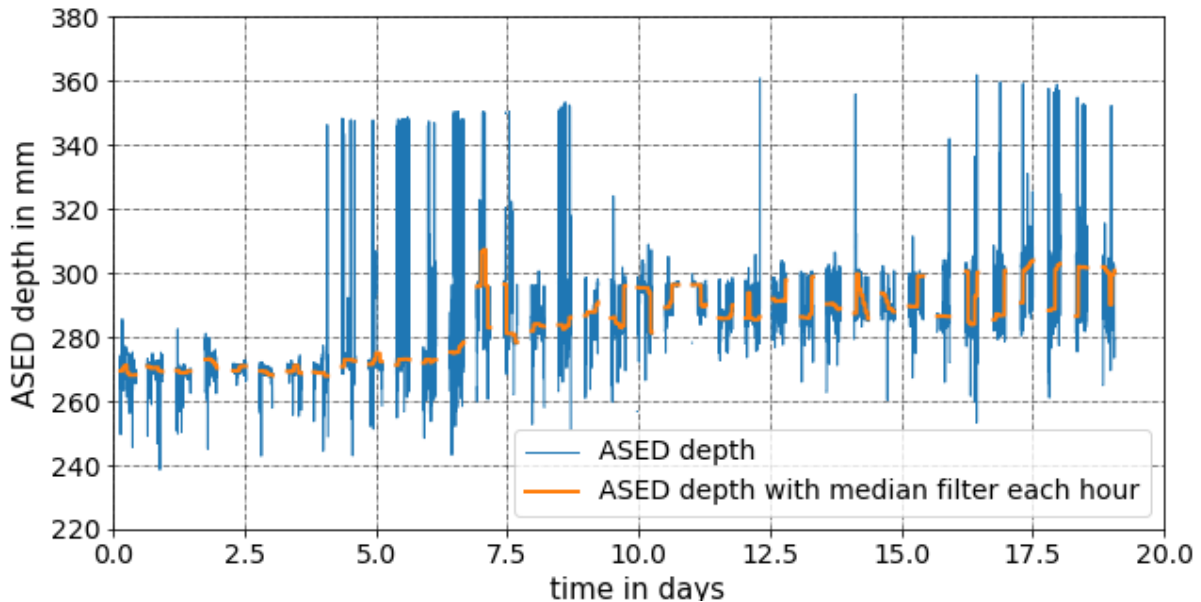


Figure 3.18: The ASED-sensor converted depth during the Western Scheldt experiment.



Figure 3.19: The water levels are retrieved from Rijkswaterstaat website at location Hansweert. The ASED-sensor is placed at the Kapellebank (Western Scheldt experiment).

The water levels are obtained from Hansweert (Figure 3.19). The 31<sup>st</sup> of October is neap tide, 7<sup>th</sup> of November spring tide, 15<sup>th</sup> of November neap tide and 23<sup>rd</sup> of November spring tide (Figure 3.20). During spring tide erosion occurs (Figure 3.20). The average erosion is 9 mm measured by the erosion pins and 20 mm measured by the ASED-sensor (Figure 3.20).

The results of all inundations of the bed detected depths can be found in Appendix A.8.2.

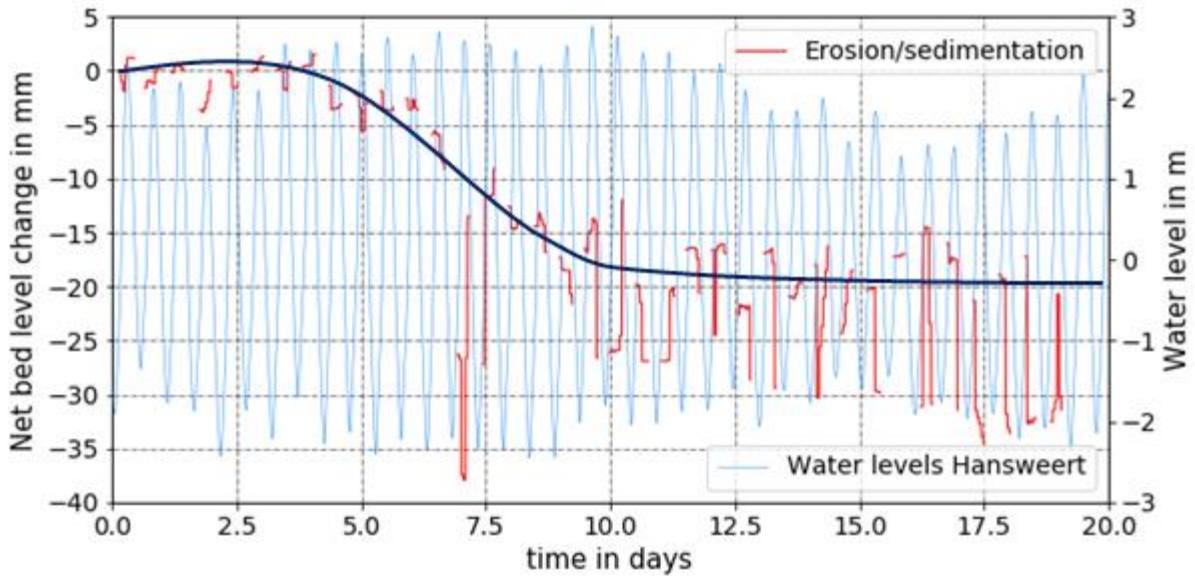


Figure 3.20: The negative values clarify erosion and the positive values indicate sedimentation during the Eastern Scheldt experiment. The black line is the trendline of the erosion/sedimentation.

### 3.3.3 Summary of the experiments converted to bed levels

The obtained ASED-sensor versus manual depths are close to the 1:1 reference line, which shows a good agreement between ASED-sensor and the manual depths (Figure 3.21). Using the data from the two methods, a fitted regression line can be obtained ( $R^2=0.993$ ). The slope of the fitted line (1.01) is close to 1. Using the data from the two methods and a 1:1 reference line gives coefficients of determination  $R^2=0.991$ . All lab experiments fit in the 95% prediction bands, which further confirms the consistency between the two measurements. Dilution 41.27% of soil type 0.48 fraction of sand measures the bed detected depth 0.031 m deeper than the manual measurement and dilution 30.94% of soil type 0.65 fraction of sand measures the bed detected depth 0.023 m deeper than the manual measurement. This indicates the dilution is too difficult to measure accurately. These dilutions will not be used for the fitted linear line and the 95% prediction bands. These dilutions are as well outside the 95% prediction bands (Figure 3.21).

For the water depth experiment, the shallower depths were detected deeper than the manual measurement and the deeper depths were detected shallower than the manual measurement during the water experiments above the metal plate (green plusses; Figure 3.21). Almost all bed detected depths were deeper than the manual measurement during the soil type experiments (pink plusses; Figure 3.21). The dilution bed detected depths are near the 1:1 reference line and the fitted linear line and are close to the manual measurement (black plusses; Figure 3.21). The bed detected depth is deeper than the manual measurement during the waves and current forcing experiments.

The bed detected depths were equal to the reference measurement during all inundation of the Eastern Scheldt experiment. The bed detected depths were deeper than the reference measurement during all inundations of the Western Scheldt experiment.

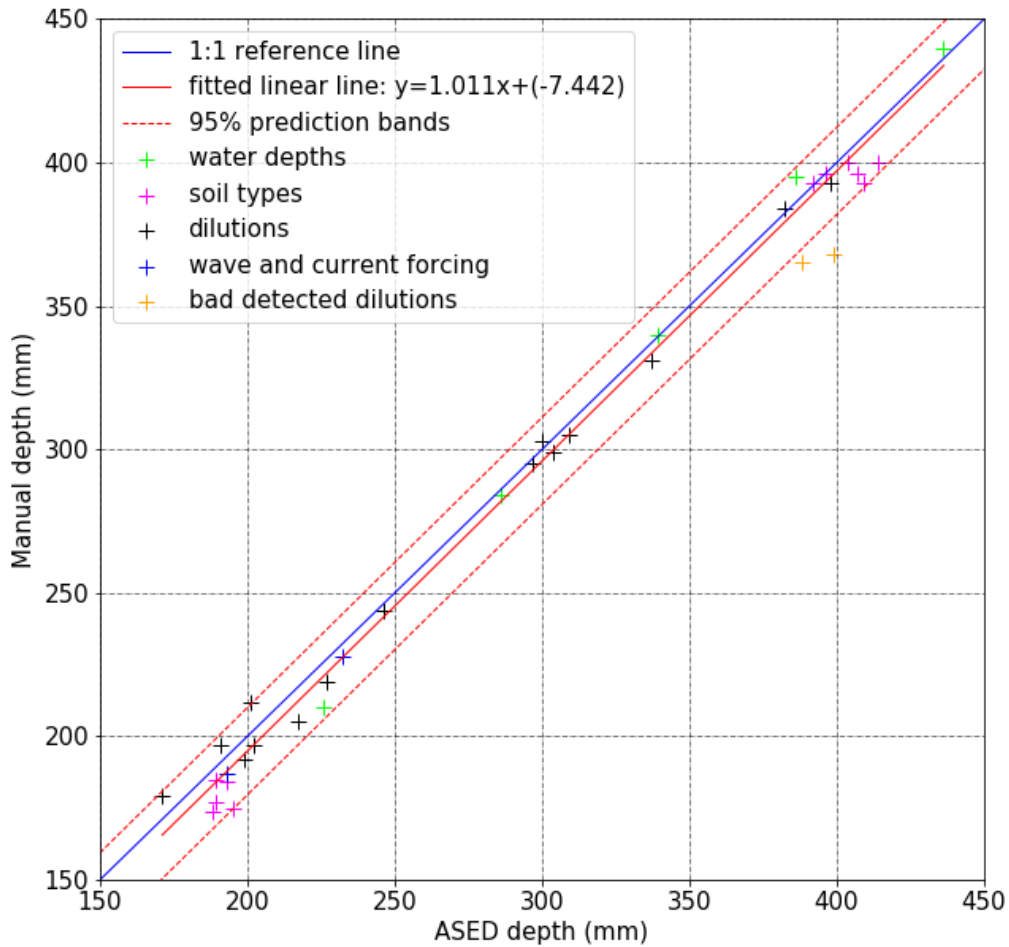


Figure 3.21: Comparison of ASED-sensor and manual measurements for all lab experiment.

### 3.4 The accuracy of the ASED-sensor

#### 3.4.1 Theoretical

The maximum achievable resolution can be determined by the sample rate of 4 MHz which gives an absolute boundary during optimal conditions of  $\frac{1500\frac{m}{s}}{2*4MHz} \approx 0.19\text{ mm}$ . Another method is the acoustic wavelength divided by 2 which gives a more realistic boundary of  $\frac{1500\frac{m}{s}}{2*300.0kHz} = 2.5\text{ mm}$ . Thus, the resolution of the ASED-sensor will be in realistic and optimal conditions 2.5 mm according to the specifications of the transducers.

#### 3.4.2 Actual

The accuracy of the whole system, the ASED-sensor and the script, can be measured with standard deviations created by averaging the bed levels over an enclosed measuring period. As the bed level is fixed during the lab experiments. During the water depth experiments the ASED-sensor measured above a metal plate which gave a strong bed reflection and an average accuracy of is 4 mm. All remained lab experiments had an average accuracy of 2 mm. The average accuracy of all lab experiments is 2 mm. The actual accuracy ranges between 2 mm and 4 mm, depending on the bed type.

## 4 Discussion

### 4.1 Measuring with the ASED-sensor

#### 4.1.1 Speed of sound

The main concern for acoustic measurement instruments is the behaviour of sound in water. Once the transducer transmits the acoustic energy into the water, many factors influence that energy's velocity and coherence (Lurton, 2010; R2Sonic, 2014). The major influence is the velocity of sound in water.

The velocity of sound in water varies both horizontally and vertically. It cannot be assumed that the velocity of sound in the water column remains constant throughout the day, even in a more local area. The main influences on sound velocity are salinity, temperature and depth (Table 4.1).

Table 4.1: Influences of temperature, salinity and depth for the speed of sound in water (R2Sonic, 2014)

Change in the influence of speed of sound in water	Change in velocity (m/s)
1°C change in temperature	4,0
1 part per thousand change in salinity	1,4
100 m change in depth (10 atm in pressure)	1,7

In these experiments, the depth did not change by 100 m (or pressure 10 atm) and therefore the speed of sound will not be affected by the depth (or pressure). The salinity is assumed constant during the conversion of the raw data into bed level data. The salinity is not constant in the Western Scheldt, it varies between 10 and 25 parts per thousand. Assuming the water temperature being 7 °C, the pressure 1.1 bar and salinities 10 and 25 parts per thousand, the speed of sound is calculated by the formula of UNESCO – Chen and Millero. The results are 1447.7 and 1453.9 m/s respectively (Table 4.2; Appendix A.6.4). The resulting calculated depth difference is 1 mm at a depth of 0.24 m (Table 4.2), which is 0.4%. This depth difference will increase linearly with depth.

Table 4.2: Influence of salinity for the speed of sound in water and for the depth.

	Water temperature (°C)	Pressure (bars)	Salinity (parts per thousand)	Speed of sound (m/s)	Depth (m)
Test 1	7	1.1	10	1447.7	0.2376
Test 2	7	1.1	25	1453.9	0.2386

##### 4.1.1.1 Temperature sensor

The ASED-sensor has a temperature sensor. The temperature measured by the ASED-sensor fluctuates (Figure 4.1). While the ASED-sensor is submerged the temperature is constant (Figure 4.1). The temperature sensor takes a few minutes to acclimatize. The temperature can increase due to power dissipation during a Wi-Fi connection. But 5 minutes after the deployment starts, the Wi-Fi connection is switched off. This was set during the experiments. In non-submerged conditions, the ASED-sensor cools down or heats up (Figure 4.1). The sensor cools down when the wind blows over the water surface and the temperature sensor is wet. The heating up effect can be caused by solar radiation or the warm environment. As the ASED-sensor gets submerged, the temperature remains constant around 7.5 °C in the Eastern Scheldt and 6 °C in the Western Scheldt (Figure 4.1).

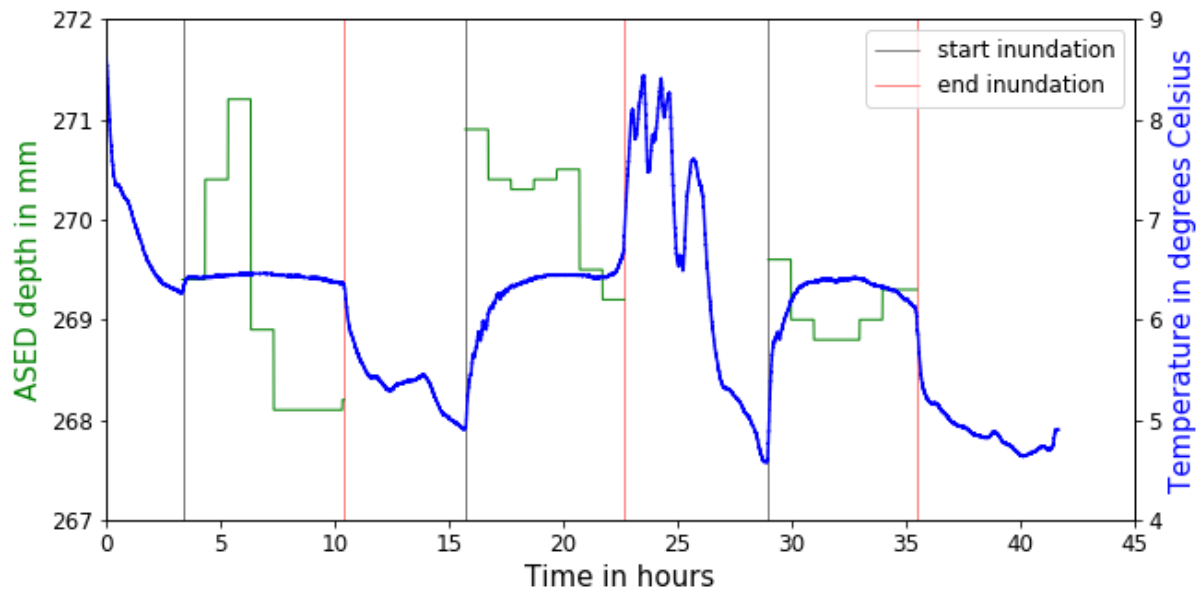


Figure 4.1: ASSED-sensor measured at a manually measured water depth of 0.258 m in the Western Scheldt. The temperature versus the ASSED-sensor measured depth in metres over the length of time of the experiment.

#### 4.1.1.2 Lime/sealer 604 Ruplo

The speed of sound of the lime/sealer 604 of Ruplo is unknown. As the ASSED-sensor measures the bed mostly deeper than the manual measurement, the lime/sealer probably delays the propagation. This is not relevant for the measurement of bed level changes by the ASSED-sensor, as the delay is constant.

#### 4.1.2 Signal attenuation

The decrease in intensity of the signal reflected by the bed during the measurement can be caused by spreading loss and by absorption (Lurton, 2010; R2Sonic, 2014). Spreading loss is due to the expanding area that the sound signal encompasses as it geometrically spreads outwards from the source. When the medium in which signal transmission occurs is unbounded, the spreading is spherical, for the wave flume and the field experiments. Whereas the medium in which signal transmission occurs is bounded, like in the water tank, the spreading is cylindrical. At shorter ranges, spreading loss plays a proportionally larger part compared to the absorption term (which has a linear relationship with range) (Burrowes *et al.*, 2011).

The absorption loss is a representation of the energy loss in the form of heat due to the viscous friction and ionic relaxation that occurs as the acoustic signal propagates outwards and this loss varies linearly with range (Burrowes *et al.*, 2011). More specifically, the absorption of sound in seawater is caused by viscosity (shear and volume); the effect of viscosity is significant at frequencies above 100 kHz (Burrowes *et al.*, 2011). There is also bottom absorption based on the sea floor terrain and composition (R2Sonic, 2014). Bottom absorption is dependent on the operating frequency of the sonar and the angle of incidence (R2Sonic, 2014). Bottom absorption will be greater for a higher frequency and large angle of incidence. It is intuitive that a mud bed will absorb more of the acoustic energy than a rock bed.

The sea is not homogenous in nature. Everything from suspended dust particles to fish, from the sea surface to the bed will scatter, that is reradiated, the acoustic energy. All the effects of individual scattering can be termed as reverberation (Lurton, 2010). The effect

of reverberation is to lessen the acoustic energy, and this leads to transmission losses (R2Sonic, 2014). In the scattering process, there is also a degree of energy which is reflected, also called backscatter (R2Sonic, 2014). This can be a cause for noise in the acoustic data.

The observed periodic noise, and the noise before the reflection of the signal by the bed can be caused by reflection by particles or inhomogeneities in the water column. Roughness on the seabed and heterogeneities in the sediment cause some energy in the acoustic wave to be scattered in different directions (R2Sonic, 2014). But during the experiments in the water tank, this can be caused as well by multiple signal reflections. The raw data of shallow depths give not only the first reflection of the signal by the bed, but also the second or even third reflection of the signal by the bed. The signal travels continuously in the water, from there periodic noise can arise.

The initial noise can be caused by the vibration after sending the pulse into the water, by (micro) bubbles underneath the head of the ASED-sensor and due to reflections of the signals in the water tank. The researchers of NIOZ noticed that the 'contact' between the ASED-sensor head and the water was not always immediately good. Probably, at the beginning of the experiment (micro) bubbles occur at the ASED-sensor head and disappear slowly during the experiment. This problem can be solved by vibrating the ASED-sensor or by patience. This phenomenon can be identified by the relative high mV of the stop mV. The stop mV is the end voltage to the transducer at the end of the pulse train. The start and stop mV cannot be adjusted manually. As the stop mV is too high (towards the battery voltage), then the transducer of the ASED-sensor cannot optimize the amplitude of the acoustic signal for detecting the bed. The start and stop mV can be adjusted in one measurement. The start and stop mV influence the strength of the reflection.

When the start and stop mV are changed during the experiment, the initial noise is lower for the first signal. But the intensity of the reflection of the first and last measurement of the experiment is the same (Figure 3.2). When the start and stop mV is similar during the experiment, the initial noise is the same for the first and last signal, but the intensity of the reflection of the last signal by the bed is lower (Figure 3.3). A small variation in the bed can have a big influence on the intensity of the reflection.

## 4.2 Collecting raw data

During lab experiments, the manual measurements can be less accurate at shallow depths. The water tank has a height of 84 cm, and the bucket with sediment is approximately 10 cm. It is difficult to go upside-down in the water tank to measure the distance accurately. The metal plate mounting on the tape measure helped a bit with the accuracy, but another method should be found to measure this more accurately. From here the ASED-sensor can be calibrated properly.

The last signal of 0.4 fraction of sand at a manual depth of 0.175 m and the last signal of dilution 26.11% of 0.8 fraction of sand at a manual depth of 0.307 m are shifted to the right (deeper) compared to the first signal. The intensity of the first and last signal is equal for 0.4 fraction of sand, but the intensity of the last signal decreases for dilution of 0.8 fraction of sand. The decrease in intensity of the last signal could be due to the soil which got in suspension.

Before the soil is put in the bucket, the soil is mixed well, and the soil can get airy. Therefore, the soil can settle during the measurement. The soil was spread equally by a

plate during the lab experiment in the water tank. Another possibility is that the upper layer of the soil got in suspension at the beginning of the experiment and settled during the experiment. Possibly, the soil in suspension is reflected as bed instead of the upper layer of the soil in the bucket.

At the time of the waves and current forcing experiments, also mussel experiments were going on in the wave flume. Therefore, no sediment could be added to the bed. The mussels were placed in a box with sand; therefore, a little sand was in suspension. The bed level of the sand was the same as the bed level of the wave flume. As the mussel experiment should not be interfered with, the ASED-sensor measured to the bed level of the wave flume, instead of to the bed level of the sand box.

During field experiments, the raw signal of the ASED-sensor changes over time. This can be due to the SSC, the deformation of the bed or the sediment of the upper layer of the bed getting in suspension just above the bed.

At the time of the field experiments, the ASED-sensor had a frame with two poles in the ground (Figure 2.15). This frame was not very stable. The ASED-sensor did not perform well during vibrating conditions. This might influence the bed detected depth. NIOZ already built a new frame with three poles in the ground instead of two (Figure 4.2). Both ASED-sensors with this three-pole mounting gave a stable bed detected depth during two inundations. These results look promising.



*Figure 4.2: New frame of the ASED-sensor with three poles in the bed.*

### 4.3 Converting raw data to bed level data

The raw signal of the ASED-sensor changes over time, as does the Kalman filter line (Figure 4.3 and Figure 4.4). The sudden increase in amplitude is easily detected (Figure 4.3 and Figure 4.4). The first bed detection starts from a water depth of 0.210 m. The bed detection of the first and the last signal is at a different depth. For the first signal, the bed detection is at time step 609 (=0.226 m) where this is for the last signal at time step 626 (=0.229 m) (Figure 3.11 and Figure 4.4). This is a difference of 3 mm during a

measurement with a flat (metal plate) and fixed bottom. The initial and periodic noise already have a small influence during the lab experiments.

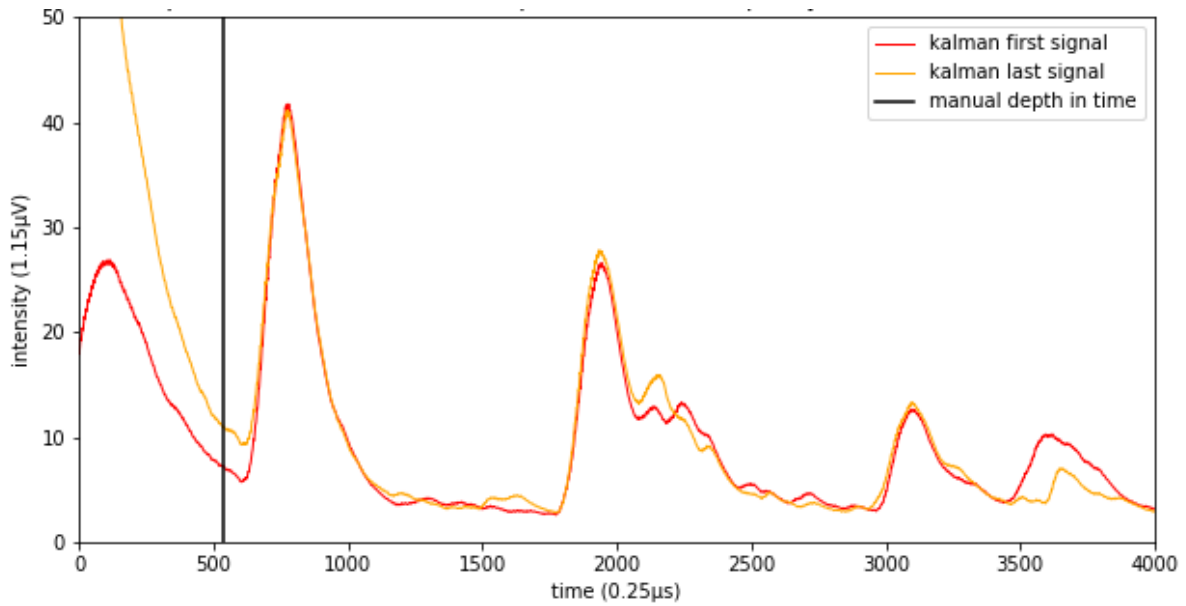


Figure 4.3: Kalman filter line of the first and last signal. The ASED-sensor measured above metal plate at a manually measured water depth of 0.210 m converted to time 536-time steps.

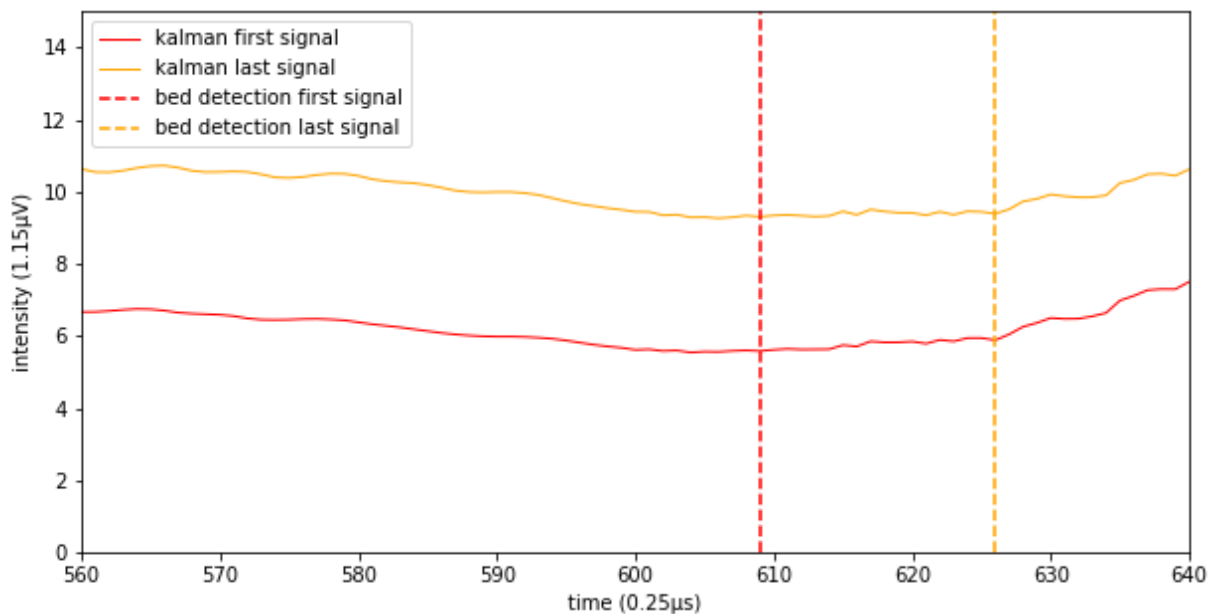


Figure 4.4: Zoomed in. Kalman filter line of the first and last signal. The ASED-sensor measured above metal plate at a manually measured water depth of 0.210 m converted to time 536-time steps.

For the water depths experiments, the shallow depths ( $\leq 0.30$  m) are detected shallower than the manual measurement above the metal plate. The deeper depths ( $> 0.30$  m) are detected deeper compared to the manual measurement. But this only occurred during the water depth experiment. Probably, this was caused by the strong reflection of the signal by the metal plate and interference of the reflected signals.

During the soil type and dilution experiments, the measured depth decreases over time ( $\approx 15$  minutes). This can be explained by settling of suspension. Dilution 41.27% of 0.48 fraction of sand had a bed detected depth of 0.399 m, whereas the manual measurement

was 0.368 m. This is a difference in depth of 0.031 m. The amount of soil dilution in the bucket has a height of 0.10 m. Probably, the ASED-sensor measured through the dilution and gets delayed by the dilution, due to scattering or a lower speed of sound in the dilution. First, the ASED-sensor sent 1 pulse and now 5 pulses. With 1 pulse the ASED-sensor could not measure through the SSC, but with 5 pulses the ASED-sensor can measure through a 10 cm layer of suspended sediment.

During the field experiments, the bed detected depth fluctuated a lot, this could be due to SSC, the deformation of the bed or the sediment of the upper layer of the bed getting in suspension just above the bed. The ASED-sensor is not continuously sending at the same frequency of 300 kHz, this can be obtained with the FFT-analysis.

As the field measurements have multiple peaks in the signal reflected by the bed, the script should not only find the maximum peak but should also find the first peak within the signal reflected by the bed. The sudden increase in amplitude will be searched for starting 300-time steps backwards in time from the maximum peak. Therefore, the parameter setting does not need to be adjusted.

During the Western Scheldt experiment, the difference between the ASED-sensor and the erosion pin measurements is likely caused by the fact that these two measurements did not measure the exact same spots. The erosion pins were located at 2 metres from the ASED-sensor. The distance between the erosion pins was 1 metre. The erosion pins were not spread around the ASED-sensor. Footsteps (Figure 2.10) were made by placing the ASED-sensor and the erosion pins. The footsteps were up to 30 cm deep; this influenced the local bed level dynamics. Hereby, the bed level dynamics can change per meter. Three weeks after the ASED-sensor was removed, the footsteps were still visible. The erosion pins measured for 4 more days compared to the ASED-sensor.

#### 4.4 Comparison with the SED-sensor

The SED-sensor is a stand-alone device that measures the bed level using 194 light cells of 2 mm each. The SED-sensor is placed vertically in the ground and detects the boundary between light (air) and dark (soil). The SED-sensor monitors continuously during non-submerged and diurnal conditions with a high vertical resolution (2mm) (Hu *et al.*, 2015). The measure domain of the SED-sensor is 388 mm. The accuracy of the SED-sensor script can be measured with standard deviations created by averaging the bed levels over an enclosed measuring period. On average the accuracy for the bed level prediction is 4 mm (2 cells) (De Mey, 2016). The uncertainty increases as the scouring height is predicted, here standard deviation could increase up to 16 mm (8 cells) (De Mey, 2016).

The ASED-sensor uses a pulsed acoustic signal of approximately 300 kHz to measure bed levels during submerged and nocturnal conditions. The ASED-sensor is placed with a frame above the bed (Figure 2.15). The ASED-sensor contains a high vertical resolution of 2.5 mm, with a measure domain of 0.25 m, which is almost half of the measure domain of the SED-sensor. The accuracy of the ASED-sensor script can be measured with standard deviations created by averaging the bed levels over an enclosed measuring period, during the lab experiments. On average the accuracy for the bed level is between 2 mm and 4 mm.

## 4.5 Further possibilities ASED-sensor

### 4.5.1 Inclination angle

In the Eastern Scheldt experiment, the inclination angle between the ASED-sensor and the vertical is negligible, causing a limited effect on the bed level measurement. However, the inclination angle can be larger in other situations. Especially in the environments with soft bed substance, like the Western Scheldt, the inclination angle may vary slightly during events with strong hydrodynamic forces (Hu *et al.*, 2015). Including additional inclination angle measurements in order to record the sensor movement during extreme conditions and to correct the corresponding bed-level measurement is useful (Hu *et al.*, 2015).

The ASED-sensor is equipped with an inclinometer and is recorded during all experiments. The inclinometer registers the angle of the ASED-sensor in an acceleration range from -1000 to 1000 which stand for -2G to 2G. The G stands for gravitational force. This is a measurement of the type of acceleration that causes a perception of weight. The inclination angle of the ASED-sensor can be calculated in Equation 2.

$$\phi = \cos^{-1} \left( \frac{A_{Z,OUT}}{\sqrt{A_{X,OUT}^2 + A_{Y,OUT}^2 + A_{Z,OUT}^2}} \right) \quad (2)$$

Where A is the axis in X, Y and Z (Figure 4.5).  $\phi$  ranges only from 0° to 180°. During the lab experiments, it can be checked whether the ASED-sensor detected the depth under an incident angle. During the field experiments, it can be checked whether waves affected the position of the ASED-sensor.

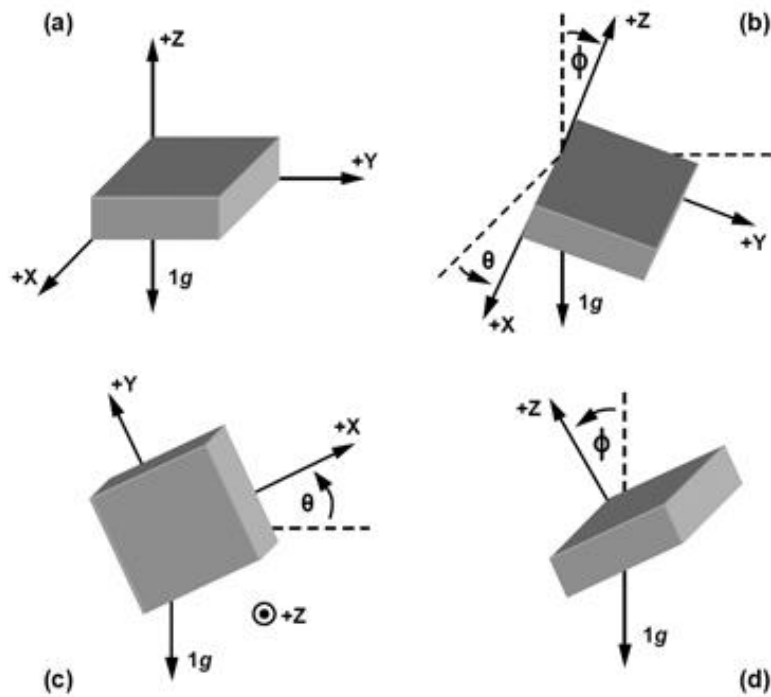


Figure 4.5: Angles of the spherical coordinate system for calculating the inclination of the ASED-sensor (Fisher, 2011).

## 4.6 Extra measurements

The extra measurements which were done, were to measure fluid mud and SSC. The ASED-sensor was placed upside-down to measure through the fluid mud. The idea was to recognize the boundary of air and fluid mud. First, this test was done with seawater from the Eastern Scheldt, to see if the border air and water was easily detected. Thereafter, the dilutions of soil type 0.12 sand fraction were used. The dilutions were 33%, 47% and 67%. Unfortunately, due to lack of time, this measurement was not analysed.

The reflection of the signal by the bed was undetectable for the SSC experiment (Appendix A.9). Therefore, this experiment was not further analysed.

### 4.6.1 Extra validation measurements

At most outside lab experiments the Echologger EU400 was used as an extra validation for the ASED-sensor (Appendix A.9). The echologger measures with a measurement frequency of 450 kHz and has a measurement interval of 3 seconds. The echologger is combined with the Trimble R8s Global Navigation Satellite System (GNSS) receiver. This GNSS receiver receives a Real Time Kinematic (RTK) correction signal. This will make the position accurate up to 1 cm horizontally and 3 cm vertically (Feng *et al.*, 2008). The water tank was positioned outside because the Trimble receiver does not receive the GPS signal in buildings. The echologger does not collect data without a GPS receiver. The GPS data (3 cm) is less accurate than the Echologger data (1 mm). For the depth values, only the echologger data is used and the GPS data is left out for further potential research.

## 5 Conclusions

The objective of this research was to assess the applicability of the ASED-sensor for measuring bed level changes in intertidal areas. This research objective was achieved by elaborating three different research questions, that are enumerated below.

*(1) What is the ASED-sensor?*

The ASED-sensor is a stand-alone device that measures the propagation time of an acoustic signal reflected by the bed. The reflection of the signal by the bed is detected by a sudden increase in amplitude. The signal has a frequency of approximately 300 kHz; the return signal is sampled at 4MHz.

*(2) For what range of environmental conditions can the ASED-sensor detect a bed?*

The practical measurement domain for the ASED-sensor is from 0.20 m to 0.45 m, according to the raw data analysis of all lab experiments. The ASED-sensor can detect the bed for all evaluated soil types, but it cannot determine the soil type from the shape of the signal. With a 0.8 fraction of sand, the ASED-sensor can detect a reflection of the signal by the bed up to 45.47% dilution. Likewise, with a 0.48 fraction of sand, the ASED-sensor can detect a signal reflected by the bed up to 41.27% dilution. For the 0.65, 0.40 and 0.12 fractions of sand, the signal reflected by the bed cannot be detected for dilutions higher than 40%. During the waves and current forcing, the bed was easily detected in the wave flume. And during the field experiments, the bed was easily detected as well. The shape of the signal reflected by the bed changed during the longer duration experiments. This can be due to the SSC, the deformation of the bed or the sediment of the upper layer of the bed getting in suspension just above the bed.

*(3) What converting method is suitable for detecting the bed using the raw data of the ASED-sensor?*

The lab and field experiments were set up to evaluate the capabilities of the newly developed ASED-sensor. An algorithm needed to be developed to detect the first strong reflection in the raw data. Three methods have been analysed to convert the raw data of the ASED-sensor into bed levels, namely the FFT analysis, the envelope method and the Kalman filter. The computation time of the FFT analysis is short, but the frequency of the FFT analysis fluctuated a lot. The envelope method has a high computation time for calculating the envelopes of the raw data. The envelope method results fluctuate even more than the FFT analysis. Therefore, the FFT analysis and the envelope method are not suitable. Finally, the Kalman filter method is evaluated. The Kalman filter smoothes the raw data of the ASED-sensor and can detect the reflection of the signal by the bed at the sudden increase in amplitude.

The newly developed script with the Kalman Filter shows promising results in the lab and field experiments, despite several uncertainties within the experiment itself. The coefficient of determination ( $R^2$ ) between the depth values detected by the script and the manual measurements was 0.99 for the lab experiments. The standard deviation of the script is 2 mm, obtained from the lab experiments.

The theoretical resolution is 2.5 mm according to the specifications of the transducer. The actual accuracy of the whole system, the ASED-sensor and the script, can be measured with standard deviations created by averaging the bed levels over an enclosed measuring period, during the lab experiments. The bed level is fixed during the lab experiments. The actual accuracy is 2 mm to 4 mm, obtained from the lab experiments.

## 6 Recommendations

1. The ASED-sensor does not measure with a constant frequency of 300 kHz. Therefore, the depth can fluctuate in detecting the bed level. A constant measure frequency of 300 kHz would be recommended during the experiments.
2. A lot of initial and periodic noise occurred during the lab experiments in the water tank. Whereas, a little initial and periodic noise occurred during the wave flume and field experiments. Most likely, the signal is reflected multiple times in the water tank. Therefore, for further research a bigger water tank or acoustic damping at the bottom and on the sides of the water tank is required during lab experiments in a water tank.
3. The script can be used to convert raw data of the ASED-sensor into bed level data. During the field experiments, the reflection of the signal by the bed had multiple peaks. First, the maximum peak was at the beginning of the bed reflection but over time the maximum peak shifted to the right (deeper). The sudden increase in amplitude will be searched starting from 300-time steps backwards in time to the maximum peak, this is the default parameter setting. Therefore, this parameter setting needs to be adjusted to a larger value. Another possibility is to find the multiple peaks of the signal reflected by the bed. Not the maximum peak should be used but the first peak of the signal reflected by the bed.
4. During the experiments, the salinity was assumed to be constant. But the salinity varies in the Western Scheldt, due to tide, fresh water from the river and the season. Therefore, the salinity should be measured or retrieved from the Rijkswaterstaat website. This can already give a depth difference of 2 mm at a depth of 0.45 m.
5. The erosion pins should be placed around the ASED-sensor set-up during field experiments, instead of at one location with 1 m between the erosion pins. Creating footsteps in the area around the set-up of the ASED-sensor was unavoidable. Therefore, the bed level dynamics can change locally.
6. The ASED-sensor is applicable at a measurement domain from 0.20 m to 0.45 m. The ASED-sensor can measure a silty bed, as at the Kapellebank in the Western Scheldt. Therefore, the ASED-sensor is applicable at intertidal areas at the coasts, with a silty bed, as at the Kapellebank.

# References

- Adam, S., Vitse, I., Johannsen, C. and Monbaliu, J. (2006) 'Sediment type unsupervised classification of the Molenplaat, Westerschelde Estuary, the Netherlands', *EARSeL eProceedings*, 5(2), pp. 146–160.
- Allen, J. R. L. (2000) 'Morphodynamics of Holocene salt marshes : a review sketch from the Atlantic and Southern North Sea coasts of Europe', *Pergamon*, p. 77.
- Van den Berg, J. H., Jeuken, C. J. L. and van der Spek, A. J. F. (1996) 'Hydraulic processes affecting the morphology and evolution of the Westerschelde estuary', in Nordstrom, K. E. and Roman, C. T. (eds) *Estuarine shores : evolution, environments, and human alterations*. John Wiley & Sons Ltd., pp. 157–184.
- Bouma, T. J. *et al.* (2014) 'Identifying knowledge gaps hampering application of intertidal habitats in coastal protection : Opportunities & steps to take', *Coastal Engineering*. Elsevier B.V., 87, pp. 147–157. doi: 10.1016/j.coastaleng.2013.11.014.
- Bouma, T. J., van Belzen, J., Balke, T., van Dalen, J., Klaassen, P., Hartog, A. M., Callaghan, D. P., Hu, Z., Stive, M. J. F., Temmerman, S. and Herman, P. M. J. (2016) 'Short-term mudflat dynamics drive long-term cyclic salt marsh dynamics', *Limnology and Oceanography*, 61(6), pp. 2261–2275. doi: 10.1002/lno.10374.
- Bouma, T. J., De Vries, M. B., Low, E., Kusters, L., Herman, P. M. J., Tánčzos, I. C., Temmerman, S., Hesselink, A., Meire, P. and Van Regenmortel, S. (2005) 'Flow hydrodynamics on a mudflat and in salt marsh vegetation: Identifying general relationships for habitat characterisations', *Hydrobiologia*, 540(1–3), pp. 259–274. doi: 10.1007/s10750-004-7149-0.
- Burrowes, G. and Khan, J. Y. (2011) *Short-Range Underwater Acoustic Communication Networks, Autonomous Underwater Vehicles*. doi: 978-953-307-432-0.
- Callaghan, D. P., Bouma, T. J., Klaassen, P., van der Wal, D., Stive, M. J. F. and Herman, P. M. J. (2010) 'Hydrodynamic forcing on salt-marsh development: Distinguishing the relative importance of waves and tidal flows', *Estuarine, Coastal and Shelf Science*. Elsevier Ltd, 89(1), pp. 73–88. doi: 10.1016/j.ecss.2010.05.013.
- Christiansen, T., Wiberg, P. L. and Milligan, T. G. (1999) 'Flow and Sediment Transport on a Tidal Salt Marsh', *Estuarine, Coastal and Shelf Science*, pp. 315–331. doi: 10.1006/ecss.2000.0548.
- Corbishley, P. and Rodriguez-Villegas, E. (2007) 'A nanopower bandpass filter for detection of an acoustic signal in a wearable breathing detector', *IEEE Transactions on Biomedical Circuits and Systems*, 1(3), pp. 163–171. doi: 10.1109/TBCAS.2007.913129.
- Van Damme, S., Struyf, E., Maris, T., Ysebaert, T., Dehairs, F., Tackx, M., Heip, C. and Meire, P. (2005) 'Spatial and temporal patterns of water quality along the estuarine salinity gradient of the Scheldt estuary ( Belgium and The Netherlands ): results of an integrated monitoring approach', *Hydrobiologia*, 540(1), pp. 29–45. doi: 10.1007/s10750-004-7102-2.
- Doody, J. P. (2004) "'Coastal squeeze" – an historical perspective', *Journal of Coastal Conservation*, 10(1), p. 129. doi: 10.1652/1400-0350(2004)010[0129:CSAHP]2.0.CO;2.
- Fagherazzi, S., Kirwan, M. L., Mudd, S. M., Guntenspergen, G. R., Temmerman, S.,

- Rybczyk, J. M., Reyes, E., Craft, C. and Clough, J. (2012) 'Numerical models of salt marsh evolution: Ecological, geomorphic, and climatic factors', *Review of Geophysics*, 50(2011), pp. 1–28. doi: 10.1029/2011RG000359.1.INTRODUCTION.
- Feng, Y. and Wang, J. (2008) 'GPS RTK Performance Characteristics and Analysis', *Journal of Global Positioning Systems*, 7(1), pp. 1–8. doi: 10.5081/jgps.7.1.1.
- Fettweis, M., Sas, M. and Monbaliu, J. (1998) 'Seasonal , Neap-spring and Tidal Variation of Cohesive Sediment Concentration in the Scheldt Estuary', *Estuarine, Coastal and Shelf Science*, pp. 21–36.
- Fisher, C. J. (2011) *Using An Accelerometer for Inclination Sensing, Convergence Promotions LLC*. Available at: <https://www.digikey.nl/en/articles/techzone/2011/may/using-an-accelerometer-for-inclination-sensing>.
- Friedrichs, C. T. (2012) *Tidal Flat Morphodynamics: A Synthesis, Treatise on Estuarine and Coastal Science*. Elsevier Inc. doi: 10.1016/B978-0-12-374711-2.00307-7.
- Ganthy, F., Sottolichio, A. and Verney, R. (2013) 'Seasonal modification of tidal flat sediment dynamics by seagrass meadows of *Zostera noltii* (Bassin d'Arcachon, France)', *Journal of Marine Systems*. Elsevier B.V., 109–110(SUPPL.), pp. S233–S240. doi: 10.1016/j.jmarsys.2011.11.027.
- Gedan, K. B. ., Kirwam, M. L. ., Wolanski, E., Barbier, E. B. . and Silliman, B. R. (2011) 'The present and future role of coastal wetland vegetation in protecting shorelines: answering recent challenges to the paradigm', *Climatic Change*, 106, pp. 7–29. doi: 10.1007/s10584-010-0003-7.
- Green, M. O. and Coco, G. (2014) 'Review of wave driven sediment resuspension and transport in estuaries', *Reviews of Geophysics*, 52(1), pp. 77–117. doi: 10.1002/2013RG000437.Received.
- Hartmann, D. L. (2008) *ATM 552 Time Series Analysis-Spectral Section 6b*. doi: 10.1016/B978-0-7506-7444-7/50068-6.
- Haykin, S. (2002) 'Kalman Filtering and Neural Networks', in Haykin, S. (ed.) *Kalman Filtering and Neural Networks*. 1st edn. Wiley-Interscience, pp. 1–21. doi: 10.1002/0471221546.ch1.
- Le Hir, P., Roberts, W., Cazaillet, O., Christie, M., Bassoullet, P. and Bacher, C. (2000) 'Characterization of intertidal flat hydrodynamics', *Continental Shelf Research*, 20(12–13), pp. 1433–1459. doi: 10.1016/S0278-4343(00)00031-5.
- Horstman, E., Balke, T., Bouma, T., Dohmen-Janssen, M. and Hulscher, S. (2011) 'Optimizing Methods To Measure Hydrodynamics in Coastal Wetlands: Evaluating the Use and Positioning of Adv, Adcp and Hr-Adcp', *Coastal Engineering Proceedings*, 1(32), pp. 1–11. doi: 10.9753/icce.v32.waves.51.
- Hu, Z., Lenting, W., van der Wal, D. and Bouma, T. J. (2015) 'Continuous monitoring bed-level dynamics on an intertidal flat: Introducing novel, stand-alone high-resolution SED-sensors', *Geomorphology*, 245(December), pp. 223–230. doi: 10.1016/j.geomorph.2015.05.027.
- Julier, S. J. and Uhlmann, J. K. (1997) 'A new extension of the Kalman filter to nonlinear systems', *SPIE*, 3068, p. 12. doi: 10.1117/12.280797.
- Kongsberg (2017) 'Multibeam echo sounder EM2040', p. 2.

- Kongsberg Maritime AS (2017) 'EA440 Hydrographic Single Beam Echo Sounder', (September). Available at: <http://www.amloceanographic.com/Technical-Demo/Single-Beam-Echo-Sounder>.
- Lawler, D. M. (2008) 'Advances in the continuous monitoring of erosion and deposition dynamics: Developments and applications of the new PEEP-3T system', *Geomorphology*, 93(1–2), pp. 17–39. doi: 10.1016/j.geomorph.2006.12.016.
- De Leeuw, J., Apon, L. P., Herman, P. M. J., Demunck, W. and Beeftink, W. G. (1992) 'Vegetation response to experimental and natural disturbance in 2 salt-marsh plant-communities in the Southwest Netherlands', *Netherlands Journal of Sea Research*, 30(568), pp. 279–288. doi: 10.1016/0077-7579(92)90066-n.
- Leonard, L. A. and Luther, M. E. (1995) 'Flow hydrodynamics in tidal marsh canopies', *Limnology and Oceanography*, 40(8), pp. 1474–1484. doi: 10.4319/lo.1995.40.8.1474.
- Louis, R. H. S., Siems, W. F. and Hill, H. H. (1992) 'Apodization Functions in Fourier Transform Ion Mobility Spectrometry', *Analytical Chemistry*, 64(2), pp. 171–177. doi: 10.1021/ac00026a015.
- Lurton, X. (2010) *An Introduction to Underwater Acoustics: Principles and Applications*. Second. Edited by P. Blondel, X. Lurton, L. Leviandier, M. Collins, Y. Le Gall, G. Llorc-Pujol, C. Sintès, G. Lapierre, V. Mazauric, C. Vrignaud, A. Pacault, and S. De Ruiter. Berlin: Springer-Praxis.
- Lyon, D. (2009) 'The discrete fourier transform, part 4: Spectral leakage', *Journal of Object Technology*, 8(7), pp. 23–34. doi: 10.5381/jot.2009.8.7.c2.
- McLelland, S. J. and Nicholas, A. P. (2000) 'A new method for evaluating errors in high-frequency ADV measurements', *Hydrological Processes*, 14(2), pp. 351–366. doi: 10.1002/(SICI)1099-1085(20000215)14:2<351::AID-HYP963>3.0.CO;2-K.
- Mendelsohn, R., Emanuel, K., Chonabayashi, S. and Bakkensen, L. (2011) 'The Impact of Climate Change on Global Tropical Storm Damages', *Nature Climate Change*, 2(February), pp. 1–39. doi: 10.1038/nclimate1357.
- De Mey, J. M. G. (2016) 'Sedimentation and erosion in intertidal vegetated foreshores, analysing foreshores by developing a bed level script for the SED Sensor', p. 68.
- Möller, I. (2006) 'Quantifying saltmarsh vegetation and its effect on wave height dissipation: Results from a UK East coast saltmarsh', *Estuarine, Coastal and Shelf Science*, 69(3–4), pp. 337–351. doi: 10.1016/j.ecss.2006.05.003.
- Möller, I., Kudella, M., Rupprecht, F., Spencer, T., Paul, M., Van Wesenbeeck, B. K., Wolters, G., Jensen, K., Bouma, T. J., Miranda-Lange, M. and Schimmels, S. (2014) 'Wave attenuation over coastal salt marshes under storm surge conditions', *Nature Geoscience*, 7(10), pp. 727–731. doi: 10.1038/NGEO2251.
- Möller, I., Spencer, T., French, J. R., Leggett, D. J. and Dixon, M. (1999) 'Wave Transformation Over Salt Marshes : A Field and Numerical Modelling Study from North Norfolk ', *Estuarine, Coastal and Shelf Science*, 49, pp. 411–426.
- Nielsen, P. (2009) *Coastal and estuarine processes*.
- Nolte, S., Koppenaar, E. C., Esselink, P., Dijkema, K. S., Schuerch, M., De Groot, A. V., Bakker, J. P. and Temmerman, S. (2013) 'Measuring sedimentation in tidal marshes: A review on methods and their applicability in biogeomorphological studies', *Journal of Coastal Conservation*, 17(3), pp. 301–325. doi: 10.1007/s11852-013-0238-3.

- NPL National Physical Laboratory (2000) 'Underwater Acoustics Technical Guides - Speed of Sound in Sea-Water', 340, pp. 1–7.
- R2Sonic (2014) 'Sonic 2024/2022', 001(96000001), p. 210.
- Ranwell, D. D. (1964) 'Spartina Salt Marshes in Southern England : II. Rate and Seasonal Pattern of Sediment Accretion', *British Ecological Society Stable*, 52(1), pp. 79–94.
- Ridd, P. V. (1992) 'A sediment level sensor for erosion and siltation detection', *Estuarine, Coastal and Shelf Science*, 35(4), pp. 353–362. doi: 10.1016/S0272-7714(05)80032-0.
- Riegl, B., Walker, B., Moyer, R., Hernandex-Cruz, L., Foster, J. G. and Foster, C. (2004) *Development of GIS Maps for Southeast Florida Coral Reefs*. Diana Beach.
- Stokes, D. J., Healy, T. R. and Cooke, P. J. (2010) 'Expansion Dynamics of Monospecific, Temperate Mangroves and Sedimentation in Two Embayments of a Barrier-Enclosed Lagoon, Tauranga Harbour, New Zealand', *Journal of Coastal Research*, 26(26), pp. 113–122. doi: 10.2112/08-1043.1.
- Thorne, P. D. and Hanes, D. M. (2002) 'A review of acoustic measurement of small-scale sediment processes', *Continental Shelf Research*, 22, pp. 603–632.
- USACE (1989) 'Environmental Engineering for Coastal Protection', *U.S. Army Corps of Engineers, Engineer Manual*, 15(11), p. 129. doi: 10.1093/ntr/nts294.
- Volkenborn, N., Martin, D. and Reise, K. (2008) 'Sediment destabilizing and stabilizing bio-engineers on tidal flats : cascading effects of experimental exclusion', *Springer*, pp. 27–35. doi: 10.1007/s10152-008-0140-9.
- Vuik, V., Jonkman, S. N., Borsje, B. W. and Suzuki, T. (2016) 'Nature-based flood protection: The efficiency of vegetated foreshores for reducing wave loads on coastal dikes', *Coastal Engineering*. Elsevier B.V., 116, pp. 42–56. doi: 10.1016/j.coastaleng.2016.06.001.
- van der Wal, D., Wielemaker- van den Dool, A. and Herman, P. M. J. (2008) 'Spatial patterns, rates and mechanisms of saltmarsh cycles (Westerschelde, The Netherlands)', *Estuarine, Coastal and Shelf Science*, 76, pp. 357–368. doi: 10.1016/j.ecss.2007.07.017.
- Wamsley, T. V., Cialone, M. A., Smith, J. M., Atkinson, J. H. and Rosati, J. D. (2010) 'The potential of wetlands in reducing storm surge', *Ocean Engineering*. Elsevier, 37(1), pp. 59–68. doi: 10.1016/j.oceaneng.2009.07.018.
- Willemsen, P. W. J. M., Borsje, B. W., Hulscher, S. J. M. ., Van der Wal, D., Zhu, Z., Oteman, B., Evans, B., Möller, I. and Bouma, T. J. (2018) 'Quantifying bed level dynamics at the transition of tidal flat and salt marsh : can we understand the lateral location of the marsh edge?', *Journal of Geophysical Research: Earth Surface*.
- Yang, S. L., Shi, B. W., Bouma, T. J., Ysebaert, T. and Luo, X. X. (2012) 'Wave Attenuation at a Salt Marsh Margin : A Case Study of an Exposed Coast on the Yangtze Estuary', *Estuaries and Coasts*, 35, pp. 169–182. doi: 10.1007/s12237-011-9424-4.

# A Appendices

## A.1 ASED-sensor

### A.1.1 The transducer



#### Applications:

- Level measurement
- Automation control
- Proximity
- Obstacle avoidance
- Robotics

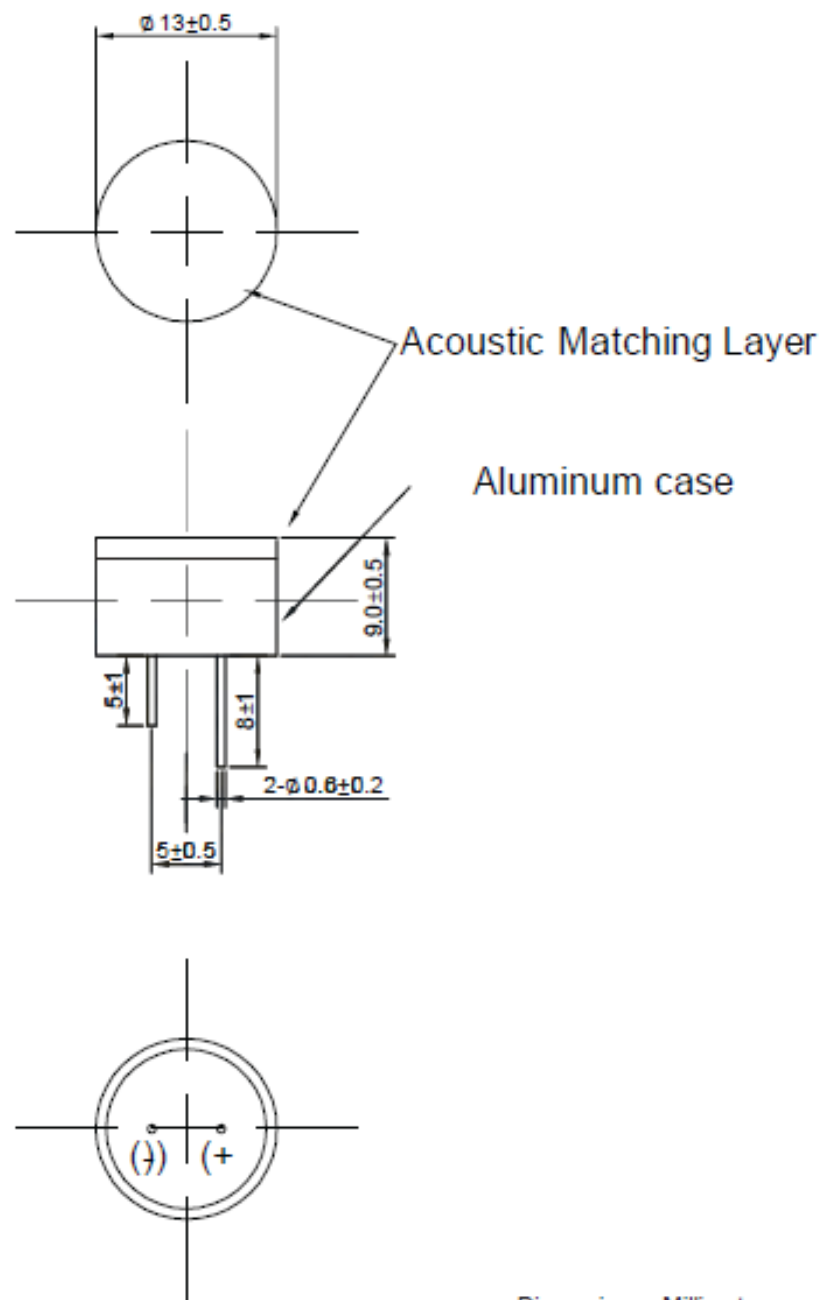
#### Features:

- Rugged sealed construction
- Cylindrical design allows for installation in various applications
- Short-range measurement capabilities

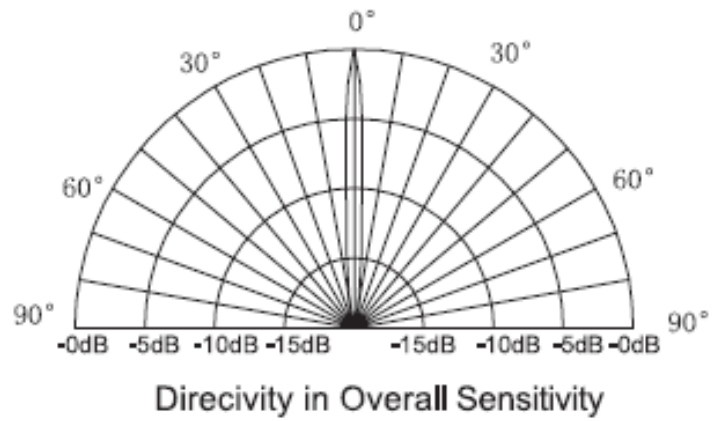
#### Technical Terms:

No	Item	Specification
1	Part Number	MCUSD13A300B09RS
2	Construction	Water Proof
3	Using Method	Dual Use
4	Centre Frequency	300 ± 15kHz
5	Receive Sensitivity Echo (V)	≥800mV (driven signal: 200Vp-p, 300kHz, at 20cm)
6	Capacitance (pF)	300 ± 25% at 1kHz
7	Max. Input Voltage	400Vp-p
8	Directivity (-3dB)	10 ± 2
9	Distance of Detection	0.04m to 1m
10	Protection Class	IP65
11	Material	Aluminium
12	Operating Temperature Range	-20°C to +80°C
13	Storage Temperature Range	-35°C to +85°C

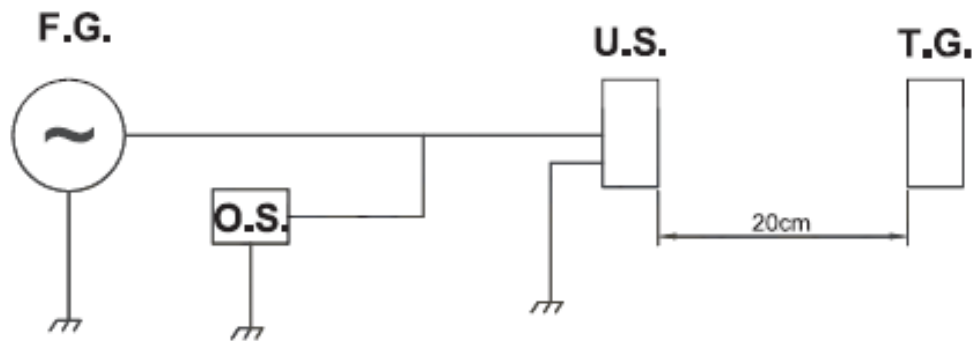
Drawing:



### Beam Pattern:



### Test Circuit:



- F.G. : Function Generator
- U.S. : Ultrasonic Sensor
- T.G. : Target
- O.S. : Oscilloscope



# 10-Bit, 40 MSPS, 3 V, 74 mW A/D Converter

## AD9203

### FEATURES

- CMOS 10-Bit, 40 MSPS sampling A/D converter
- Power dissipation: 74 mW (3 V supply, 40 MSPS)  
17 mW (3 V supply, 5 MSPS)
- Operation between 2.7 V and 3.6 V supply
- Differential nonlinearity:  $-0.25$  LSB
- Power-down (standby) mode, 0.65 mW
- ENOB: 9.55 @  $f_{IN} = 20$  MHz
- Out-of-range indicator
- Adjustable on-chip voltage reference
- IF undersampling up to  $f_{IN} = 130$  MHz
- Input range: 1 V to 2 V p-p differential or single-ended
- Adjustable power consumption
- Internal clamp circuit

### APPLICATIONS

- CCD imaging
- Video
- Portable instrumentation
- IF and baseband communications
- Cable modems
- Medical ultrasound

### GENERAL DESCRIPTION

The AD9203 is a monolithic low power, single supply, 10-bit, 40 MSPS analog-to-digital converter, with an on-chip voltage reference. The AD9203 uses a multistage differential pipeline architecture and guarantees no missing codes over the full operating temperature range. Its input range may be adjusted between 1 V and 2 V p-p.

The AD9203 has an onboard programmable reference. An external reference can also be chosen to suit the dc accuracy and temperature drift requirements of an application.

An external resistor can be used to reduce power consumption when operating at lower sampling rates. This yields power savings for users who do not require the maximum sample rate. This feature is especially useful at sample rates far below 40 MSPS. Excellent performance is still achieved at reduced power. For example, 9.7 ENOB performance may be realized with only 17 mW of power, using a 5 MHz clock.

A single clock input is used to control all internal conversion cycles. The digital output data is presented in straight binary or twos complementary output format by using the DFS pin. An

#### Rev. B

Information furnished by Analog Devices is believed to be accurate and reliable. However, no responsibility is assumed by Analog Devices for its use, nor for any infringements of patents or other rights of third parties that may result from its use. Specifications subject to change without notice. No license is granted by implication or otherwise under any patent or patent rights of Analog Devices. Trademarks and registered trademarks are the property of their respective owners.

### FUNCTIONAL BLOCK DIAGRAM

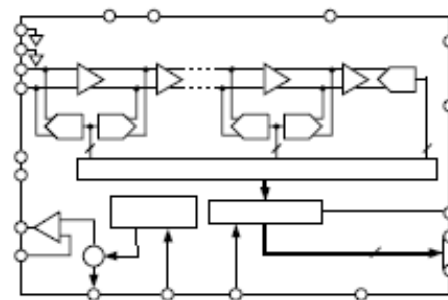


Figure 1.

out-of-range signal (OTR) indicates an overflow condition that can be used with the most significant bit to determine over- or underrange.

The AD9203 can operate with a supply range from 2.7 V to 3.6 V, an attractive option for low power operation in high-speed portable applications.

The AD9203 is specified over industrial ( $-40^{\circ}\text{C}$  to  $+85^{\circ}\text{C}$ ) temperature ranges and is available in a 28-lead TSSOP package.

### PRODUCT HIGHLIGHTS

**Low Power**—The AD9203 consumes 74 mW on a 3 V supply operating at 40 MSPS. In standby mode, power is reduced to 0.65 mW.

**High Performance**—Maintains better than 9.55 ENOB at 40 MSPS input signal from dc to Nyquist.

**Very Small Package**—The AD9203 is available in a 28-lead TSSOP.

**Programmable Power**—The AD9203 power can be further reduced by using an external resistor at lower sample rates.

**Built-In Clamp Function**—Allows dc restoration of video signals.

One Technology Way, P.O. Box 9106, Norwood, MA 02062-9106, U.S.A.  
Tel: 781.329.4700 [www.analog.com](http://www.analog.com)  
Fax: 781.326.8703 © 2004 Analog Devices, Inc. All rights reserved.

## SPECIFICATIONS

AVDD = 3 V, DRVDD = 3 V, F<sub>S</sub> = 40 MSPS, input span from 0.5 V to 2.5 V, internal 1 V reference, PWRCON = AVDD, 50% clock duty cycle, T<sub>MIN</sub> to T<sub>MAX</sub> unless otherwise noted.

Table 1.

Parameter	Symbol	Min	Typ	Max	Unit	Conditions
RESOLUTION			10		Bits	
MAX CONVERSION RATE	F <sub>S</sub>	40			MSPS	
PIPELINE DELAY				5.5	Clock Cycles	
DC ACCURACY						
Differential Nonlinearity	DNL		± 0.25 ± 0.7	LSB		
Integral Nonlinearity	INL		± 0.65 ± 1.4	LSB		
Offset Error	E <sub>ZS</sub>		± 0.6 ± 2.8	% FSR		
Gain Error	E <sub>F<sub>S</sub></sub>		± 0.7 ± 4.0	% FSR		
ANALOG INPUT						
Input Voltage Range	A <sub>IN</sub>	1		2	V p-p	
Input Capacitance	C <sub>IN</sub>		1.4		pF	
Aperture Delay	T <sub>AP</sub>		2.0		ns	
Aperture Uncertainty (Jitter)	T <sub>AJ</sub>		1.2		ps rms	
Input Bandwidth (-3 dB)	BW		390		MHz	
Input Referred Noise			0.3		mV	Switched, Single-Ended
INTERNAL REFERENCE						
Output Voltage (0.5 V Mode)	VREF		0.5		V	REFSENSE = VREF
Output Voltage (1 V Mode)	VREF		1		V	REFSENSE = GND
Output Voltage Tolerance (1 V Mode)			± 5	± 30	mV	
Load Regulation			0.65	1.2	mV	1.0 mA Load
POWER SUPPLY						
Operating Voltage	AVDD	2.7	3.0	3.6	V	
	DRVDD	2.7	3.0	3.6	V	
Analog Supply Current	I <sub>AVDD</sub>		20.1	22.0	mA	
Digital Supply Current	I <sub>DRVDD</sub>		4.4	6.0	mA	f <sub>IN</sub> = 4.8 MHz, Output Bus Load = 10pF
			9.5	14.0	mA	f <sub>IN</sub> = 20 MHz, Output Bus Load = 20 pF
Power Consumption			74	84.0	mW	f <sub>IN</sub> = 4.8 MHz, Output Bus Load = 10pF
			88.8	108.0	mW	f <sub>IN</sub> = 20 MHz, Output Bus Load = 20 pF
Power-Down	P <sub>D</sub>		0.65	1.2	mW	
Power Supply Rejection Ratio	PSRR		0.04	± 0.25	% F <sub>S</sub>	
DYNAMIC PERFORMANCE (A <sub>IN</sub> = 0.5 dBFS)						
Signal-to-Noise and Distortion	SINAD					
f = 4.8 MHz			59.7		dB	
f = 20 MHz		57.2	59.3		dB	
Effective Bits	ENOB					
f = 4.8 MHz			9.6		Bits	
f = 20 MHz		9.2	9.55		Bits	
Signal-to-Noise Ratio	SNR					
f = 4.8 MHz			60.0		dB	
f = 20 MHz		57.5	59.5		dB	
Total Harmonic Distortion	THD					
f = 4.8MHz			-76.0		dB	
f = 20 MHz			-74.0	-65.0	dB	
Spurious-Free Dynamic Range	SFDR					
f = 4.8 MHz <sup>1</sup>			80		dB	
f = 20 MHz		67.8	78		dB	

# AD9203

Parameter	Symbol	Min	Typ	Max	Unit	Conditions
Two-Tone Intermodulation Distortion	IMD		68		dB	$f = 44.49$ MHz and $45.52$ MHz
Differential Phase	DP		0.2		Degree	NTSC 40 IRE Ramp
Differential Gain	DG		0.3		%	
<b>DIGITAL INPUTS</b>						
High Input Voltage	$V_{IH}$	2.0			V	
Low Input Voltage	$V_{IL}$			0.4	V	
Clock Pulse Width High		11.25			ns	
Clock Pulse Width Low		11.25			ns	
Clock Period <sup>2</sup>			25		ns	
<b>DIGITAL OUTPUTS</b>						
High-Z Leakage	$I_{OZ}$			$\pm 5.0$	$\mu$ A	Output = 0 to DRVDD
Data Valid Delay	$t_{OD}$		5		ns	$C_L = 20$ pF
Data Enable Delay	$t_{DEN}$		6		ns	$C_L = 20$ pF
Data High-Z Delay	$t_{DHZ}$		6		ns	$C_L = 20$ pF
<b>LOGIC OUTPUT (with DRVDD = 3 V)</b>						
High Level Output Voltage ( $I_{OH} = 50$ $\mu$ A)	$V_{OH}$	2.95			V	
High Level Output Voltage ( $I_{OH} = 0.5$ mA)	$V_{OH}$	2.80			V	
Low Level Output Voltage ( $I_{OL} = 1.6$ mA)	$V_{OL}$			0.3	V	
Low Level Output Voltage ( $I_{OL} = 50$ $\mu$ A)	$V_{OL}$			0.05	V	

<sup>1</sup> Differential Input (2 V p-p).

<sup>2</sup> The AD9203 will convert at clock rates as low as 20 kHz.

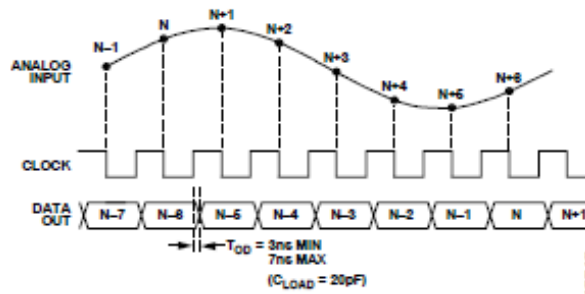


Figure 2. Timing Diagram

## OUTLINE DIMENSIONS

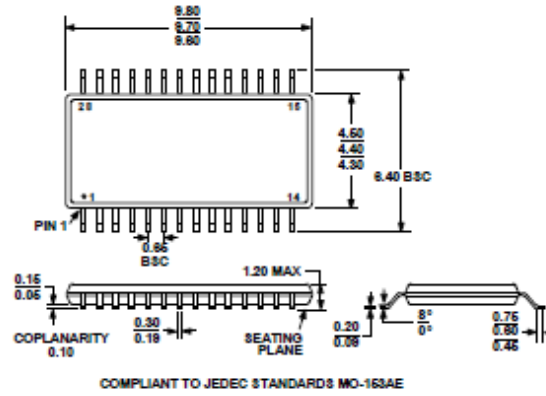


Figure 47. 28-Lead Thin Shrink Small Outline Package  
(RU-28)  
Dimensions shown in inches and (millimeters)

## ORDERING GUIDE

Model	Temperature Range	Package Description	Package Option
AD9203ARU	-40°C to +85°C	28-Lead Thin Shrink Small Outline	RU-28
AD9203ARURL7	-40°C to +85°C	28-Lead Thin Shrink Small Outline	RU-28
AD9203ARUZ <sup>1</sup>	-40°C to +85°C	28-Lead Thin Shrink Small Outline	RU-28
AD9203ARUZRL7 <sup>1</sup>	-40°C to +85°C	28-Lead Thin Shrink Small Outline	RU-28
AD9203-EB		Evaluation Board	

<sup>1</sup> Z = Pb-free part.

### A.1.3 The sedsonar file

Table A.6.1: Abbreviations with the description of the sedsonar file

Sec	Time: seconds since 1-Jan-2001. The difference with the common (epoch) year 1970 is 978307200.
Msec	0.999 measures in msec, which makes the start time more accurate.
Temp	Celsius * 100
Pressure	Pressure in bar * 10000, eenheid/resolutie is dus 0.1mbar
Run_ns	Total time in ns from broadcasting, waiting time and recording of all the reflected signals
Rf_ns	“rangefinder_ns”: number of nanoseconds between start measurement and the 1 <sup>st</sup> bottom reflection. Follows from “mark”. After the software update, this value will also include the blanking distance.
Ax ay az	Acceleration, range -1000 to 1000 stands for -2G to +2G. Gives orientation of the sensor using the gravity. Kind of a motion sensor.
Mx my mz	Magnetic field, range -2048 to 2047 stands for -1.3 to +1.3 Gauss
Dac0	0 to 4095, roughly a measure for energy in an acoustic signal. It is limited by the battery voltage.
Battery	Battery voltage in mV
Startmv stopmv	Start and end voltage from the management of the acoustic signal, the voltage from “dac0” with battery voltage as a limit.
Deadtime	Waiting time in 0.25 $\mu$ s units between sending and receiving: 400 = 100 $\mu$ s = 75mm (1500 m/s geluidssnelheid)
Flags	Needs to be zero
Txadj	Number of times that dac0/startmv (stopmv) are adjusted for an optimal amplitude per acoustic session. A high value is 7. This happens when for example a fish swims below the transducer.
Mark	1 to 3999, index in 4000 audio samples where the firmware 1 <sup>st</sup> reflection from the bottom detects, when zero it is unknown.
Buf	4000 samples in range -128 to 127. Sample rate is 4M (=4000 samples (t1 to t3999)) so this digital shot covers 1ms in time.

### A.1.4 Running the parse.py script

For analyses, the output files of the ASED-sensor need to be converted to a readable file. This is done using the script parse.py. The script parse.py creates 4 output files, namely: XXX-XXXA.params, XXX-XXXA.pressure, XXX-XXXA.sedsonar and XXX-XXXA.sync. The file settings are saved in the params file. The pressure values are subscribed in the pressure file. The sedsonar file contains all raw data measurements. The sync file synchronises the pressure values with the sedsonar values. The raw data of the ASED-sensor will be used for finding a suitable method to analyse the performance of the ASED-sensor.

```

Windows PowerShell
PS E:\UTwente\Master\Afstuderen\experiment_data\input> python parse.py .\002-064A.SE2
processing .\002-064A.SE2
done
PS E:\UTwente\Master\Afstuderen\experiment_data\input>
  
```

Figure A.6.1: Run the parse.py file in Windows PowerShell by the selected file of the ASED-sensor.

	002-064A.SE2	30/10/2018 09:30	SE2 File	8,628 KB
	002-064A.SE2.params	12/02/2019 19:40	PARAMS File	2 KB
	002-064A.SE2.sedsonar	12/02/2019 19:40	SEDSONAR File	24,808 KB
	002-064A.SE2.sync	12/02/2019 19:40	SYNC File	48 KB

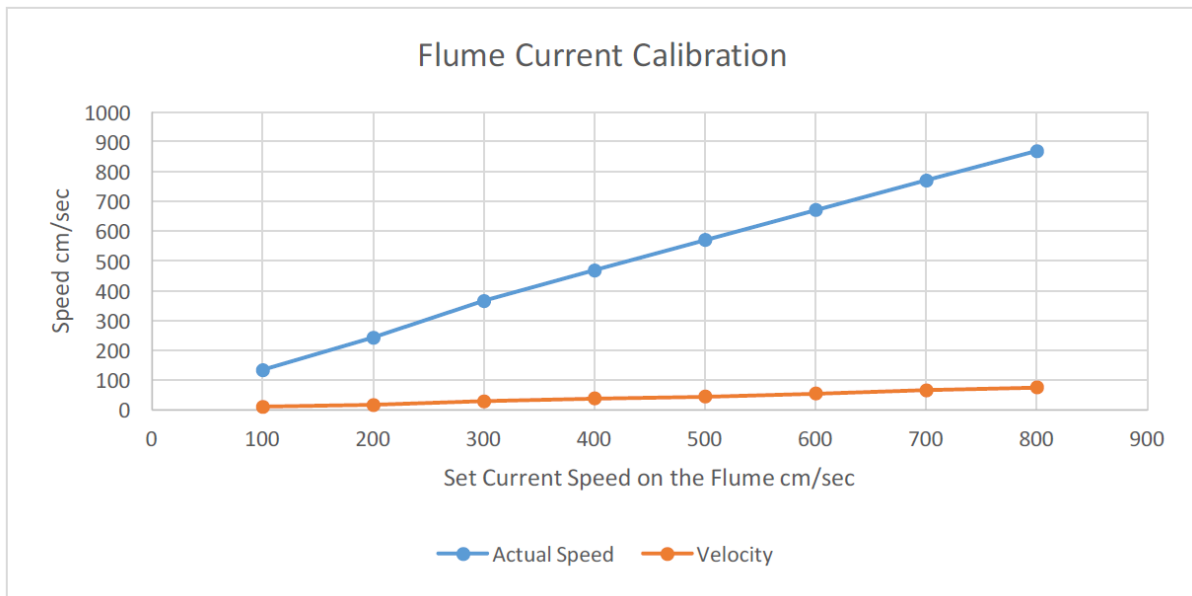
Figure A.6.2: The output of running the parse.py script.

## A.2 Sediment distribution

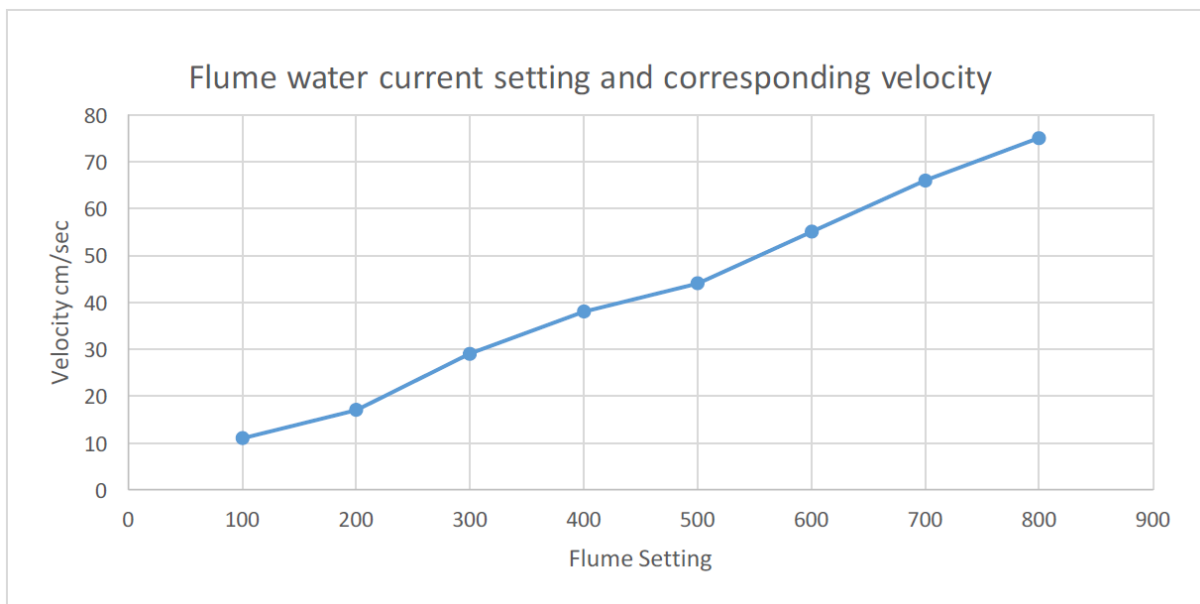
Table A.6.2: Sediment distribution ranging from sand fraction 1.00, 0.80, 0.65, 0.48, 0.40, 0.12 and 0.07.

% sand in soil type	Fract ion Sand	10% boundary (10% smaller than ... $\mu\text{m}$ )	90% boundary (90% smaller than ... $\mu\text{m}$ )	Modus grainsize in $\mu\text{m}$	Median grainsize D50 from Malvern in $\mu\text{m}$	Median grainsize D50 from Malvern in PHI	Coarse sand % fraction PHI 0-1, 500-1000 $\mu\text{m}$	Medium sand % fraction PHI 1-2, 250-500 $\mu\text{m}$ in %	Fine sand % fraction PHI 2-3, 125-250 $\mu\text{m}$ in %	Very Fine sand % fraction PHI 3-4, 62.5-125 $\mu\text{m}$	Silt % < 63 $\mu\text{m}$	% water in sediment
100.0	1.00	165.69	414.92	262.458	262.34	1.93	2.97	52.2	43.58	1.25	0	10.5
100.0		168.15	421.27	266.082	266.18	1.91	3.37	53.35	42.21	1.07	0	10.9
100.0		167.17	417.45	264.832	264.51	1.92	3.08	52.99	42.79	1.14	0	11.8
78.3	0.80	11.94	397.92	256.073	221.5	2.17	2.67	38.15	35.39	2.06	21.72	22.2
80.8		14.45	404.46	262.42	230.8	2.12	2.8	40.88	35.33	1.79	19.2	22.2
81.0		13.42	373.39	246.679	220.62	2.18	1.37	37.83	39.93	1.87	18.99	22.1
64.1	0.65	6.42	398.26	263.868	179.38	2.48	3.33	30.18	26.5	4.15	35.88	28.4
64.9		6.78	401.63	266.776	185.48	2.43	3.37	31.28	26.57	3.68	35.14	28.6
67.2		7	408.01	268.098	195.39	2.36	3.62	32.85	27.51	3.23	32.82	28.4
49.5	0.48	4.82	361.96	263.714	59.62	4.07	2.24	22.06	19.81	5.44	50.52	36.1
48.6		4.77	371.01	268.478	55.13	4.18	2.9	21.56	18.51	5.65	51.45	36.1
46.4		4.46	363.74	267.942	46.12	4.44	2.65	20.56	17.82	5.47	53.57	36.5
42.9	0.40	4.23	333.63	259.206	39.54	4.66	1.6	17.77	16.98	6.6	57.14	41.2
36.9		4.59	327.98	273.248	31.55	4.99	1.92	15.65	13.12	6.32	63.09	41.0
39.1		4.7	307.25	253.371	32.98	4.92	0.96	15.31	15.96	6.99	60.88	41.1
13.2	0.12	2.98	75.71	20.811	16.97	5.88	1.1	0.87	2.55	8.8	86.84	52.8
12.0		2.87	70.37	19.47	16.21	5.95	0.5	0.81	2.23	8.56	88.05	52.9
10.1		2.77	63.51	15.369	14.47	6.11	0	0.27	1.91	8.09	89.86	53.0
7.6	0.07	2.84	55.38	9.371	12.66	6.3	0	0.08	0.94	6.73	92.39	70.4
5.7		2.8	50	9.366	12.05	6.37	0	0	0.25	5.57	94.3	70.4

### A.3 Flume calibration



Calibration of the current speeds in the flume. “Set Current Speed” referring to the speed setting on the flume; “Actual Speed” referring to the actual speed the setting induces; “Velocity” referring to the x-reading from the portable ADV.



## A.4 SSC lab experiment

### A.4.1 Set-up SSC level

The set-up for measuring the SSC level consists of an air compressor (Figure A.6.3.1) which sucks the air, a safety Erlenmeyer flask (Figure A.6.3.2) and an Erlenmeyer flask (Figure A.6.3.3) with a clip and a glass funnel (Figure A.6.3.4). All of them connected with rubber hoses; therefore, the air sucks the water in the Erlenmeyer flask. Between the glass funnel and the Erlenmeyer flask is a small piece of filter paper, which stops the sediment going into the Erlenmeyer flask. The filter paper is measured before and after the SSC experiments. The SSC can be calculated from the amount of sediment on the paper and the amount of water in the syringe which is put in the glass funnel.



Figure A.6.3: Set-up for the SSC analysis

### A.4.2 SSC experiment

The number of pulses is important for the propagation of the signal into the water. If there is a lot of SSC, a signal with one pulse will measure the SSC instead of the bed. While sending a signal with 5 pulses will measure the bed instead of the SSC. The soil type of 80% sand was put in the bucket. This soil type had the best signal reflection and no noise occurred at the beginning of the signal. The distance from the soil to the ASSED-sensor was 39.6 cm. The SSC was first sieved with a sieve opening of 425  $\mu\text{m}$  and, thereafter sieved with a sieve opening of 125  $\mu\text{m}$ . From now on the very fine silt is called sludge.

Before the sludge was put in the water tank, 3 water samples were taken. The water samples were taken by a 60 ml syringe. Each time some sludge was added to the tank, the water was well mixed with a mixer powered by an electrical drilling machine (Figure 2.14) and 3 new water samples were taken near the transducer head. The SSC in seawater from the Eastern Scheldt is 29.1 mg/l. The ASSED-sensor with only one pulse could not measure the bottom after adding one tea spoon of sludge. Therefore, as the first test, one tea spoon of sludge was added. The SSC is then increased every 10 minutes until an SSC of 3743.2 mg/l (Table A.6.3). The measurement of the SSC in the water tank is clarified in

*Table A.6.3: 80% sand with different SSC in the water tank at a water depth of 39.6 cm*

<b>Information about the addition into the Eastern Scheldt water in the water tank</b>	<b>SSC in mg/l</b>
Eastern Scheldt water	29.1
One teaspoon sludge added	29.2
One spoon sludge added	40.4
One spoon sludge added	51.0
Two spoons sludge added	64.7
Water added to sludge 2.4 cm of 10 L mayonnaise bucket added	966.2
The same mixture as water added to the sludge: 3 cm of 10 L mayonnaise bucket added	3743.2

The experiment of the SSC could not find a reflection of the signal by the bed, because the reflection of the signal by the bed was too weak. The initial and periodic noise occurred during this measurement. The periodic noise did not have high-intensity peaks. Therefore, this experiment will not be further analysed.

## A.5 Analysed methods

### A.5.1 Frequency analysis method

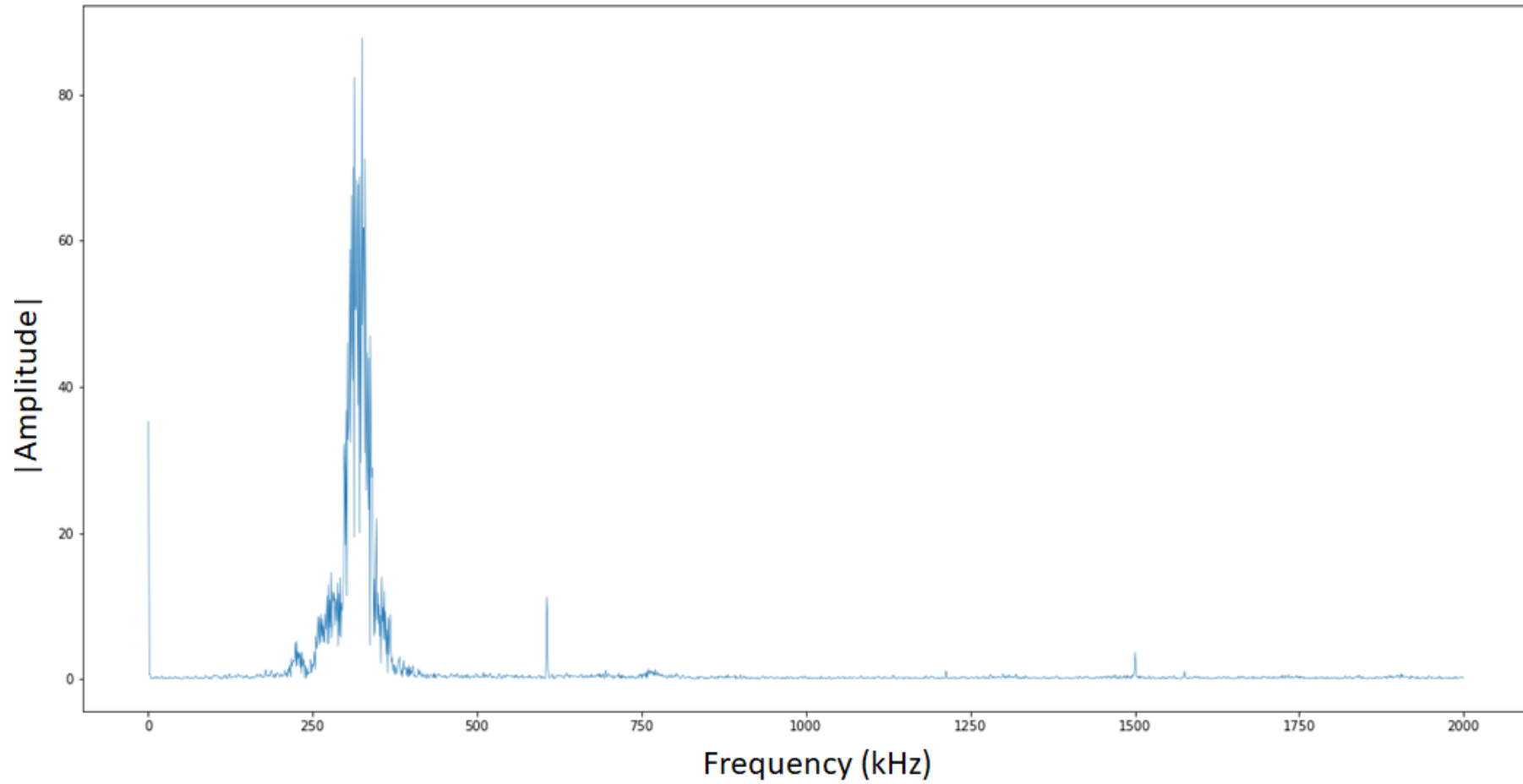


Figure A.6.4: The FFT analysis. The manual depth is 0.284 m. The frequency with the highest amplitude is 325 kHz.

Table A.6.4: The FFT analysis by calculating the frequencies into depths

file 52	handmeasured depth [m]		0.284						
	0	1	2	3	4	5	6	7	grouped
freq [Hz]	325163	314157	325163	314157	314157	325163	325163	325163	325163
depth [m]	0.313	0.295	0.313	0.296	0.295	0.312	0.312	0.312	0.312

### A.5.1.1 Windowing

Windowing reduces the amplitude of the samples at the beginning and end of the window, reducing leakage (Lyon, 2009). As the raw data has noise in the measurements a Hanning or Hamming window can be applied (Figure A.6.5). Those windows reduce negative side lobes and therefore slightly broaden the main lobe (Hartmann, 2008), but the main lobe is not contaminated by the sidelobes. The corner points are not considered by the Hanning window, where this is the case for the Hamming window. The high-signal and high-noise data at the low-frequency end of the spectra were removed by the Hanning window (Louis *et al.*, 1992). Therefore, the Hanning window was chosen.

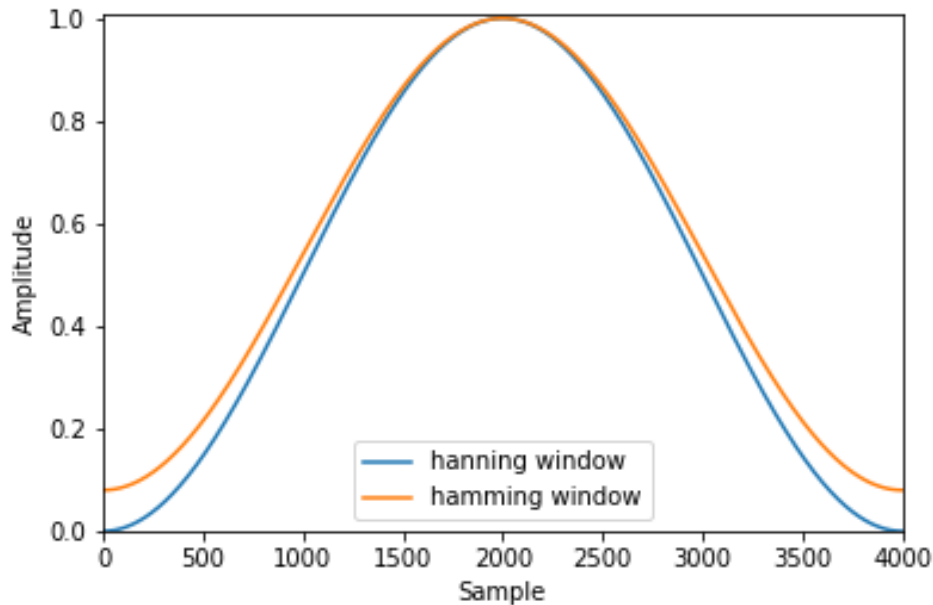


Figure A.6.5: The Hanning and Hamming window applied over the signal for the FFT analysis

### A.5.2 Envelope method

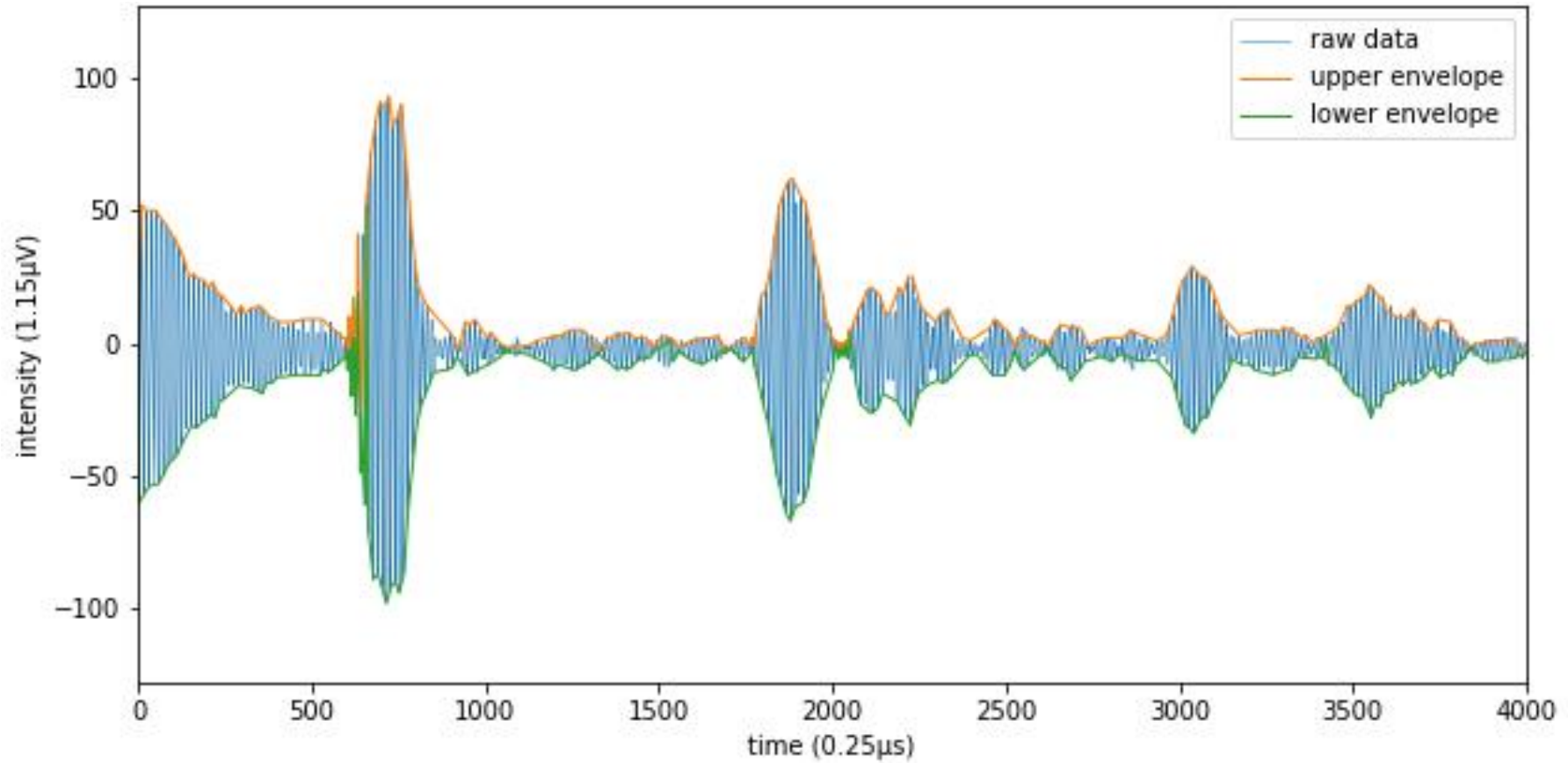
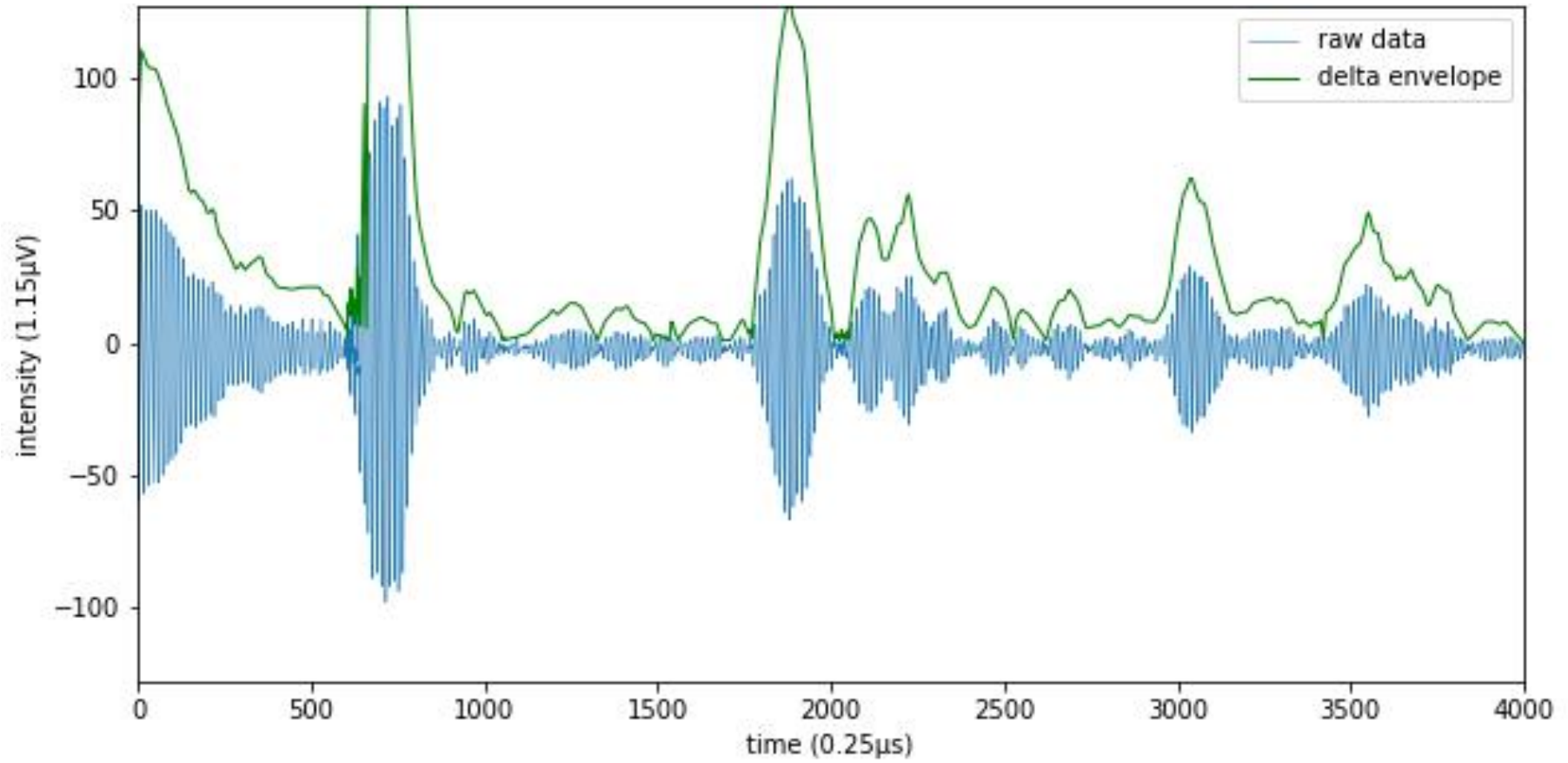


Figure A.6.6: Creating the upper and lower envelope of the raw data. This measurement was applied above a metal plate at a depth of 0.21 m.



*Figure A.6.7: Creating the delta envelope by subtracting the lower minus the upper envelope. This measurement was applied above a metal plate at a depth of 0.21 m.*

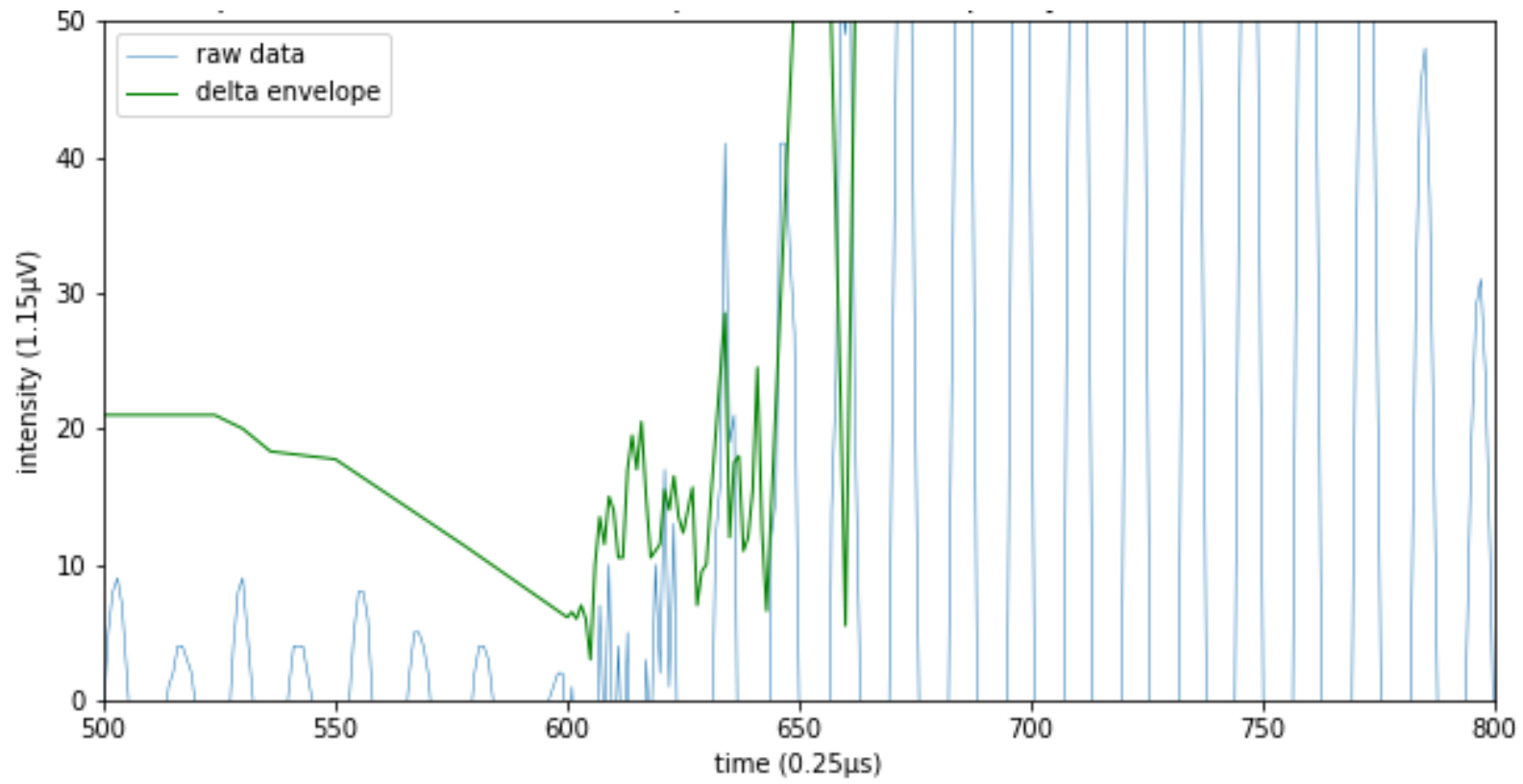


Figure A.6.8: Zoomed in. Creating the delta envelope by subtracting the lower minus the upper envelope. This measurement was applied above a metal plate at a depth of 0.21 m.

### A.5.3 Kalman filter method

#### A.5.3.1 Absolute and square

The raw data is squared, or the absolute is taken and the Kalman filter is applied (Figure A.6.9). The square Kalman filter has a higher intensity compared to the absolute Kalman filter (Figure A.6.9 and Figure A.6.10). Both methods gave the same result in bed detection. The square Kalman filter has a very high-intensity peak and for the convenience, the absolute Kalman filter will be used.

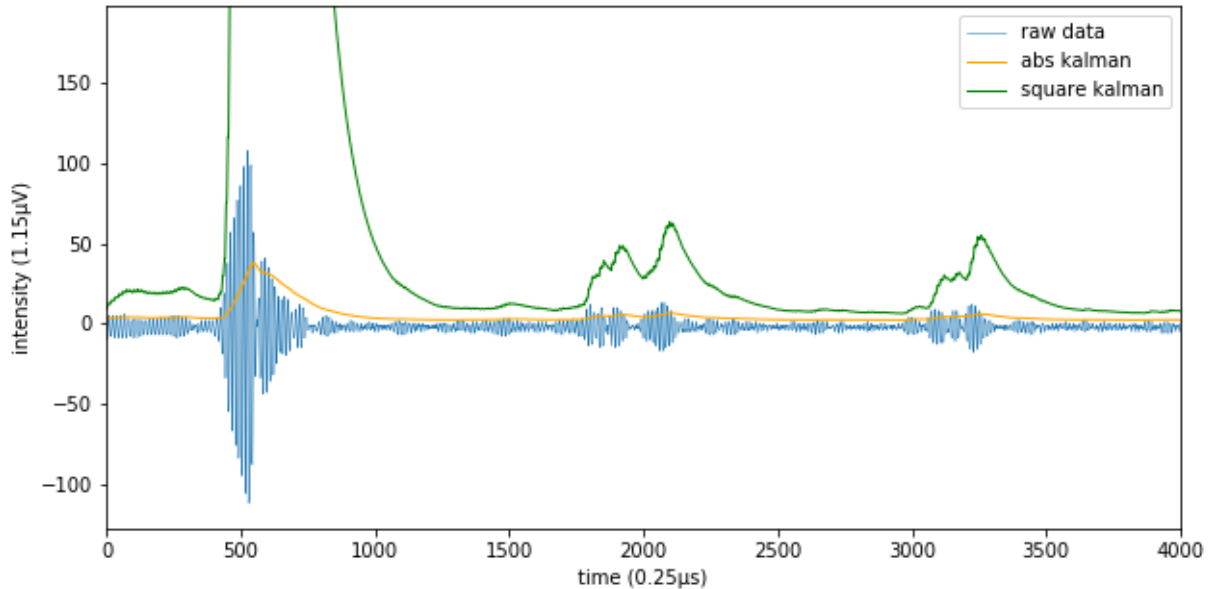


Figure A.6.9: Plotting the raw data by taking the absolute or square of the raw signal and applying the Kalman filter. The soil type was 0.48 sand fraction.

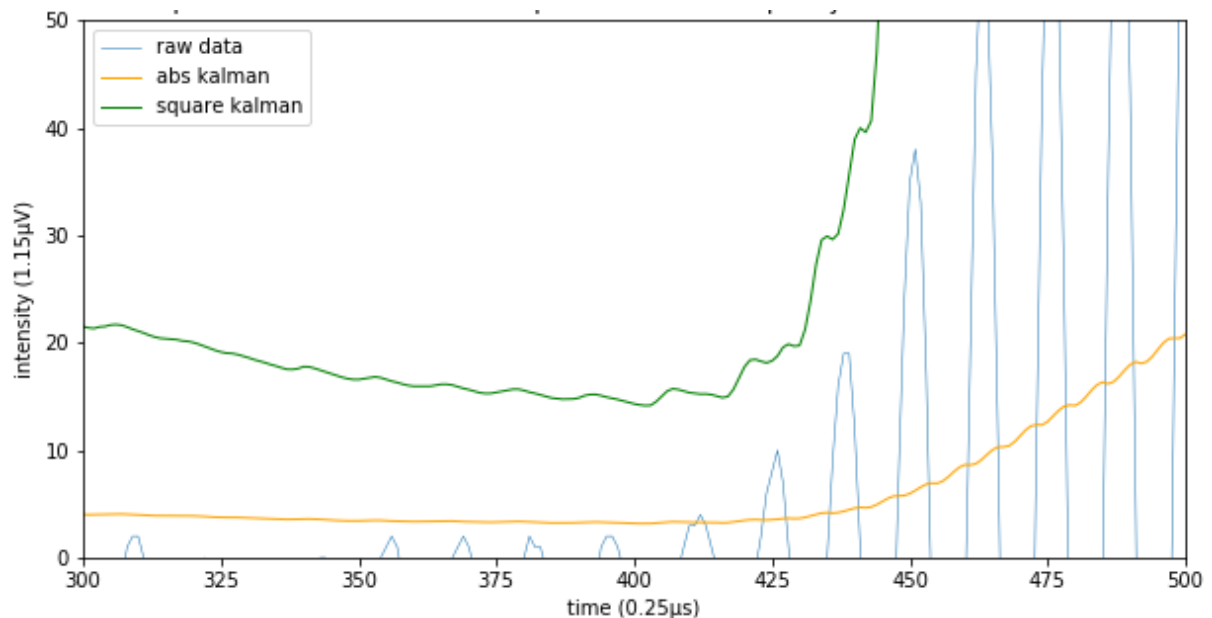


Figure A.6.10: Zoomed in. Plotting the raw data by taking the absolute or square of the raw signal and applying the Kalman filter. The soil type was 0.48 sand fraction.

#### A.5.4 Maximum value method

Maximum value: NIOZ had a method to make a first assumption of the depth. This method found the maximum value of the intensity peak (Figure A.6.11), which was written in the firmware in language C. This method is easy to implement and is fast to calculate the bed detection.

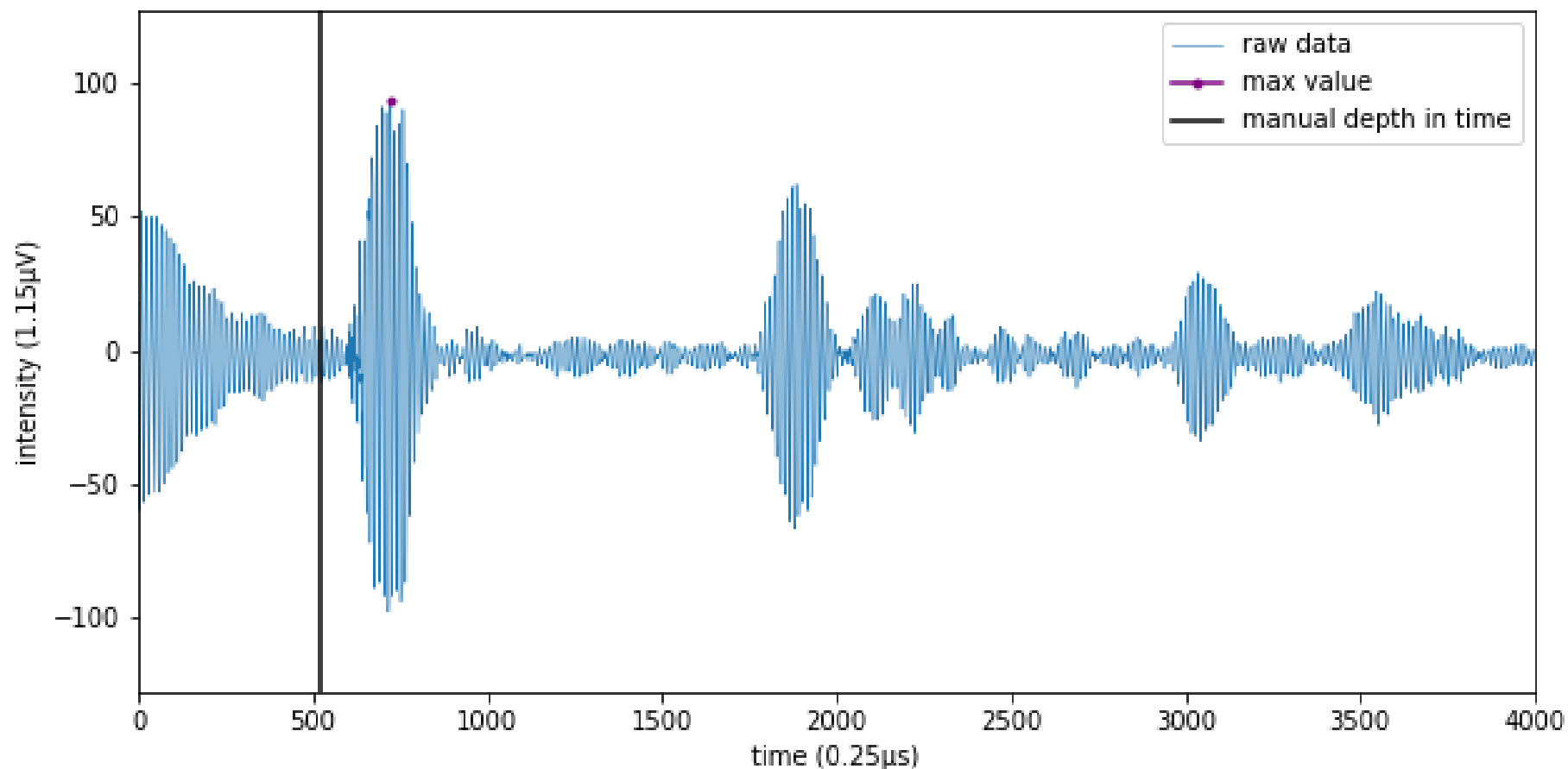


Figure A.6.11: The raw data (blue line) with a maximum value (purple dot) at time step 723. The manual depth (black line) is 0.21 m converted to time is 547-time steps of  $0.25 \mu\text{s}$

### A.5.5 Moving average method

A moving average of  $N=100$  was chosen. Because a lower moving average value did not smooth the graph.

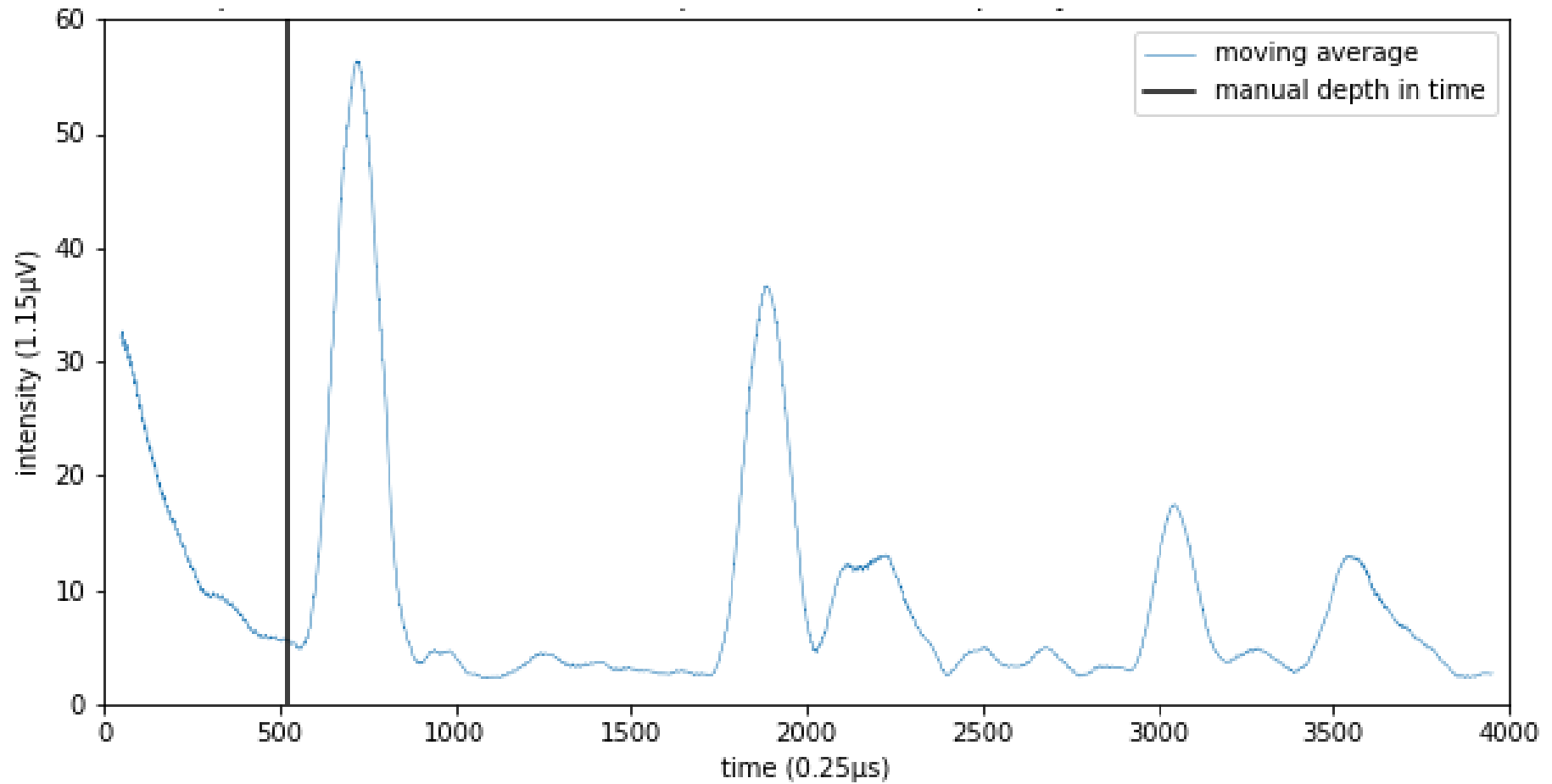


Figure A.6.12: Taking the absolute of the raw data and applying a moving average of 100 to smooth the graph. The blue line is the raw data. The manual depth (black line) is 0.21 m converted to time is 547-time steps of 0.25  $\mu\text{s}$

After the moving average value, the derivative was taken. The derivative gives an indication of the maximum and minimum values. As we are looking for the sudden increase in amplitude. First, the minimum value needs to be searched before the start of the maximum value. This was very difficult to analyse within Figure A.6.13, and therefore this method is not suitable.

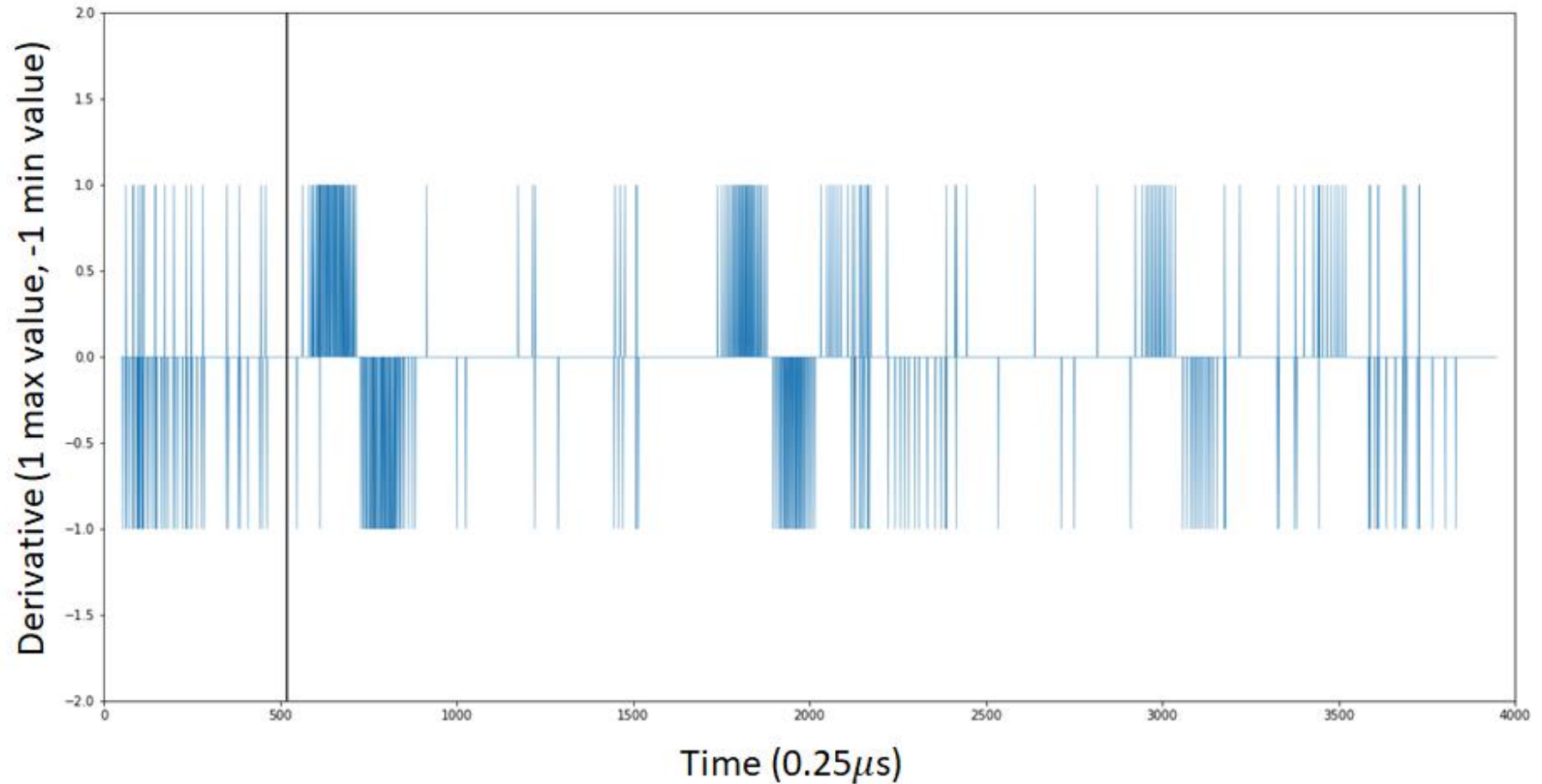


Figure A.6.13: Taking the derivative of the moving average (blue line). The manual depth (black line) is 0.21 m converted to time is 547 time steps of 0.25 µs.

## A.6 Formulas of the speed of sound

### A.6.1 The formula of Del Grosso

$$c(S, T, P) = C_{000} + \Delta C_T + \Delta C_S + \Delta C_P + \Delta C_{STP}$$

$$\Delta C_T(T) = C_{T1}T + C_{T2}T^2 + C_{T3}T^3$$

$$\Delta C_S(S) = C_{S1}S + C_{S2}S^2$$

$$\Delta C_P(P) = C_{P1}P + C_{P2}P^2 + C_{P3}P^3$$

$$\Delta C_{STP}(S, T, P) = C_{TP}TP + C_{T3P}T^3P + C_{TP2}TP^2 + C_{T2P2}T^2P^2 + C_{TP3}TP^3 + C_{ST}ST + C_{ST2}ST^2 \\ + C_{STP}STP + C_{S2TP}S^2TP + C_{S2P2}S^2P^2$$

T = temperature in degrees Celsius

S = salinity in Practical Salinity Units (PSU)

P = pressure in kg/cm<sup>2</sup>

The range of validity: temperature 0 to 30 °C, salinity 30 to 40 parts per thousand, pressure 0 to 1000 kg/cm<sup>2</sup>, where 100 kPa = 1.019716 kg/cm<sup>2</sup>.

Coefficients	Numerical values
C <sub>000</sub>	1402.392
C <sub>T1</sub>	0.5012285 * 10 <sup>1</sup>
C <sub>T2</sub>	-0.551184 * 10 <sup>-1</sup>
C <sub>T3</sub>	0.221649 * 10 <sup>-3</sup>
C <sub>S1</sub>	0.1329530 * 10 <sup>1</sup>
C <sub>S2</sub>	0.1288598 * 10 <sup>-3</sup>
C <sub>P1</sub>	0.1560592
C <sub>P2</sub>	0.2449993 * 10 <sup>-4</sup>
C <sub>P3</sub>	-0.8833959 * 10 <sup>-8</sup>
C <sub>ST</sub>	-0.1275936 * 10 <sup>-1</sup>
C <sub>TP</sub>	0.6353509 * 10 <sup>-2</sup>
C <sub>T2P2</sub>	0.2656174 * 10 <sup>-7</sup>
C <sub>TP2</sub>	-0.1593895 * 10 <sup>-5</sup>
C <sub>TP3</sub>	0.5222483 * 10 <sup>-9</sup>
C <sub>T3P</sub>	-0.4383615 * 10 <sup>-6</sup>
C <sub>S2P2</sub>	-0.1616745 * 10 <sup>-8</sup>
C <sub>ST2</sub>	0.9688441 * 10 <sup>-4</sup>
C <sub>S2TP</sub>	0.4857614 * 10 <sup>-5</sup>
C <sub>STP</sub>	-0.3406824 * 10 <sup>-3</sup>
C <sub>000</sub>	1402.392
C <sub>T1</sub>	0.5012285 * 10 <sup>1</sup>

### A.6.2 Formula of Coppens

$$c(D, S, t) = c(0, S, t) + (16.23 + 0.253 * t) * D + (0.213 - 0.1 * t) * D^2 + [0.016 + 0.0002 \\ * (S - 35)] * (S - 35) * t * D$$

$$c(0, S, t) = 1449.05 + 45.7 * t - 5.21 * t^2 + 0.23 * t^3 + (1.333 - 0.126 * t + 0.009 * t^2) \\ * (S - 35)$$

T = T/10 where T = temperature in degrees Celsius

S = salinity in parts per thousand

D = depth in metres

The range of validity: temperature 0 to 35°C, salinity 0 to 45 parts per thousands, depth 0 to 4000m.

### A.6.3 Formula of Mackenzie

$$c(D, S, T) = 1448.96 + 4.591 * T - 5.304 * 10^{-2} * T^2 + 2.374 * 10^{-4} * T^3 + 1.340 * (S - 35) + 1.630 * 10^{-2} * D + 1.675 * 10^{-7} * D^2 - 1.025 * 10^{-2} * T * (S - 35) - 7.139 * 10^{-13} * T * D^3$$

T = temperature in degrees Celsius

S = salinity in parts per thousand

D = depth in metres

The range of validity: temperature 2 to 30 °C, salinity 25 to 40 parts per thousand and depth 0 to 8000m.

### A.6.4 The formula of UNESCO: Chen and Millero

$$c(S, T, P) = C_W(T, P) + A(T, P)S + B(T, P)S^{3/2} + D(T, P)S^2$$

$$C_W(T, P) = C_{00} + C_{01}T + C_{02}T^2 + C_{03}T^3 + C_{04}T^4 + C_{05}T^5 + (C_{10} + C_{11}T + C_{12}T^2 + C_{13}T^3 + C_{14}T^4)P + (C_{20} + C_{21}T + C_{22}T^2 + C_{23}T^3 + C_{24}T^4)P^2 + (C_{30} + C_{31}T + C_{32}T^2)P^3$$

$$A(T, P) = A_{00} + A_{01}T + A_{02}T^2 + A_{03}T^3 + A_{04}T^4 + (A_{10} + A_{11}T + A_{12}T^2 + A_{13}T^3 + A_{14}T^4)P + (A_{20} + A_{21}T + A_{22}T^2 + A_{23}T^3)P^2 + (A_{30} + A_{31}T + A_{32}T^2)P^3$$

$$B(T, P) = B_{00} + B_{01}T + (B_{10} + B_{11}T)P$$

$$D(T, P) = D_{00} + D_{10}P$$

T = temperature in degrees of Celsius

S = salinity in PSU (parts per thousand)

P = pressure in bar

The range of validity: temperature 0 to 40 °C, salinity 0 to 40 parts per thousand, pressure 0 to 1000 bar.

Coefficients	Numerical values	Coefficients	Numerical values
$C_{00}$	1402.388	$A_{02}$	$7.166 * 10^{-5}$
$C_{01}$	5.03830	$A_{03}$	$2.008 * 10^{-6}$
$C_{02}$	$-5.81090 * 10^{-2}$	$A_{04}$	$-3.21 * 10^{-8}$
$C_{03}$	$3.3432 * 10^{-4}$	$A_{10}$	$9.4742 * 10^{-5}$
$C_{04}$	$-1.47797 * 10^{-6}$	$A_{11}$	$-1.2583 * 10^{-5}$
$C_{05}$	$3.1419 * 10^{-9}$	$A_{12}$	$-6.4928 * 10^{-8}$
$C_{10}$	0.153563	$A_{13}$	$1.0515 * 10^{-8}$
$C_{11}$	$6.8999 * 10^{-4}$	$A_{14}$	$-2.0142 * 10^{-10}$
$C_{12}$	$-8.1829 * 10^{-4}$	$A_{20}$	$-3.9064 * 10^{-7}$
$C_{13}$	$1.3632 * 10^{-10}$	$A_{21}$	$9.1061 * 10^{-9}$
$C_{14}$	$-6.1260 * 10^{-10}$	$A_{22}$	$-1.6009 * 10^{-10}$
$C_{20}$	$3.1260 * 10^{-5}$	$A_{23}$	$7.994 * 10^{-12}$
$C_{21}$	$-1.7111 * 10^{-6}$	$A_{30}$	$1.100 * 10^{-10}$
$C_{22}$	$2.5086 * 10^{-8}$	$A_{31}$	$6.651 * 10^{-12}$

$C_{23}$	$-2.5353 * 10^{-10}$	$A_{32}$	$-3.391 * 10^{-13}$
$C_{24}$	$1.0415 * 10^{-12}$	$B_{00}$	$-1.922 * 10^{-2}$
$C_{30}$	$-9.7729 * 10^{-9}$	$B_{01}$	$-4.42 * 10^{-5}$
$C_{31}$	$3.8513 * 10^{-10}$	$B_{10}$	$7.3637 * 10^{-5}$
$C_{32}$	$-2.3654 * 10^{-12}$	$B_{11}$	$1.7950 * 10^{-7}$
$A_{00}$	1.389	$D_{00}$	$1.727 * 10^{-3}$
$A_{01}$	$-1.262 * 10^{-2}$	$D_{10}$	$-7.9836 * 10^{-6}$

### A.6.5 Calculated speed of sounds

The variables which are used for the calculation of the speed of sound are visible in Table A.6.5.

Table A.6.5: Variables for calculating the speed of sound

Variable name	Value of variable	Unit of variable
<b>D1</b>	2.07	depth in m
<b>D2</b>	2.75	depth in m
<b>S1</b>	32.5	salinity in ppt
<b>S2</b>	40	salinity in ppt
<b>T1</b>	7.9	temperature in degrees Celsius
<b>T2</b>	20	temperature in degrees Celsius
<b>t1</b>	0.79	temperature in degrees Celsius / 1000
<b>t2</b>	2	temperature in degrees Celsius / 1000
<b>d1</b>	0.00207	depth in m / 1000
<b>d2</b>	0.00275	depth in m / 1000
<b>p1</b>	1.2454	pressure in bar
<b>p2</b>	1.3151	pressure in bar

Table A.6.6: Calculated speed of sounds from the variables of Table A.6.5 with the different speed of sound formulas

	Speed of sound in m/s		Speed of sound in m/s	Del Grosso	Speed of sound in m/s	UNESCO	Speed of sound in m/s
<b>Mackenzie</b>		<b>Coppens</b>					
D1,S1,T1	1478.922	d1,S1,t1	1478.951	p1,S1,T1	1479.123	p1,S1,T1	1479.201
D2,S2,T2	1527.183	d2,S2,t2	1527.081	p2,S2,T2	1527.307	p2,S2,T2	1527.303
D2,S2,T1	1488.376	d2,S2,t1	1488.256	p2,S2,T1	1488.466	p2,S2,T1	1488.538
D2,S1,T2	1518.671	d2,S1,t2	1518.703	p2,S1,T2	1518.887	p2,S1,T2	1518.903
D1,S2,T2	1527.172	d1,S2,t2	1527.070	p1,S2,T2	1527.296	p1,S2,T2	1527.291
D1,S1,T2	1518.659	d1,S1,t2	1518.692	p1,S1,T2	1518.875	p1,S1,T2	1518.892
D1,S2,T1	1488.365	d1,S2,t1	1488.244	p1,S2,T1	1488.455	p1,S2,T1	1488.526
D2,S1,T1	1478.933	d2,S1,t1	1478.962	p2,S1,T1	1479.134	p2,S1,T1	1479.213

As can be seen in Table A.6.6 the speed of sound does not differ a little. A better insight will be given to calculate the different speed of sound formulas into depths. This is done in Table A.6.7, the first speed of sound of each formula is used to calculate the depth. The formula of Mackenzie differs the most compared to the depths by using the formula of Coppens, Del Grosso and UNESCO. Therefore, the Mackenzie formula will not be used.

Coppens differs 0.1 mm from the UNESCO and Del Grosso depth. The most common sound velocity profilers use the UNESCO-Chen and Millero formula as well. The UNESCO algorithm is the International Standard algorithm and therefore the formula of UNESCO will be used to calculate the speed of sound (NPL National Physical Laboratory, 2000).

*Table A.6.7: Calculating the distance using the first value of the speed of sound of the different speed of sound formulas*

<b>Mackenzie in m</b>	<b>Coppens in m</b>	<b>Del Grosso in m</b>	<b>UNESCO in m</b>
0.1686	0.1683	0.1684	0.1684
0.4214	0.4208	0.4209	0.4209
0.8429	0.8417	0.8418	0.8418

## A.7 Extra results experiments

### A.7.1 Water depths

Initial noise and no periodic noise occur before the reflection of the signal by the bed at a depth of 0.210 m. The first signal has noise before the reflection of the signal by the bed for water depths 0.115 m, 0.210 m, 0.340 m, 0.440 m, 0.497 m and 0.572 m (Figure 3.3, Table A.6.8). For all depths, the last signal has noise before the reflection of the signal by the bed.

*Table A.6.8: All water depths at a manually measured depth in metres. The reflection of the signal by the bed is analysed by the raw data of the ASSED-sensor.*

Manual water depths in m	0.115	0.210	0.284	0.340	0.395	0.440	0.497	0.572
No initial noise before reflection of the signal by the bed								
No periodic noise before the reflection of the signal by the bed			x					
First signal has noise before the reflection of the signal by the bed	x	x		x		x	x	x
Last signal has noise before the reflection of the signal by the bed	x	x	x	x	x	x	x	x
First signal has stronger intensity reflection of the signal by the bed				x	x	x	x	x
Last signal has stronger intensity reflection of the signal by the bed								
The second reflection of the bed is good visible	x	x	x	x	x			
From the reflection of the signal a bed can be detected		x	x	x	x	x		
Length of experiment in min	20.5	14.8	16.15	20.15	11.95	17.3	16.3	16.15

### A.7.2 Soil types

For 0.65 fraction of sand, no initial noise occurs for a water depth around 0.20 m and 0.40 m. All sand fractions have periodic noise at a water depth of 0.40 m (Figure A.6.14; Table A.6.9). The first signal has noise before the reflection of the signal by the bed for 0.65 and 0.48 fraction of sand. The last signal has noise before the reflection of the signal by the bed for 0.12, 0.48, 0.65 and 0.80 fraction of sand (Figure A.6.14).

Most soil types have a reflection intensity around 100 ( $1.15\mu\text{V}$ ), except the last signal of soil type 0.48 fraction of sand which is around 70 ( $1.15\mu\text{V}$ ).

An extra measurement was done for 1.0 fraction of sand at a manually measured depth of 0.319 m. The start of the reflection of the signal by the bed has a lot of periodic noise and therefore unable to detect the beginning of the reflection of the signal by the bed.

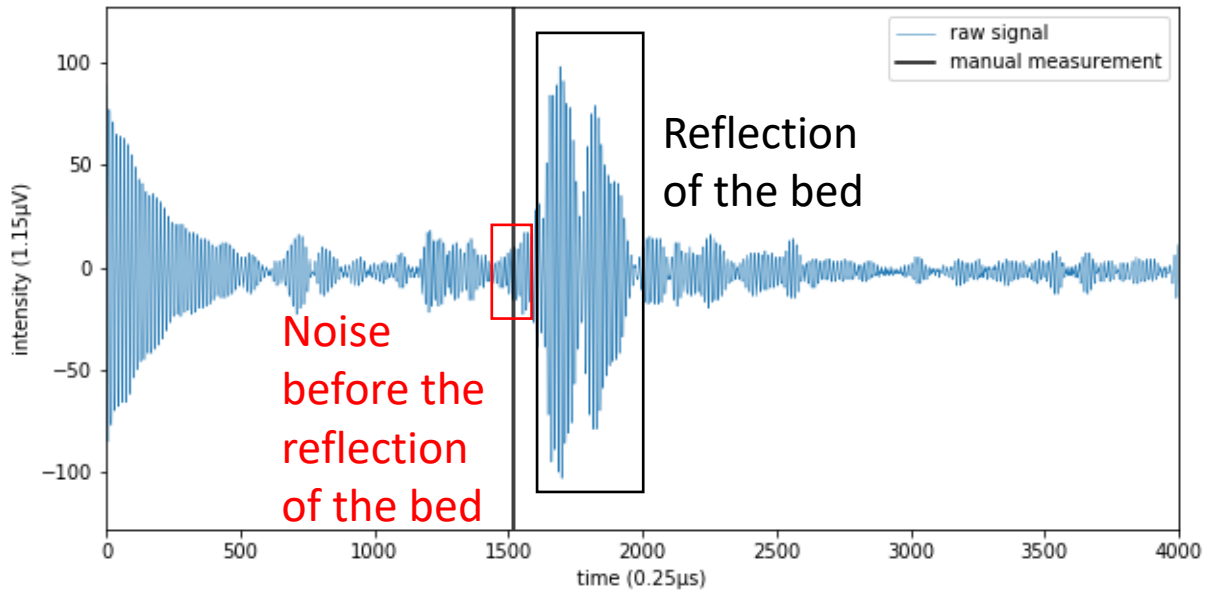


Figure A.6.14: Soil type 0.48 fraction of sand at a manually measured depth of 0.396 m = 1523 (0.25  $\mu$ s).

Table A.6.9: All soil types at a manually measured depth in metres. The reflection of the signal by the bed is analysed by the raw data of the ASED-sensor.

Fraction of sand	1.0	0.80	0.65	0.48	0.40	0.12
All measured depths in m	0.186 0.400	0.188 0.394	0.181 0.393	0.178 0.396	0.179 0.400	0.189 0.393
No initial noise before reflection of the signal by the bed		0.188	0.181 0.393			
No periodic noise before the reflection of the signal by the bed		0.188				
First signal has noise before the reflection of the signal by the bed	0.186		0.393	0.178 0.396	0.179	
Last signal has noise before the reflection of the signal by the bed	0.186	0.394	0.393	0.178 0.396	0.179	0.393
First signal has stronger intensity reflection of the signal by the bed			0.181	0.396		
Last signal has stronger intensity reflection of the signal by the bed						
The second reflection of the bed is good visible		0.188	0.181			
From the reflection of the signal a bed can be detected	0.400	0.188 0.394	0.181 0.393	0.178 0.396	0.179 0.400	0.189 0.393
Length of experiment in min (around 0.20 m)	4.0	12.1	9.9	9.65	10.0	5.3
Length of experiment in min (around 0.40 m)	7.4	4.65	5.4	7.4	4.6	4.85

### A.7.3 Dilutions

0.8 fraction of sand does not have initial noise for dilution 16.37% (0.303 m; Table A.6.10). All dilutions have periodic noise (Table A.6.10). The intensity peak of the bed is stronger than the periodic noise.

Most dilutions have a reflection intensity around 90 (1.15 $\mu$ V), except the last signal of dilution 16.37% (0.303 m) which is around 70 (1.15 $\mu$ V) and dilution 26.22% (0.307 m) which is below 50 (1.15 $\mu$ V).

Table A.6.10: Soil type of 0.8 fraction of sand with dilutions at a manually measured depth. The raw data of the reflection of the signal by the bed of the dilutions are analysed.

<b>% of water in the soil</b>	<b>16.37</b>	<b>26.11</b>	<b>26.93</b>	<b>45.47</b>
All measured depths in m	0.219 0.303	0.212 0.307	0.393	0.384
No initial noise before reflection of the signal by the bed	0.303			
No periodic noise before the reflection of the signal by the bed				
First signal has noise before the reflection of the signal by the bed	0.219 0.303	0.212 0.307	0.393	
Last signal has noise before the reflection of the signal by the bed			0.393	
First signal has stronger intensity reflection of the signal by the bed		0.307		
Last signal has stronger intensity reflection of the signal by the bed	0.303		0.393	0.384
The second reflection of the bed is good visible	0.219 0.303			0.384
From the reflection of the signal a bed can be detected	0.219 0.303	0.212	0.393	0.384
Length of experiment in min	15.3 (0.219) 14.4 (0.303)	13.15 (0.212) 13.9 (0.307)	5.0	4.9

For 0.65 fraction of sand, no initial and periodic noise occurs for dilution 18.12% (0.197 m and 0.305 m; Table A.6.11). The reflection of the signal by the bed is comparable to Figure 3.5.

The remaining dilutions have initial and periodic noise (Figure 3.6; Table A.6.11). The first signal has less initial noise compared to the last signal with a dilution of 17.07% (0.244 m), 56.14% (0.360 m), 68.98% (0.393 m) and 90.37% (0.427 m; Figure 3.6).

Most dilutions have a reflection intensity around 90 (1.15 $\mu$ V), except for the last signal of dilutions higher than 40%.

Table A.6.11: Soil type of 0.65 fraction of sand with dilutions at a manually measured depth. The raw data of the reflection of the signal by the bed of the dilutions are analysed.

<b>% water in soil</b>	<b>17.07</b>	<b>18.12</b>	<b>30.94</b>	<b>43.86</b>	<b>68.98</b>	<b>90.37</b>
All measured depths in m	0.244 0.331	0.197 0.305	0.365	0.360	0.389	0.427
No initial noise before reflection of the signal by the bed		0.197 0.305				
No periodic noise before the reflection of the signal by the bed		0.197 0.305				
First signal has noise before the reflection of the signal by the bed	0.244 0.331		0.365	0.360	0.389	0.427
Last signal has noise before the reflection of the signal by the bed	0.244 0.331		0.365	0.360	0.389	0.427
First signal has stronger intensity reflection of the signal by the bed				0.360	0.389	0.427
Last signal has stronger intensity reflection of the signal by the bed						
The second reflection of the bed is good visible						
From the reflection of the signal a bed can be detected	0.244 0.331	0.197 0.305	0.365			
Length of experiment in min	14.55 (0.244) 17.1 (0.331)	14.85 (0.197) 14.3 (0.305)	8.3	6.1	20.9	12.5

All dilutions of 0.48 fraction of sand have initial and periodic noise (Figure 3.7; Table A.6.12). The last signal contains more initial noise than the first signal for dilutions 19.95% (0.309 m (Figure 3.7)), 41.27% and 52.45%.

Most dilutions have a reflection intensity around 90 (1.15 $\mu$ V), except the last signal of dilution 19.95% (0.309 m).

*Table A.6.12: Soil type of 0.48 fraction of sand with dilutions at a manually measured depth. The raw data of the reflection of the signal by the bed of the dilutions are analysed.*

<b>% of water in the soil</b>	<b>19.95</b>	<b>20.00</b>	<b>41.27</b>	<b>52.45</b>
All measured depths in m	0.192 0.309	0.179 0.295	0.368	0.361
No initial noise before reflection of the signal by the bed				
No periodic noise before the reflection of the signal by the bed				
First signal has noise before the reflection of the signal by the bed	0.309	0.295	0.368	0.361
Last signal has noise before the reflection of the signal by the bed		0.295	0.368	0.361
First signal has stronger intensity reflection of the signal by the bed		0.295		
Last signal has stronger intensity reflection of the signal by the bed				
The second reflection of the bed is good visible				
From the reflection of the signal a bed can be detected	0.192	0.179 0.295	0.368	
Length of experiment in min	17.0 (0.192) 13.8 (0.309)	13.8 (0.179) 13.6 (0.295)	10.1	11.2

Dilution 21.75% (0.197 m) with 0.4 fraction of sand has no initial and no periodic noise (Table A.6.13). The first signal has a stronger intensity reflection of the signal by the bed for dilution 20.26% (0.205 m (Table A.6.13)).

Most dilutions have a reflection intensity around 90 (1.15 $\mu$ V), except the last signal of dilution 20.26% (0.205 m) which has an intensity of 40 (1.15 $\mu$ V) and dilutions 20.26% (0.287 m) and 44.47% (0.385 m), which have an intensity of around 10 (1.15 $\mu$ V).

*Table A.6.13: Soil type of 0.4 fraction of sand with dilutions at a manually measured depth. The raw data of the reflection of the signal by the bed of the dilutions are analysed.*

<b>% of water in the soil</b>	<b>20.26</b>	<b>21.75</b>	<b>44.47</b>	<b>52.42</b>	<b>65.19</b>
All measured depths in m	0.205 0.287	0.197 0.299	0.385	0.374	0.380
No initial noise before reflection of the signal by the bed		0.197			
No periodic noise before the reflection of the signal by the bed		0.197			
First signal has noise before the reflection of the signal by the bed	0.205 0.287	0.299	0.385	0.374	0.380
Last signal has noise before the reflection of the signal by the bed	0.205 0.287	0.299	0.385	0.374	0.380
First signal has stronger intensity reflection of the signal by the bed	0.205				
Last signal has stronger intensity reflection of the signal by the bed					
The second reflection of the bed is good visible					

From the reflection of the signal a bed can be detected	0.205	0.197 0.299			
Length of experiment in min	13.6 (0.205) 15.6 (0.287)	16.5 (0.197) 13.8 (0.299)	8.9	4.5	7.8

All dilutions have a reflection intensity of around 90 ( $1.15\mu\text{V}$ ).

*Table A.6.14: Soil type of 0.12 fraction of sand with dilutions at a manually measured depth. The raw data of the reflection of the signal by the bed of the dilutions are analysed.*

<b>% of water in the soil</b>	<b>57.50</b>	<b>63.13</b>	<b>72.45</b>
All measured depths in m	0.366	0.358	0.357
No initial noise before reflection of the signal by the bed			
No periodic noise before the reflection of the signal by the bed			
First signal has noise before the reflection of the signal by the bed	0.366	0.358	0.357
Last signal has noise before the reflection of the signal by the bed	0.366	0.358	0.357
First signal has stronger intensity reflection of the signal by the bed			
Last signal has stronger intensity reflection of the signal by the bed			
The second reflection of the bed is good visible			
From the reflection of the signal a bed can be detected			
Length of experiment in min	6.8	4.6	6.5

## A.8 Inundations of the field experiments

### A.8.1 Eastern Scheldt

For the first inundation, the n-value fluctuates between 2.2 and 3.5 and the bed detected depth fluctuates between 0.382 m and 0.388 m. With a constant bed detected depth of 0.382 m in the middle of the first inundation. The second inundation has a fluctuating n-value between 2.2 and 2.6, and a bed detected depth between 0.376 m and 0.388 m. After three hours of inundation, the bed detected depth is constant at 0.384 m until, in the last half hour, it increases to 0.387 m. The third inundation has a constant n-value of 2.2 and bed detected depth. The bed detected depth is 0.385 m for the first hour and the last 1.5 hour, in between the bed detected depth is 0.384 m. The fourth inundation has a fluctuating n-value between 2.2 and 10.5. The bed detected depth fluctuates around 0.389 m. The last inundation has for the first 5.5 hours a constant n-value of 2.2 and the last 2.5 hour a fluctuating n-value to 11.2. The bed detected depth is more constant during the first 5.5 hours at a depth around 0.389 m, thereafter the bed detected depth fluctuates a lot between 0.360 m and 0.420 m (Table A.6.15). The fluctuating can be caused by SSC.

*Table A.6.15: Inundations during the Eastern Scheldt experiment*

<b>Inundation</b>	<b>1</b>	<b>2</b>	<b>3</b>	<b>4</b>	<b>5</b>
Manually measured depth in m	0.387	0.387	0.387	0.387	0.387
Averaged ASSED depth in m	0.383	0.384	0.384	0.389	0.389
Difference manual - ASSED depth in m	0.004	0.003	0.003	-0.002	-0.002
Minimum ASSED depth in m	0.366	0.367	0.384	0.361	0.355
Maximum ASSED depth in m	0.388	0.391	0.385	0.438	0.421
Standard deviation ASSED depth in m	0.0035	0.0038	0.0005	0.0107	0.0088
Averaged n-value	2.4	2.4	2.2	5.1	3.8
Minimum n-value	2.2	2.2	2.2	2.2	2.2
Maximum n-value	3.5	6.5	2.3	19.7	17.1
Standard deviation n-value	0.25	0.58	0.03	3.14	3.00
Length of inundation in time (HH:MM)	07:50	07:50	06:40	07:35	08:10

### A.8.2 The Western Scheldt

The bed detected depth fluctuates more and therefore the standard deviation is higher. The average standard deviation was 0.0148 m (Table A.6.16) during the 3-week experiment. This is due to the shape change of the signal reflected by the bed over time. At the beginning of the inundation, the first part of the maximum intensity peak is the signal reflected by the bed (Figure 3.9). Later during the inundation, the second part or even the third part of the maximum intensity peak has the highest intensity of the signal reflected by the bed (Figure 3.9). Therefore, three different depths will be converted. This occurs for inundations 9 to 16, 31 to 37 which have multiple bed detected depths, around 0.27 m, 0.31 m and 0.35 m. The n-value increases to more than 15, during this period.

Table A.6.16: Inundations during the Western Scheldt experiment

<b>Inundation</b>	<b>All</b>	<b>1</b>	<b>2</b>	<b>3</b>	<b>4</b>	<b>5</b>	<b>6</b>	<b>7</b>	<b>8</b>	<b>9</b>	<b>10</b>
Manually measured depth in m	0.262	0.262	0.262	0.262	0.262	0.262	0.262	0.262	0.262	0.262	0.262
Averaged ASED depth in m	0.285	0.270	0.270	0.269	0.272	0.270	0.269	0.270	0.269	0.276	0.277
Difference manual - ASED depth in m	-0.023	-0.008	-0.008	-0.007	-0.010	-0.008	-0.007	-0.008	-0.007	-0.014	-0.015
Minimum ASED depth in m	0.239	0.246	0.239	0.250	0.245	0.265	0.243	0.255	0.244	0.243	0.251
Maximum ASED depth in m	0.568	0.286	0.275	0.282	0.281	0.273	0.272	0.274	0.346	0.348	0.348
Standard deviation ASED depth in m	0.0151	0.0042	0.0033	0.0024	0.0031	0.0011	0.0022	0.0018	0.0047	0.0153	0.0106
Averaged n-value	4.5	2.9	2.3	2.3	2.3	2.3	2.3	2.3	2.3	3.7	5.2
Minimum n-value	2.2	2.3	2.3	2.3	2.3	2.3	2.3	2.3	2.3	2.3	2.3
Maximum n-value	19.9	16.3	3.8	6.7	3.0	5.0	5.6	3.5	15.0	19.7	19.7
Standard deviation n-value	4.20	1.61	0.10	0.32	0.08	0.22	0.20	0.08	0.64	4.42	5.11
Length of inundation in time (HH:MM)	454:06	07:05	06:57	06:43	05:19	05:56	05:52	06:27	06:34	06:08	05:56

<b>Inundation</b>	<b>11</b>	<b>12</b>	<b>13</b>	<b>14</b>	<b>15</b>	<b>16</b>	<b>17</b>	<b>18</b>	<b>19</b>	<b>20</b>	<b>21</b>
Manually measured depth in m	0.262	0.262	0.262	0.262	0.262	0.262	0.262	0.262	0.262	0.262	0.262
Averaged ASED depth in m	0.291	0.275	0.284	0.298	0.288	0.285	0.293	0.288	0.287	0.291	0.294
Difference manual - ASED depth in m	-0.029	-0.013	-0.022	-0.036	-0.026	-0.023	-0.031	-0.026	-0.025	-0.029	-0.032
Minimum ASED depth in m	0.255	0.249	0.243	0.260	0.262	0.253	0.251	0.261	0.260	0.266	0.275
Maximum ASED depth in m	0.349	0.347	0.350	0.350	0.350	0.301	0.353	0.298	0.324	0.309	0.305
Standard deviation ASED depth in m	0.0306	0.0116	0.0206	0.0182	0.0162	0.0062	0.0201	0.0047	0.0071	0.0067	0.0039
Averaged n-value	8.0	3.9	5.4	9.5	6.0	4.4	6.7	2.7	4.3	4.9	5.4
Minimum n-value	2.3	2.3	2.3	2.3	2.3	2.3	2.3	2.3	2.3	2.3	2.3
Maximum n-value	19.8	19.7	19.8	19.9	19.8	16.0	19.6	16.2	15.5	18.0	12.3
Standard deviation n-value	7.32	3.73	5.91	6.39	6.43	4.62	5.65	1.59	3.45	3.04	2.50
Length of inundation in time (HH:MM)	06:05	05:53	06:08	06:05	05:54	05:48	05:43	06:02	06:40	06:37	06:11

<b>Inundation</b>	<b>22</b>	<b>23</b>	<b>24</b>	<b>25</b>	<b>26</b>	<b>27</b>	<b>28</b>	<b>29</b>	<b>30</b>	<b>31</b>	<b>32</b>
Manually measured depth in m	0.262	0.262	0.262	0.262	0.262	0.262	0.262	0.262	0.262	0.262	0.262
Averaged ASED depth in m	0.293	0.288	0.289	0.292	0.290	0.292	0.291	0.290	0.293	0.288	0.293
Difference manual - ASED depth in m	-0.031	-0.026	-0.027	-0.030	-0.028	-0.030	-0.029	-0.028	-0.031	-0.026	-0.031
Minimum ASED depth in m	0.284	0.273	0.274	0.277	0.266	0.271	0.279	0.260	0.267	0.266	0.253
Maximum ASED depth in m	0.300	0.298	0.361	0.304	0.301	0.306	0.356	0.302	0.311	0.342	0.362
Standard deviation ASED depth in m	0.0040	0.0050	0.0074	0.0056	0.0066	0.0061	0.0071	0.0038	0.0055	0.0058	0.0131
Averaged n-value	6.2	3.5	4.2	4.3	4.1	3.8	4.4	2.4	3.8	2.9	6.2
Minimum n-value	2.3	2.3	2.3	2.3	2.3	2.3	2.3	2.3	2.3	2.2	2.3
Maximum n-value	15.6	18.5	18.9	18.9	15.5	14.8	15.9	7.7	16.4	15.7	19.6
Standard deviation n-value	4.22	2.73	3.01	3.35	3.08	2.69	3.65	0.58	1.81	1.96	4.96
Length of inundation in time (HH:MM)	06:12	06:18	06:37	06:11	05:39	06:09	06:23	05:47	06:36	05:32	05:27

<b>Inundation</b>	<b>33</b>	<b>34</b>	<b>35</b>	<b>36</b>	<b>37</b>
Manually measured depth in m	0.262	0.262	0.262	0.262	0.262
Averaged ASED depth in m	0.290	0.301	0.301	0.300	0.294
Difference manual - ASED depth in m	-0.028	-0.039	-0.039	-0.038	-0.032
Minimum ASED depth in m	0.279	0.281	0.261	0.275	0.265
Maximum ASED depth in m	0.360	0.359	0.359	0.355	0.352
Standard deviation ASED depth in m	0.0092	0.0084	0.0228	0.0136	0.0094
Averaged n-value	5.2	8.3	7.1	8.3	6.4
Minimum n-value	2.3	2.3	2.3	2.3	2.3
Maximum n-value	19.4	19.9	19.7	19.8	19.5
Standard deviation n-value	4.91	3.85	5.40	5.38	4.44
Length of inundation in time (HH:MM)	05:18	05:31	05:12	05:12	05:13

## A.9 Performed experiments

All the measurements will be obtained with the ASED-sensor with a fixed measurement frequency of 300 kHz, and as validation with a tape measure and with the echologger EU400 (SBES) in a water tank.

*Table A.6.17: Different water depths in metres for the echologger and the ASED-sensor*

<b>SBES</b>	0.137	0.197	0.260	0.336	0.392	0.442	0.496	0.556
<b>ASED-sensor</b>	0.115	0.210	0.284	0.340	0.395	0.440	0.497	0.572

The values in Table A.6.18 are the water depths measured by the tape measure.

*Table A.6.18: Different soil types versus the water depth for the echologger and the ASED-sensor*

<b>Fraction sand in soil</b>	<b>1.0</b>	<b>0.80</b>	<b>0.65</b>	<b>0.48</b>	<b>0.40</b>	<b>0.12</b>
<b>ASED-sensor</b>	0.186	0.188	0.181	0.178	0.179	0.189
	0.400	0.394	0.393	0.396	0.400	0.393
<b>SBES</b>	0.200	0.197	0.194	0.194	0.195	0.198
	0.403	0.392	0.393	0.402	0.406	0.391

All the measured depths in metres are the manually measured depths in Table A.6.19.

*Table A.6.19: Manually measured water depths in metres of the dilutions of soil types*

<b>Fraction sand</b>	<b>0.8</b>	<b>0.65</b>	<b>0.48</b>	<b>0.4</b>	<b>0.12</b>
<b>% of water in the soil</b>	<b>16.37</b>	<b>17.07</b>	<b>19.95</b>	<b>21.75</b>	
<b>ASED</b>	0.219	0.244	0.192	0.197	
<b>SBES</b>	0.192	0.223	0.176	0.181	
<b>ASED</b>	0.299	0.327	0.305	0.295	
<b>SBES</b>	0.284	0.315	0.31	0.3	
<b>% of water in the soil</b>	<b>26.11</b>	<b>18.12</b>	<b>20</b>	<b>20.26</b>	
<b>ASED</b>	0.212	0.197	0.179	0.205	
<b>SBES</b>	0.192	0.214	0.195	0.173	
<b>ASED</b>	0.307	0.305	0.295	0.287	
<b>SBES</b>	0.313	0.305	0.296	0.27	
<b>% of water in the soil</b>	<b>26.93</b>	<b>30.94</b>	<b>41.27</b>	<b>44.47</b>	<b>57.5</b>
<b>ASED</b>	0.393	0.365	0.368	0.385	0.37
<b>SBES</b>	0.376	0.373	0.355	0.37	0.381
<b>% of water in the soil</b>	<b>45.47</b>	<b>43.86</b>	<b>52.45</b>	<b>52.42</b>	<b>63.13</b>
<b>ASED</b>	0.38	0.356	0.357	0.37	0.358
<b>% of water in the soil</b>		<b>68.98</b>		<b>65.19</b>	<b>72.45</b>
<b>ASED</b>		0.385		0.376	0.353
<b>% of water in the soil</b>		<b>90.37</b>			
<b>ASED</b>		0.423			